PROBABILISTIC SEISMIC DAMAGE ASSESSMENT AND REPAIR COST ANALYSIS OF EXISTING STEEL MOMENT FRAME BUILDINGS

A Thesis

Presented to the Faculty of the Graduate School

of Cornell University

In Partial Fulfillment of the Requirements for the Degree of

Master of Science

by

Jung Sik Yang

August 2009

ABSTRACT

The purpose of seismic reliability analysis of existing building is to estimate the probable damage due to future earthquakes and to retrofit these building for improved performance. Earthquake damage to buildings depends not only on structural model but also on the characteristics of earthquake ground motion such as duration, frequency, peak ground motion, and number of occurrences. These characteristics are considered as random. Thus, stochastic processes are used to describe earthquake occurrence, ground motions, and failure.

An existing eight-story steel moment frame building located in Los Angeles, California is chosen as a case study to illustrate the application of the stochastic methods. To evaluate the seismic reliability of the building, a large number of ground motions are generated that represent possible future earthquakes in the region. Earthquake ground motion is modeled as a Gaussian process based on recorded accelerogram of the 1994 Northridge earthquake. Under the ground motions generated, the response samples of the building are obtained by dynamic analysis method.

For the purpose of the seismic vulnerability analysis, failure rate analysis is performed to estimate the probability of exceedance of peak building response measured by peak interstory drift and floor acceleration. Besides, to develop fragility curves, incremental dynamic analysis (IDA) is performed which is a parametric analysis method to estimate structural performance under earthquake ground motions scaled to several levels of intensity measures such as first mode spectral displacement and acceleration. From IDA results, fragility curves are developed which show the conditional probability of reaching or exceeding a particular damage state as a

function of ground motion intensity measure. Fragility curves are then represented by lognormal distribution functions with two parameters.

Because the damage in terms of monetary loss provides more meaningful measure of economic impacts of earthquakes, seismic damage to the building is evaluated in terms of dollar value. Using the fragility curves, direct economic cost functions are developed to estimate economic losses as a function of ground motion intensity measure.

In order to illustrate the use of the direct economic cost functions for finding an optimal retrofit option, braced frames are designed by placing bracing elements to the existing moment frames. Although several retrofit options should be considered to find an optimal alternative, this study focuses on the concentrically braced steel frame system. The exceedance probabilities of the overall direct economic cost of the two structural systems are compared to make a decision which structural system is superior.

BIOGRAPHICAL SKETCH

Jung Sik Yang was born in Busan, South Korea on January 17, 1978. He received a Bachelor of Science in Civil Engineering with a concentration in Structural Engineering from the University of Southern California in 2006. After spending a year working in a structural engineering office, he continued his studies toward a Master of Science in Structural Engineering at Cornell University.

ACKNOWLEDGMENTS

First of all, I would like to sincerely thank my advisor, Dr. Mircea Grigoriu for his guidance and patience throughout the work that resulted in this thesis. I also wish to thank Dr. Wilkins Aquino for his contributions as a member of my committee. Finally, but most importantly, I thank my parents in Korea. I always feel their love and support that make me stay strong and focused on my career goals.

TABLE OF CONTENTS

BIOGRAPHICAL SKETCH iii
ACKNOWLEDGEMENTS iv
TABLE OF CONTENTS v
LIST OF FIGURES vii
LIST OF TABLES x
LIST OF ALGORITHMS xi

1 INTRODUCTION 1

1.1 Overview 3

2 METHODOLOGY FOR ESTIMATION OF EARTHQUAKE DAMAGE 5

2.1 Stochastic Modeling of Earthquake Occurrence and Ground Motion 5

2.1.1 Earthquake Occurrences 5
2.1.2 Autocorrelation Function and Power Spectral Density 8
2.1.3 Weakly Stationary Gaussian Process 10
2.1.4 Generation of Ground Acceleration by a Stationary Gaussian Process 11

2.2 Estimation of Earthquake Damage for SDOF Systems 15

2.2.1 Dynamic Responses for Linear Elastic SDOF Systems 16
2.2.2 Statistical Analysis of Response of SDOF systems 19
2.2.3 Failure Rate of SDOF Systems 21

2.3 Earthquake Damage Estimation for MDOF Systems 23

2.3.1 Structural Model for Linear Elastic MDOF Systems 23
2.3.2 Equations of Motion for Linear Elastic MDOF Systems 25
2.3.3 Modal Analysis 28
2.3.4 Displacement Response of the Structural Model 31
2.3.5 Statistical Analysis of Response of MDOF Systems 32
2.3.6 Failure Rate of MDOF Systems 36
2.3.7 Repair Cost Probability of the Three-Story Model 39

3 LINEAR ANALYSIS OF EIGHT-STORY BUILDING 43

3.1 Steel Moment Resisting Frame 43

3.2 Building Description 46

3.3 Seismic Response Analysis of the Eight-Story Building 48

3.3.1 Generation of Stationary Ground Motion 48
3.3.2 System Properties of the Eight-Story Building 50

3.3.3 Statistical Analysis of Responses and Evaluation of the Dominant Mode 54
3.4 Failure Rate of the Eight-Story Building 59
3.5 Fragility Curves 64
3.5.1 Damage of Structural and Nonstructural Components 64
3.5.2 Fragility Curves by a Linear Dynamic Analysis Method 66
3.6 Cost Functions for the Eight-Story Building 77
3.6.1 Discrete Damage-State Probability Curves 78
3.6.2 Repair Cost Functions for Structural and Nonstructural Damage 80
3.6.3 Monetary Losses during the Recovery time 84
3.6.4 Direct Economic Cost Functions 85
3.7 Exceedance Probability of Direct Economic Cost 88

4 NONLINEAR ANALYSIS OF EIGHT-STORY BUILDING 92
4.1 Generation of Non-stationary Ground Motion 92
4.2 Theoretical Background of Nonlinear Dynamic Analysis 96
4.2.1 Geometric and Material Nonlinearities 97
4.2.2 Equations of Motion for Nonlinear Inelastic MDOF Systems 99
4.3 Solution Method for Nonlinear Systems 100
4.4 Nonlinear Analysis of the Eight-Story Building 102
4.4.1 Force–Displacement Relations 103
4.4.2 Nonlinear Responses of the Building 106
4.4.3 Failure Rate 108
4.5 Direct Economic Cost Function 111
4.5.1 Fragility Curves 111
4.5.2 Direct Economic Cost Functions 117
4.6 Alternative Structural System: Braced Frame 119
4.6.1 Force–Displacement Relations 121
4.6.2 Direct Economic Cost Functions 124
4.7 Exceedance Probability of Direct Economic Cost 126

5 SUMMARY AND CONCLUSION 130

REFERENCES 133

LIST OF FIGURES

1.1 Fragility curves representing four damage states [18] 2

2.1 Five sample paths of earthquake occurrences generated by Method 1 and 2 8
2.2 One-Sided Power Spectral Density of $A(t)$ 11
2.3 N-S component of the El Centro Earthquake at Imperial Valley in California on May 18, 1940 (Ground motion data was obtained from Cosmos Virtual Data Center website [9]) 12
2.4 Calculated errors between $\rho(\tau)$ and $\hat{\rho}_{est}(\tau)$ of $A_s(t)$ for N-S El Centro Earthquake in 1940 13
2.5 Autocorrelation function of $A_s(t)$ for N-S El Centro Earthquake in 1940 14
2.6 One-sided spectral density of $A_s(t)$ for N-S El Centro Earthquake in 1940 ... 15
2.7 A sample of ground motion generated by a stationary Gaussian process 15
2.8 Single-degree-of-freedom system 16
2.9 A sample of displacement time history response 17
2.10 Mean of $X(t)$ of the SDOF model 20
2.11 Scaled covariance function of $X(t)$ of the SDOF model 21
2.12 Failure rate curve for the SDOF model 22
2.13 Three-story structural model 24
2.14 Natural frequencies and mode shapes for the structural model 27
2.15 Comparison of the total displacement response and displacement response due to the first mode of the three-story structure (solid line: total response; dotted line: response due to the first mode) 32
2.16 Mean of $X^{(i)}(t)$ of the three-story model (maximum and minimum values on the y-axis are set to the average of the peak values of $X_r^{(i)}(t)$) 34
2.17 Scaled covariance functions of story displacement of the three-story model .. 35
2.18 Linear relationship between two different story displacements 36
2.19 Failure rate curves of the three-story structural model (solid lines: failure rate due to an earthquake, dotted lines: lifetime failure rate) 38
2.20 Repair cost functions C_1 and C_2 in terms of interstory displacement 40
2.21 Repair cost probability functions using the repair cost function $C_1(\delta)$ (solid lines: repair cost probability due to an earthquake, dotted lines: lifetime repair cost probability) 41
2.22 Repair cost probability functions using the repair cost function $C_2(\delta)$ (solid lines: repair cost probability due to an earthquake, dotted lines: lifetime repair cost probability) 41

3.1 Typical welded moment resisting connection prior to 1994 [12] 44
3.2 Reduced Beam Section (RBS) connection [11] 45
3.3 Plan view of the eight-story building and elevation view of the N-S moment frame 47

3.4 Ground motion acceleration of the 1994 Northridge earthquake (component: 360 deg) recorded at UCLA station (Ground motion data was obtained from Cosmos Virtual Data Center website [9]) 48
3.5 Normalized autocorrelation function and one-sided PSD of the 1994 Northridge earthquake 49
3.6 A sample of ground motion acceleration modeled by a stationary Gaussian process based on the time history record of the 1994 Northridge earthquake . 50
3.7 Modes of the eight-story building 53
3.8 Mean of the responses for the eight-story building 55
3.9 Scaled covariance of story displacement of the eight-story building 56
3.10 Scaled covariance of story acceleration of the eight-story building 57
3.11 Exact solutions and responses due to *n*-th mode of the 1st story 58
3.12 Failure rates of the eight-story building in terms of interstory drift ratio 61
3.13 Failure rates of the eight-story building in terms of floor acceleration 62
3.14 Twenty IDA curves for the 1st and 5th stories 69
3.15 Twenty IDA curves of the 1st story 70
3.16 A simple example of fragility curves 71
3.17 Example of linear regression method to estimate the two parameters of lognormal CDF 74
3.18 Comparison of fragility curves constructed from IDA data and lognormal CDF 74
3.19 Fragility curves for the 1st and 5th stories of the eight-story building (dotted lines: by IDA data, solid lines: by a lognormal fit) 76
3.20 Flowchart for developing the direct economic loss functions 78
3.21 Discrete damage-state probability curves for the 1st and 5th stories 79
3.22 Repair cost functions for structural damage in the 1st and 5th stories 82
3.23 Repair cost functions for nonstructural damage in the 1st and 5th stories 83
3.24 Monetary loss functions during the recovery time for the 1st and 5th stories . 85
3.25 Direct economic cost function for the 1st story 86
3.26 Direct economic cost functions for the eight-story building 87
3.27 Distribution of intensity measures for an earthquake occurrence obtained from 10,000 samples of stationary ground motion (Section 3.3.1) 88
3.28 Probability curves of the direct economic cost for each story (solid line: probability due to an earthquake; dotted line: lifetime probability) 89
3.29 Probability curves of the direct economic cost for the eight-story building (solid line: probability due to an earthquake; dotted line: lifetime probability) 91

4.1 Acceleration time history of the 1994 Northridge earthquake (Ground motion data was obtained from Cosmos Virtual Data Center website [9]) 94
4.2 A sample of stationary ground acceleration 95
4.3 Deterministic modulate envelope function $w(t)$ 95
4.4 A sample of non-stationary ground acceleration 95

4.5 Distribution of possible intensity measures obtained from the 10,000 samples of non-stationary ground acceleration 96
4.6 P-Δ effects on a structural model 97
4.7 A moment frame in the 2nd story modeled in MASTAN2 103
4.8 Plastic hinges on deflected shape of the 2nd story moment frame..... 104
4.9 Force and displacement relationship of the 2nd story moment frame..... 104
4.10 Comparison of the different cases of structural analysis..... 107
4.11 Failure rates of the eight-story building in terms of interstory drift ratio 109
4.12 Failure rates of the eight-story building in terms of floor acceleration..... 110
4.13 IDA curves for the 1st story of the eight-story building subjected to four different accelerograms 113
4.14 IDA curves for the 1st story showing an extreme case of hardening..... 113
4.15 Ten IDA curves for the 1st and 5th stories..... 114
4.16 Fragility curves for the 1st and 5th stories of the eight-story building (dotted lines: by IDA data, solid lines: by a lognormal fit) 116
4.17 Direct economic cost functions for the eight-story building 118
4.18 Braced frames in the N-S direction (plan view in Figure 3.3) 120
4.19 Static pushover analysis of the 2nd story braced frame 121
4.20 Force and displacement relationship of the 2nd story braced frame 122
4.21 Direct economic cost functions for the braced frame building 125
4.22 Exceedance probabilities of the direct economic cost due to an earthquake occurrence..... 127
4.23 Exceedance probabilities of the direct economic cost during the lifetime..... 128
4.24 Exceedance probabilities of direct economic cost of the entire buildings 129

LIST OF TABLES

2.1 Modal parameters of the three-story structure for *n*-th mode 31

3.1 Moment of inertia of the N-S moment frame elements [1] 51
3.2 Significant Los Angeles Earthquakes [37] 63
3.3 Threshold of moment frames for structural damage [18] 65
3.4 Thresholds of moment frames for nonstructural damage [18] 66
3.5 Cumulative damage state probabilities for the example 71
3.6 A set of data points obtained to estimate two parameters of lognormal CDF 73
3.7 Estimated parameters of fragility function for the eight-story building 75
3.8 Repair cost ratios and damage state costs of the eight-story building [18] 81

4.1 Parameters of the envelope function $w(t)$ 94
4.2 Yield forces and lateral stiffness of the eight-story building 105
4.3 Bracing elements 119
4.4 Yield forces and story stiffnesses of the braced frame structure 124
4.5 Thresholds of braced frames for structural damage [18] 124

LIST OF ALGORITHMS

2.1 Methods to generate sample paths of earthquake occurrences 7
2.2 Newmark's method: Solution method for linear SDOF systems [7],[14] 18
2.3 Newmark's method: Solution method for linear MDOF systems [7],[14] 30

3.1 Construction of IDA Curves [4],[38],[39] 67

4.1 Wilson's Method: Solution method for nonlinear MDOF systems [7] 101
4.2 Modified Newton-Raphson Iteration [7] 102
4.3 Tangent stiffness matrix for moment frames 106
4.4 Tangent stiffness matrix for braced frames (tri-linear force-displacement relationship) 123

CHATER 1

INTRODUCTION

Earthquakes are unpredictable and potentially severe natural hazards. Structural failures in recent earthquakes such as Northridge earthquake in southern California and Sichuan earthquake in China have caused casualties and monetary losses inducing significant social and economic impacts. These events provide information on the seismic reliability of existing buildings. The purpose of seismic reliability analysis of existing buildings is to estimate the probable damage due to future earthquakes and to retrofit these buildings for improved performance. In general, structural reliability is expressed in terms of probability because of the uncertainty in seismic loads.

This thesis provides methodologies for building performance evaluation under earthquake loads and damage loss estimation related to structural and nonstructural damage as well as economic aspects of the damage. As a case study, an existing eight-story steel moment frame building located in Los Angeles, California is selected. In the Los Angeles region, high seismic risk area, most recently the 1994 Northridge earthquake caused the billions of dollars in damage in addition to fear of earthquakes.

For the purpose of the seismic vulnerability analysis, failure rate analysis is a useful approach. The failure rate analysis estimates the exceedance probability of structural damage in terms of different damage measures such as peak interstory drift ratio and floor acceleration. Since the accuracy of this approach depends on the number of samples of seismic response, it is necessary to generate a large number of ground motions that represent future earthquakes in the region. Based on the spectral density of a time history record, artificial ground motions can be modeled as a random process to take the random nature of earthquakes into consideration. Then the seismic response data can be obtained from dynamic analysis.

Fragility curves can be used to characterize the relationship between seismic intensity measure and building damage. The fragility curves provide the conditional probability of reaching or exceeding a particular damage state as a function of spectral displacement, spectral acceleration, or peak ground acceleration [18]. Figure 1.1 shows typical fragility curves representing four damage states: Slight, Moderate, Extensive, and Complete.

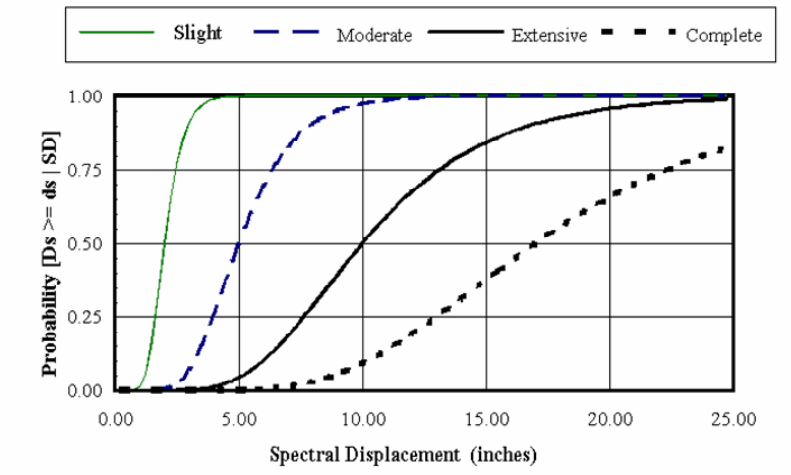

Figure 1.1: Fragility curves representing four damage states [18]

In general, the fragility curves can be developed using either of actual damage data from previous earthquakes or analytical methods. If the real damage data is not available or sufficient for a certain structure, fragility curves are generated from seismic response data obtained by means of dynamic analysis of structure subjected to artificial ground motions [8].

A method to construct analytical fragility curves is Incremental Dynamic Analysis (IDA). IDA, which involves simulating curves of damage measure versus seismic intensity measure, is a parametric analysis method to estimate structural performance under several earthquake ground motions [21],[38]. Based on IDA results,

structural and nonstructural damage can be classified into the four different damage states of the fragility curves, independently, based on threshold values which are given in terms of damage measures.

The estimation of the potential economic loss is also important criteria to determine the seismic vulnerability of structures. To assess the loss due to earthquakes in terms of dollar value, the formulation of reliable cost functions is required. The cost function can be developed from the fragility curves. Because each damage state is related to an expected repair cost or loss, the monetary damage of a building can be estimated as the mean economic loss which is the sum of the products of discrete damage state probability and expected damage cost [12],[18].

1.1 Overview

This thesis contains five chapters, the first of which is this brief introduction. The second chapter presents basic concepts underlying the seismic response analysis of linear single- and multi-degree-of-freedom systems. The first part of the chapter is concerned with modeling earthquake ground motion as a stationary process using an acceleration time history record. Then numerical methods to determine the response of structures subjected to artificial ground motion are presented and demonstrated with sample structural models. Subsequently, the responses of the structures are used as a measure of failure rate under the effect of ground motions.

In the third chapter, seismic damage analysis of an existing steel moment frame building located in Los Angeles is performed assuming linear elastic behavior. The artificial earthquakes are generated based on the acceleration time history of the 1994 Northridge earthquake. By utilizing the methods of response analysis developed in chapter two, the procedure to develop the fragility curves are discussed. Then loss

estimation functions are developed by converting the damage state probabilities to dollar equivalent.

In the fourth chapter, nonlinear analysis of the existing building is performed under the effect of non-stationary ground motion for more reliable estimation of structural performance. For nonlinear multi-degree-of-freedom systems, the governing equations of motion and methodologies for solving these equations are introduced. For the estimation of direct economic cost, the overall process described in chapter three is used. Lastly, an alternative structural system is presented as a retrofit option, and its level of safety is compared with that of the existing structural system.

The final chapter presents conclusions and discusses the findings of this study.

CHAPTER 2

METHODOLOGY FOR ESTIMATION OF EARTHQUAKE DAMAGE

Earthquakes occur randomly at any instant of time in seismically active regions. Due to their inherent uncertainty and the limited knowledge about the causes involved in this phenomenon, probability theories are widely used to incorporate the uncertainties. As a mean of protecting the built environment from earthquakes, probabilistic approaches are developed to estimate seismic damage to existing buildings or new buildings to be constructed.

In this chapter, modeling of earthquake-induced ground motion is first illustrated, and then basic topics in structural dynamics and their applications to earthquake response analysis are discussed. Failure rate analysis is then carried out considering simple structural models, which provides insight into structural reliability.

2.1 Stochastic Modeling of Earthquake Occurrence and Ground Motion

As a first step of seismic hazard estimation, this section discusses stochastic methods for modeling earthquake occurrences and generating artificial ground motion time histories.

2.1.1 Earthquake Occurrences

A Poisson process is commonly used to model an event with a long return period that can randomly occur at any time instant. Because earthquakes could occur in a seismic zone randomly in time and have a long recurrence time interval, the occurrence of earthquakes is assumed to follow a Poisson process [3].

Thus, the number of possible earthquake occurrences in a time *t* is governed by the Poisson probability mass function (PMF). If $N_{eq}(t)$ is the number of earthquakes in time interval (0, *t*), then

$$p(N_{eq}(t) = n_{eq}) = \frac{(\lambda t)^{n_{eq}}}{n_{eq}!} e^{-\lambda t} \tag{2.1}$$

where λ is the mean occurrence rate. It follows then that the mean number of occurrences in *t* is λt [3].

Under the assumption that earthquake occurrences follow a Poisson distribution, the time intervals between two consecutive occurrences are independent, exponentially distributed random variables with mean $1/\lambda$. Because of the memoryless property of the exponential distributions, the inter-arrival time of the future events is independent of the past [3]. Algorithm 2.1 shows two methods for simulating sample paths of earthquake occurrences over a specified period of time (0, *t*).

Numerical Example

The two methods are applied to the following numerical example. Suppose 30 earthquakes have been reordered over 50 years. Then the mean occurrence rate of earthquakes is estimated as $\hat{\lambda} = 0.6$ quakes/year. Under the assumption that earthquake occurrences can be modeled by a Poisson process, sample paths can be generated based on $\hat{\lambda}$. By each method in Algorithm 2.1, five sample paths of earthquake occurrences within the next 50 years are generated in Figure 2.1.

Algorithm 2.1: Methods to generate sample paths of earthquake occurrences

<table>
<tr><td rowspan="2"><u>Method 1</u>:</td><td>Input: t: time period of interest $(0, t)$
λ: mean occurrence rate

Output: t_i: occurrence time
EQ_i: the number of earthquakes at t_i</td></tr>
<tr><td>(a) Define initial values
$t_0=0$ and $EQ_0=0$

(b) Generate exponential random number T
$T \sim exponential(\lambda)$
where T: recurrence time

(c) Update time t_i
$t_i=t_{i-1}+T$

(d) Update the number of earthquakes EQ
If $t_i \le t$,
then $EQ_i=EQ_{i-1}+1$ and go to step (b)
If $t_i > t$,
then stop</td></tr>
<tr><td rowspan="2"><u>Method 2</u>:</td><td>Input: t: time period of interest $(0, t)$
λ: mean occurrence rate

Output: t_i: occurrence time
EQ_i: the number of earthquakes at t_i</td></tr>
<tr><td>(a) Generate Poisson random number N_{eq}
$N_{eq} \sim Poisson(\lambda t)$
where N_{eq} : the number of earthquake occurrences within time t

(b) Generate uniform random numbers t_i
$t_i \sim uniform(0,t)$
where t_i: occurrence time for each earthquake

(c) Arrange t_i in ascending order</td></tr>
</table>

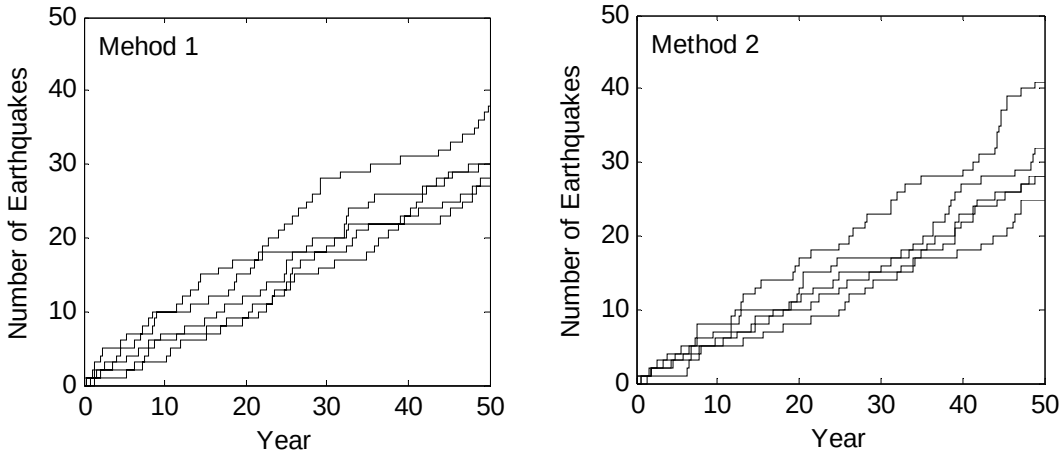

Figure 2.1: Five sample paths of earthquake occurrences generated by Method 1 and 2

2.1.2 Autocorrelation Function and Power Spectral Density

Power spectral density (PSD) represents the distribution of the power of a time series as a function of frequency. By definition, the PSD is the Fourier transform of the autocorrelation of a time series. For stationary processes $A(t)$, the autocorrelation function $r(\tau)$ depends only on lag time τ [20].

$$r(\tau) = E[A(t)A(t+\tau)] \tag{2.2}$$

The following two equations, a Fourier pair, show the relationship between the autocorrelation function $r(\tau)$ and the PSD $s(\nu)$.

$$r(\tau) = 2\int_0^\infty s(\nu)\cos(\nu t)d\nu \tag{2.3}$$

$$s(\nu) = \frac{1}{\pi}\int_0^\infty r(\tau)\cos(\nu\tau)d\tau \tag{2.4}$$

where $s(\nu)$ is a positive and even function of frequency ν [15],[34]. In engineering applications, the one-sided PSD function

$$\begin{aligned} g(\nu) &= 2s(\nu) \qquad \nu > 0 \\ &= 0 \qquad\quad \text{otherwise} \end{aligned} \tag{2.5}$$

is preferred because only the positive frequency range is considered [15],[34].

If a time history record a_j is given by discrete values, its autocorrelation and one-sided PSD functions can be estimated respectively as

$$r_l = r(l\Delta\tau) = \frac{1}{N_s - l}\sum_{j=1}^{N_s - l} a_j a_{j+l} \tag{2.6}$$

$$g_l = g\left(\frac{l\nu_c^{'}}{m_{lag}}\right) = \frac{\Delta\tau}{\pi}\left[r_0 + 2\sum_{j=1}^{m_{lag}-1} r_j \cos\frac{\pi jl}{m_{lag}} + (-1)^l r_{m_{lag}}\right] \tag{2.7}$$

where $l = 0,1,2,\cdots,m_{lag}$, m_{lag} is the maximum lag number, and $\nu_c^{'} = 1/2\Delta\tau$ is the cutoff frequency [25]. To reduce possible instabilities that may occur in the calculation of the autocorrelation function, m_{lag} should be less than one-tenth of the sample size N_s. The one-sided PSD given in Equation (2.7) is a biased estimate because of finite record length. In order to reduce the uncertainty errors and the variability of the PSD estimate, a smoothing procedure using a lag window weighting function is necessary [25]. The lag window weighing function is defined by

$$\begin{aligned} D_j = D(j\Delta\tau) &= \frac{1}{2}\left(1 + \cos\frac{\pi j}{m_{lag}}\right) && j = 0,1,2,\cdots,m_{lag} \\ &= 0 && j > m_{lag} \end{aligned} \tag{2.8}$$

Then the smooth estimate of one-sided PSD can be obtained as [25]

$$\hat{g}_l = \hat{g}\left(\frac{l\nu_c^{'}}{m_{lag}}\right) = \frac{\Delta\tau}{\pi}\left[r_0 + 2\sum_{j=1}^{m_{lag}-1} D_j r_j \cos\frac{\pi jl}{m_{lag}}\right] \tag{2.9}$$

2.1.3 Weakly Stationary Gaussian Process

Let $A(t)$ be a zero-mean, real-valued, stationary Gaussian process with the autocorrelation function $r(\tau) = E[A(t)A(t+\tau)]$ and one-sided power spectral density $g(\nu)$. Then $A(t)$ has the spectral representation of

$$A(t) = \int_0^\infty [\cos \nu t dU(\nu) + \sin \nu t dV(\nu)] \tag{2.10}$$

in which $U(\nu)$ and $V(\nu)$ are independent Gaussian processes with real-valued, zero-mean, and orthogonal increments. Equation (2.10) is impractical to generate the samples of the process $A(t)$ because the equation involves an infinite number of random variables in the processes of $U(\nu)$ and $V(\nu)$ [16],[34].

Therefore, samples of $A(t)$ are generated by a discrete approximation of order q of Equation (2.10) which is given by

$$A_q(t) = \sum_{k=1}^{q} \sigma_k \{V_k \cos(\nu_k t) + W_k \sin(\nu_k t)\} \tag{2.11}$$

where V_k and W_k are the independent Gaussian random variables with zero mean and unit variance, and ${\sigma_k}^2$ ($k = 1, 2, ..., q$) are defined by

$$\begin{aligned} {\sigma_k}^2 &= \int_{\nu'_{k-1}}^{\nu'_k} g(\nu) d\nu \\ &\approx g(\nu_k) \Delta \nu_k \end{aligned} \tag{2.12}$$

in which ν_k is the midpoint of a frequency interval (ν'_{k-1}, ν'_k), and $g(\nu)$ is the one-sided PSD of $A(t)$ [16],[34].

Figure 2.2 illustrates the spectral density $g(\nu)$ of $A(t)$ and a partition of frequency range $(0, \nu'_c)$ in q nonoverlapping intervals. The cutoff frequency ν'_c must be large enough to include most of the power of the process. ${\sigma_k}^2$ represents the contribution of the power in the frequency interval (ν'_{k-1}, ν'_k) to the total variance of the process $A(t)$ [16],[34].

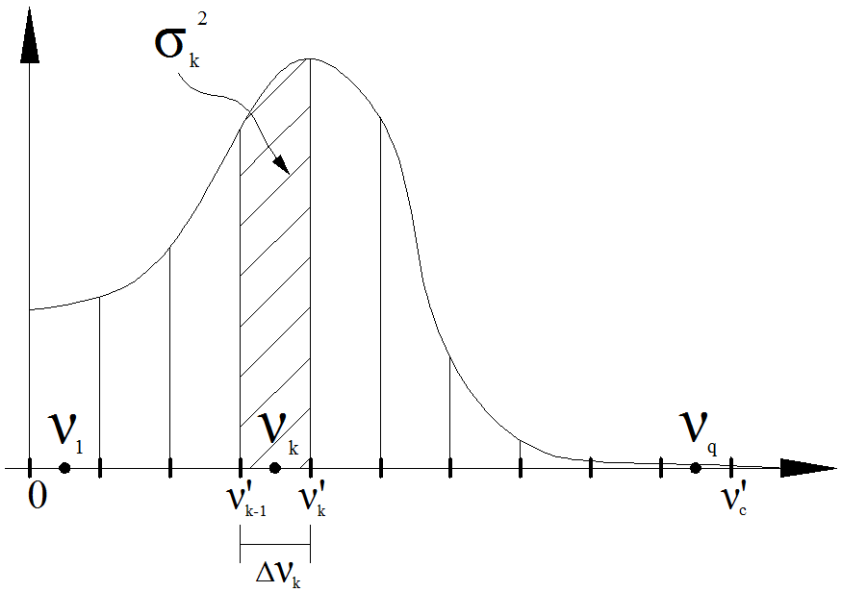

Figure 2.2: One-Sided Power Spectral Density of $A(t)$

2.1.4 Generation of Ground Acceleration by a Stationary Gaussian Process

As an example of modeling of earthquake ground motion by a stationary process, consider the acceleration time history record of the1940 El Centro earthquake in Figure 2.3. Earthquake ground motion is nonstationary random processes in general [34]. However, the strong ground motion portion corresponding to the time range of 1.3 to 5.9 seconds can be assumed to be a sample of a stationary process. Assuming the strong ground acceleration portion is the sum of a large number of independent stochastic processes, the ground acceleration can be approximated by a Gaussian process based on the central limit theorem [34].

However, the reference ground motion data in $t = [1.3, 5.9]$ seconds is insufficient to accurately estimate the autocorrelation function of the process. Thus, an additional assumption is made that the strong motion portion is a sample of stationary first-order Gaussian Markov process with zero-mean.

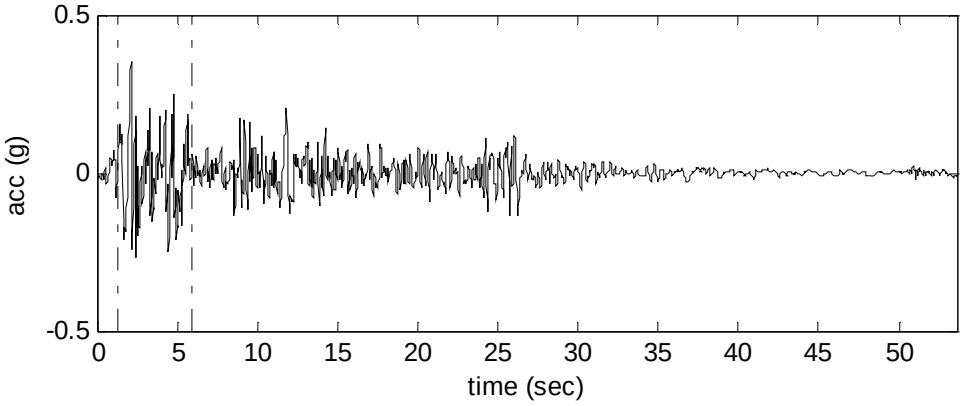

Figure 2.3: N-S component of the El Centro Earthquake at Imperial Valley in California on May 18, 1940 (Ground motion data was obtained from Cosmos Virtual Data Center website [9])

Let $A_s(t)$ denote a stationary first-order Gaussian Markov process with zero-mean; that is, $A_s(t)$ is the solution of the following stochastic differential equation

$$dA_s(t) = -\kappa A_s(t)dt + \sigma\sqrt{2\kappa}dB(t) \tag{2.13}$$

where $A_s(0) \sim N(0,\sigma^2)$, and $dB(t)$ is the increment of Brownian motion [15],[32]. Then the autocorrelation function of $A_s(t)$ is

$$r(\tau) = \sigma^2 e^{-\kappa|\tau|} \tag{2.14}$$

where κ is the positive constant, and σ^2 is the variance of $A_s(t)$ [23],[32],[34]. Substituting $r(\tau)$ to Equation (2.4) and using Equation (2.5) gives the one-sided spectral density function of $A_s(t)$ [34],

$$g(\nu) = \frac{2\sigma^2\kappa}{\pi(\nu^2 + \kappa^2)} \tag{2.15}$$

From the reference ground motion record, the variance of $A_s(t)$ is estimated as $\hat{\sigma}^2 = 0.0145$ g^2. Then to estimate the positive constant κ in Equation (2.15), let the estimated normalized autocorrelation function of $A_s(t)$ be

$$\hat{\rho}_{est}(\tau_l) = \frac{\hat{r}(\tau_l)}{\hat{\sigma}^2} \tag{2.16}$$

in which $\hat{r}(\tau_l)$ can be estimated using Equation (2.6). The estimator of κ can be obtained using the quadratic equation (2.17) in which the estimator $\hat{\kappa}$ minimizes the sum of squared differences between $\rho(\tau_l) = e^{-\kappa|\tau_l|}$ and $\hat{\rho}_{est}(\tau_l)$.

$$\varepsilon(\kappa) = \sum_l \left(\rho(\tau_l) - \hat{\rho}_{est}(\tau_l)\right)^2 \tag{2.17}$$

As shown in Figure 2.4, $\varepsilon(\kappa)$ is minimized at $\hat{\kappa} = 17.02$. Based on the optimized κ, $\rho(\tau)$ is compared to $\hat{\rho}_{est}(\tau)$ in Figure 2.5.

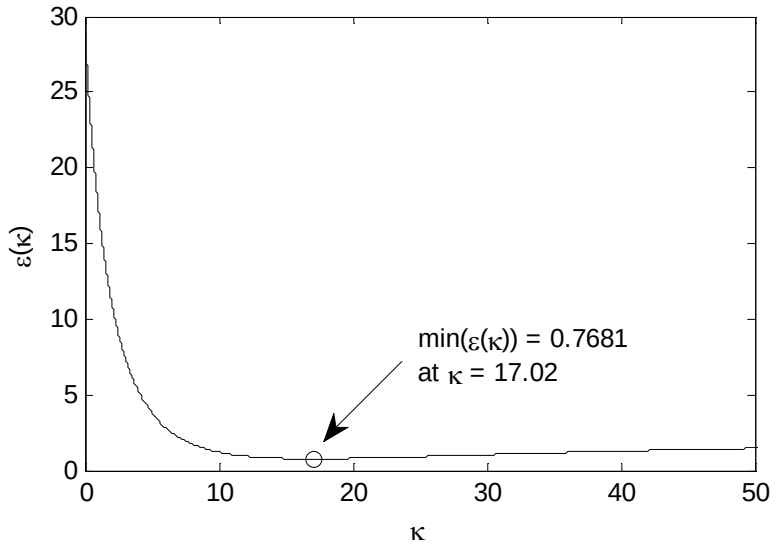

Figure 2.4: Calculated errors between $\rho(\tau)$ and $\hat{\rho}_{est}(\tau)$ of $A_s(t)$ for N-S El Centro Earthquake in 1940

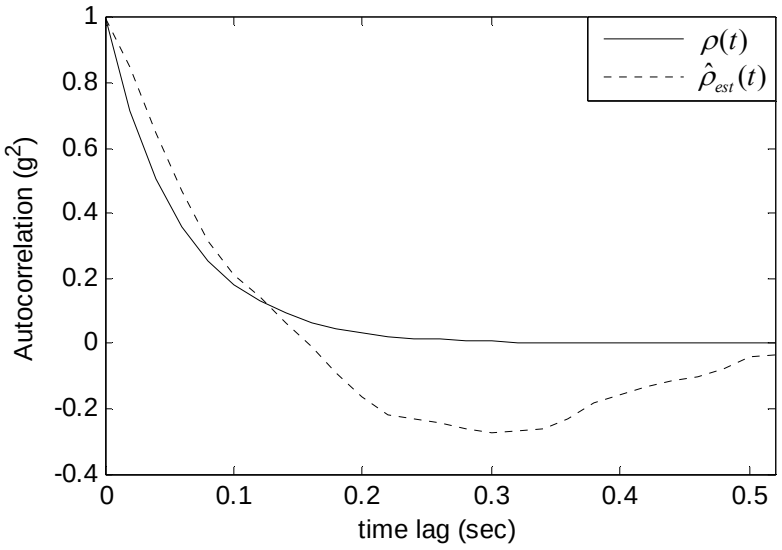

Figure 2.5: Autocorrelation function of $A_s(t)$ for N-S El Centro Earthquake in 1940

Using Equation (2.15) with the estimated parameters $\hat{\sigma}^2$ and $\hat{\kappa}$, the one-sided spectral density of $A_s(t)$ is presented in Figure 2.6. Assuming that most of power is included in the frequency range (0, ν_c') in which the cutoff frequency ν_c' is 250 rad/sec, 10,000 independent ground accelerograms are generated using Equation (2.11) with 5,000 non-overlapping intervals, i.e. $\Delta\nu_k = 0.05$ rad/sec. A sample of stationary ground accelerograms is presented in Figure 2.7.

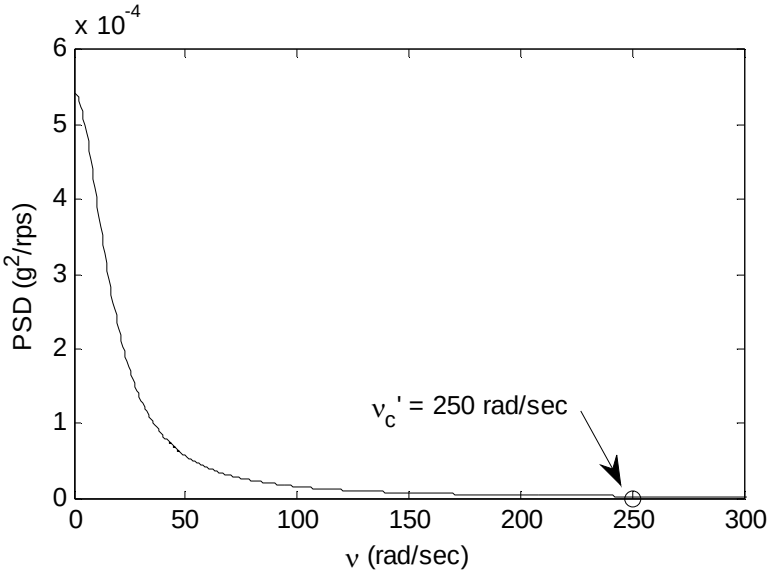

Figure 2.6: One-sided spectral density of $A_s(t)$ for N-S El Centro Earthquake in 1940

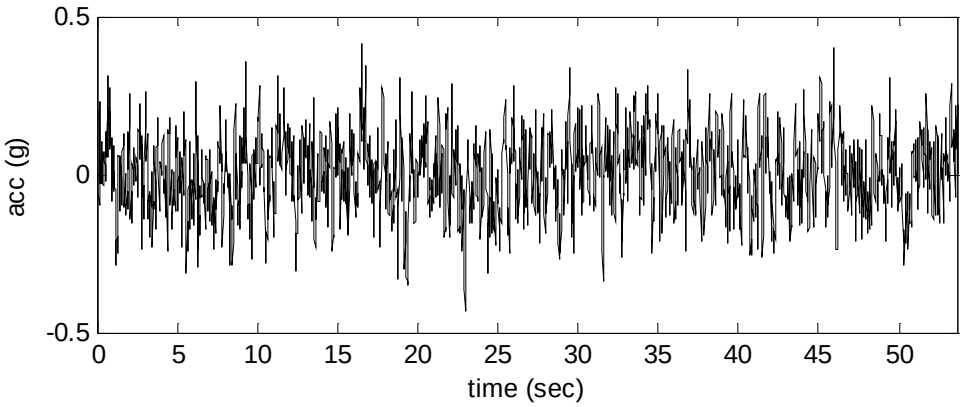

Figure 2.7: A sample of ground motion generated by a stationary Gaussian process

2.2 Estimation of Earthquake Damage for SDOF Systems

A one-story structure can be idealized with a concentrated mass supported by a massless frame providing stiffness to the system and a viscous damper. The idealized system is shown in Figure 2.8 with lumped mass *m*, lateral stiffness *k*, and damping coefficient *c*. For dynamic analysis, such a structural system is called a single-degree-

of-freedom (SDOF) system in which the system has only one DOF–lateral displacement [7].

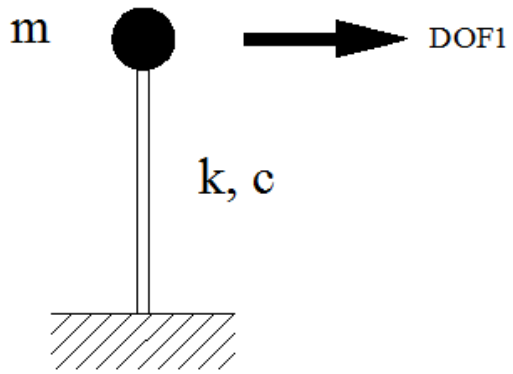

Figure 2.8: Single-degree-of-freedom system

Consider the linear elastic SDOF system (Figure 2.8) with the following properties: the mass m is 0.0283 lb-sec^2/in, the stiffness k is 18.5790 lb/in, and the damping ratio ζ is 0.05. Using this structural model, this section introduces (1) the numerical evaluation of dynamic response of SDOF systems, (2) input-output relation of linear time invariant systems subjected to stationary ground excitation, and (3) failure probability analysis.

2.2.1 Dynamic Responses for Linear Elastic SDOF Systems

The equation of motion for a linear elastic SDOF system subjected to an external force $p(t)$ is

$$m\ddot{x}(t) + c\dot{x}(t) + kx(t) = p(t) \tag{2.18}$$

where m is the mass, k is the stiffness, and c is the damping coefficient. When the SDOF model is subjected to earthquake ground motion, the external force $p(t)$ can be

replaced by the earthquake force which equals to the mass m times the ground acceleration $a(t)$.

$$p(t) = -ma(t) \tag{2.19}$$

Substituting Equation (2.19) in Equation (2.18) and dividing by the mass *m*, the equation of motion can be rewritten as

$$\ddot{x}(t) + 2\zeta\omega\dot{x}(t) + \omega^2 x(t) = -a(t) \tag{2.20}$$

where ζ is the damping ratio, and ω is the natural frequency. The solution to the differential equation (2.20) can be obtained by Newmark's method (see Algorithm 2.2) [7],[14].

The response of the structural model (Figure 2.8) under ground acceleration can be computed by the Newmark's method. As an input to Algorithm 2.2, the natural frequency is computed as $\omega = \sqrt{k/m} =$ 25.6223 rad/sec. Using the 10,000 samples of stationary Gaussian ground acceleration (generated in Section 2.1.4) with a constant time step size $\Delta t = 0.02$ sec, 10,000 samples of displacement response $X(t)$ are obtained. Figure 2.9 shows a sample of $X(t)$.

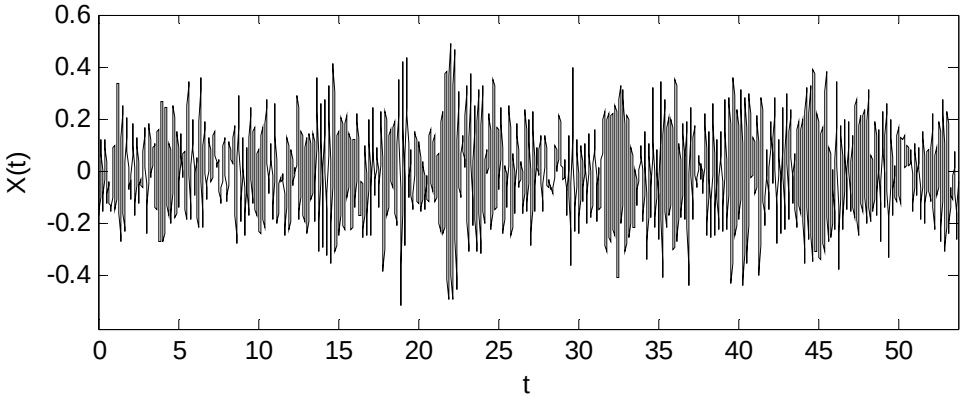

Figure 2.9: A sample of displacement time history response

Algorithm 2.2: Newmark's method: Solution method for linear SDOF systems [7],[14]

Input Parameters: ω, ζ, Δt, and $a(t)$
Output Parameters: $\ddot{x}(t)$, $\dot{x}(t)$, and $x(t)$
($\gamma = 1/2$ and $\beta = 1/6$ for linear acceleration method)

(a) Initial conditions

$x_0 = 0$ and $\dot{x}_0 = 0$

(b) Mass, stiffness, and damping

$m = 1$, $k = \omega^2 m$, and $c = 2\zeta\omega m$

(Note: *m*, *k*, and *c* are not real values of the system.)

(c) External force

$$p(t) = -ma(t)$$

(d) Initial calculations

$$\ddot{x}_0 = \frac{p_0 - c\dot{x}_0 - kx_0}{m}$$

$$\hat{k} = k + \frac{\gamma}{\beta\Delta t}c + \frac{1}{\beta(\Delta t)^2}m$$

$$A = \frac{1}{\beta\Delta t}m + \frac{\gamma}{\beta}c$$

$$B = \frac{1}{2\beta}m + \Delta t\left(\frac{\gamma}{2\beta} - 1\right)c$$

(e) Repeat calculations for each time steps

$$\Delta p_i = p_i - p_{i-1}$$

$$\Delta\hat{p}_i = \Delta p_i + A\dot{x}_{i-1} + B\ddot{x}_{i-1}$$

$$\Delta x_i = \frac{\Delta\hat{p}_i}{\hat{k}}$$

$$\Delta\dot{x}_i = \frac{\gamma}{\beta\Delta t}\Delta x_i - \frac{\gamma}{\beta}\dot{x}_i + \Delta t\left(1 - \frac{\gamma}{2\beta}\right)\ddot{x}_i$$

$$\Delta\ddot{x}_i = \frac{1}{\beta(\Delta t)^2}\Delta x_i - \frac{1}{\beta\Delta t}\dot{x}_i - \frac{1}{2\beta}\ddot{x}_i$$

$x_i = x_{i-1} + \Delta x_i$, $\dot{x}_i = \dot{x}_{i-1} + \Delta\dot{x}_i$, and $\ddot{x}_i = \ddot{x}_{i-1} + \Delta\ddot{x}_i$

2.2.2 Statistical Analysis of Response of SDOF systems

An important property of a linear system is that if the input excitation is a stationary process then the output response is also a stationary process. Hence, the expected value and covariance function of the output response are independent of time. In a particular case, the input process has zero-mean then so does the output [10],[13].

Because the structural model (Figure 2.8) is assumed to be linear elastic and the input ground excitation is a zero-mean stationary Gaussian process, the displacement response $X(t)$ is also a stationary Gaussian process with zero-mean and a time independent covariance function.

(a) Mean of displacement response

Using the 10,000 samples of $X(t)$ obtained in Section 2.2.1, the mean of $X(t)$ is estimated as

$$E[X(t)] \approx \frac{1}{10,000} \sum_{r=1}^{10,000} X_r(t) \tag{2.21}$$

where $X_r(t)$ are the samples of displacement response. As shown in Figure 2.10 in which maximum and minimum values on the y-axis are set to the average of the peak values of $X_r(t)$, ± 0.5524 inches, the estimated mean of $X(t)$ is approximately zero at any time.

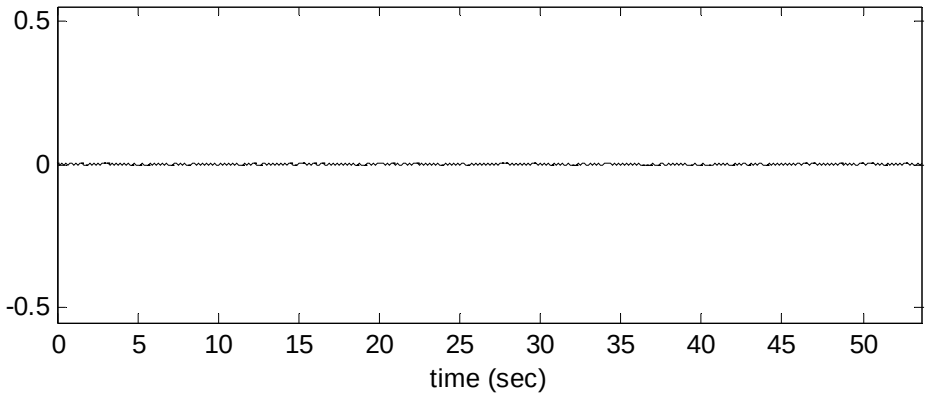

Figure 2.10: Mean of $X(t)$ of the SDOF model

(b) Covariance of displacement response

Covariance function $c_{XX}(t,\tau)$ of $X(t)$ is

$$c_{XX}(t,\tau) = E[(X(t+\tau) - \mu_{X(t+\tau)})(X(t) - \mu_{X(t)})] \tag{2.22}$$

where $\mu_{X(t)}$ is the expected value of $X(t)$, and τ is the time lag. When $X(t)$ is given at discrete values of time t_i, $X(t_i)$, the covariance can be represented in a matrix form, called a covariance matrix, Σ.

$$\Sigma = \begin{bmatrix} \mathrm{var}(X(t_1)) & \mathrm{cov}(X(t_1), X(t_2)) & \cdots & \mathrm{cov}(X(t_1), X(t_n)) \\ \mathrm{cov}(X(t_2), X(t_1)) & \mathrm{var}(X(t_2)) & \cdots & \mathrm{cov}(X(t_2), X(t_n)) \\ \vdots & \vdots & \ddots & \vdots \\ \mathrm{cov}(X(t_n), X(t_1)) & \mathrm{cov}(X(t_n), X(t_2)) & \cdots & \mathrm{var}(X(t_n)) \end{bmatrix} \tag{2.23}$$

where $X(t_1), X(t_2), ..., X(t_n)$ are column vectors of random variables corresponding to time t_i [33]. The covariance matrix is symmetric, and the diagonal elements are the variances which equal to $c_{XX}(t,0)$.

The scaled covariance function or coefficient of correlation is

$$\xi_{XX}(t,\tau) = \frac{c_{XX}(t,\tau)}{\sigma_{X(t+\tau)}\sigma_{X(t)}} \tag{2.24}$$

where $\sigma_{X(t)}$ is the standard deviation of $X(t)$.

The covariance and coefficient of correlation measure the dependency between two random variables. The covariance is zero for two independent random variables; otherwise, the covariance has non-zero value which changes according to the measure of the dependency of random variables. In addition, the scaled covariance has the limits of [-1, 1], and zero implies that two random variables are uncorrelated [3],[33]. Under the assumption of a stationary process, the covariance function of the displacement samples only depends on time lag τ but is independent of time *t*. Figure 2.11 shows the scaled covariance function estimated from the 10,000 samples of $X(t)$. As shown in the figure, the covariance function has a maximum value equal to one at $\tau = 0$ and decreases as time lag increases.

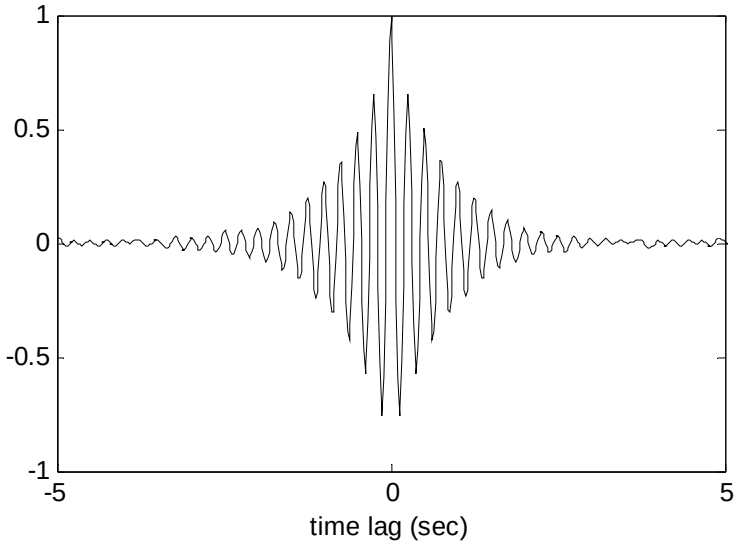

Figure 2.11: Scaled covariance function of $X(t)$ of the SDOF model

2.2.3 Failure Rate of SDOF Systems

Failure of a structure implies that a structure dose not performed as what it is designed. There are several factors related to the failure such as temperature, pressure, and

fatigue. The failure can occur when the response $Y(t)$ of a structure first reaches a certain critical value y_{cr}, when a fraction of time in which $Y(t) \geq y_{cr}$ exceeds a predetermined fraction limit, or when an accumulation of small amount of damage reaches a certain fixed total damage [10].

The failure in this chapter only refers that lateral displacement of a structure exceeds a critical threshold. Then failure rate can be estimated by counting the number of times that peak value of each displacement sample $\max_t |X_r(t)|$ equals or exceeds a critical displacement x_{cr} and then dividing by the total number of samples, n_s

$$P_F \approx \frac{1}{n_s} \sum_{r=1}^{n_s} 1\left(\max_t |X_r(t)| \geq x_{cr} \right) \tag{2.25}$$

Using the 10,000 samples of $X(t)$, the failure rate P_F of the structural model is estimated using Equation (2.25) with an approximate accuracy of 0.001. As a rule of thumb, a minimum number of samples n_s should be equal to or greater than $10/P_F$ in order to estimate the failure probability P_F accurately [16].

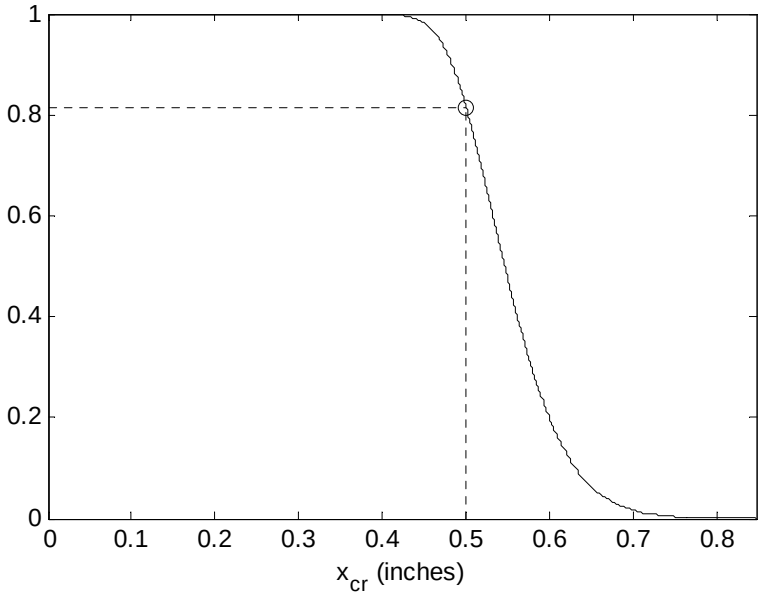

Figure 2.12: Failure rate curve for the SDOF model

The resulting failure rate curve in Figure 2.12 shows the probability that the lateral displacement caused by an earthquake equals or exceeds a critical displacement. For example, the probability of earthquake-induced lateral displacement equal to or greater than 0.50 inches is estimated as 0.8155 (Refer to the dotted line in Figure 2.12). In other words, if the system is endurable against the maximum lateral displacement of 0.50 inches, the probability of failure is estimated to be 0.8155.

2.3 Earthquake Damage Estimation for MDOF Systems

The approach to failure probability analysis of SDOF systems developed in Section 2.2 can be extended to multi-degree-of-freedom (MDOF) systems. The equations of motion are developed first for a MDOF system subjected to earthquake-induced ground motion. Subsequently, the modal analysis procedure is introduced to determine the response of MDOF systems.

As an illustrative example, a three-story structural model is selected. Based on the response of the structural model under the ground motion generated in Section 2.1.4, the failure probability and the exceedance probability of repair cost are estimated.

2.3.1 Structural Model for Linear Elastic MDOF Systems

The three-story structural model in Figure 2.13(a) consists of steel columns which support aluminum floor slabs. Each aluminum floor slab is 12 inches in length, 18 inches in width, and 0.53 inches in thickness and has a density of 165 pcf. The steel columns with the cross-sectional area of 0.25" × 0.125" and 14.5 inches in height are oriented with their weak axis in the direction of the ground motion. The material properties of the steel columns are listed as follows: the density is 490 pcf, the modulus of elasticity E is 29,000 ksi, and the moment of inertia I is 4.0690×10^{-5} in^4.

Assumptions

In order to simplify the dynamic analysis, the three-story structural model is idealized as a lumped mass model with three degrees of freedom (see Figure 2.13(b)). Then the following assumptions are made in the dynamic analysis: (1) the floors are infinitely stiff, (2) all connections are rigid, (3) the mass of the columns is negligible because it is less than 5% of the floor mass, (4) the structural response is linear elastic, and (5) Rayleigh damping is used with a damping ratio of 0.05 for the first two modes.

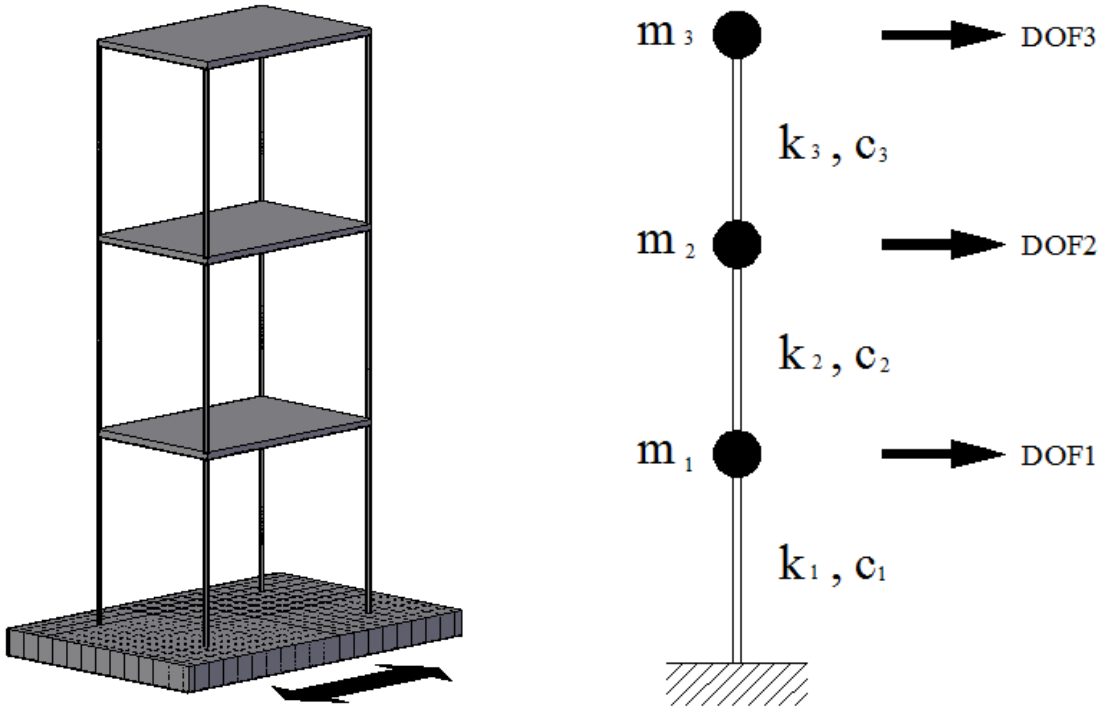

(a) Isometric view (b) Simplified model

Figure 2.13: Three-story structural model

2.3.2 Equations of Motion for Linear Elastic MDOF Systems

The equations of motion for linear elastic MDOF systems subjected to external forces $\underline{p}(t)$ are

$$\underline{m}\ddot{\underline{x}}(t) + \underline{c}\dot{\underline{x}}(t) + \underline{k}\underline{x}(t) = \underline{p}(t) \tag{2.26}$$

where $\underline{m}$ is the mass matrix, $\underline{c}$ is the damping matrix, $\underline{k}$ is the stiffness matrix, and $\underline{p}(t)$ is the vector of external forces. When MDOF systems are subjected to ground motion, the external forces $\underline{p}(t)$ in Equation (2.26) can be replaced by

$$\underline{p}(t) = -\underline{m}\ \underline{1}\ a(t) \tag{2.27}$$

where $\underline{1}$ is the vector of ones, and $a(t)$ is the ground acceleration. Substituting Equation (2.27) in Equation (2.26), the equations of motion can be rewritten as

$$\underline{m}\ddot{\underline{x}}(t) + \underline{c}\dot{\underline{x}}(t) + \underline{k}\underline{x}(t) = -\underline{m}\ \underline{1}\ a(t) \tag{2.28}$$

For the three-story structural model in Figure 2.13, Equation (2.28) contains three coupled equations. Thus, the system properties $\underline{m}$, $\underline{c}$, $\underline{k}$ can be expressed by 3×3 matrices.

Mass Matrix for the Structural Model

The mass of each floor is

$$m_i = 0.0283 \text{ lb-sec}^2/\text{in}, \quad i = 1, 2, 3 \tag{2.29}$$

Then the mass matrix for the three-story structural model is

$$\underline{m} = \begin{bmatrix} m_1 & 0 & 0 \\ 0 & m_2 & 0 \\ 0 & 0 & m_3 \end{bmatrix} \tag{2.30}$$

Stiffness Matrix for the Structural Model

The story stiffness k_i is the sum of the lateral stiffness of all columns in the story. Assuming linear elastic behavior and infinitely stiff floors, the story stiffness of the three-story structural model is computed as [7]

$$k_i = 4k_{col} = 4\frac{12EI_c}{h^3} = 18.5790 \text{ lb/in}, \quad i = 1,2,3 \tag{2.31}$$

With the story stiffness determined, the stiffness matrix is constructed as

$$\underline{k} = \begin{bmatrix} k_1 + k_2 & -k_2 & 0 \\ -k_2 & k_2 + k_3 & -k_3 \\ 0 & -k_3 & k_3 \end{bmatrix} \tag{2.32}$$

Natural Frequencies and Mode Shapes for the Structural Model

The natural frequencies and mode shapes are obtained by solving the matrix eigenvalue problem below [7]

$$\left[\underline{k} - \omega_n^{\,2}\underline{m}\right]\underline{\phi}_n = 0, \quad n = 1,2,\ldots,N_m \tag{2.33}$$

where ω_n is the natural frequency, $\underline{\phi}_n$ is the mode shape vector of the *n*-th mode, and N_m is the total number of modes. The natural frequencies and corresponding mode shapes for the three-story structural model are shown in Figure 2.14.

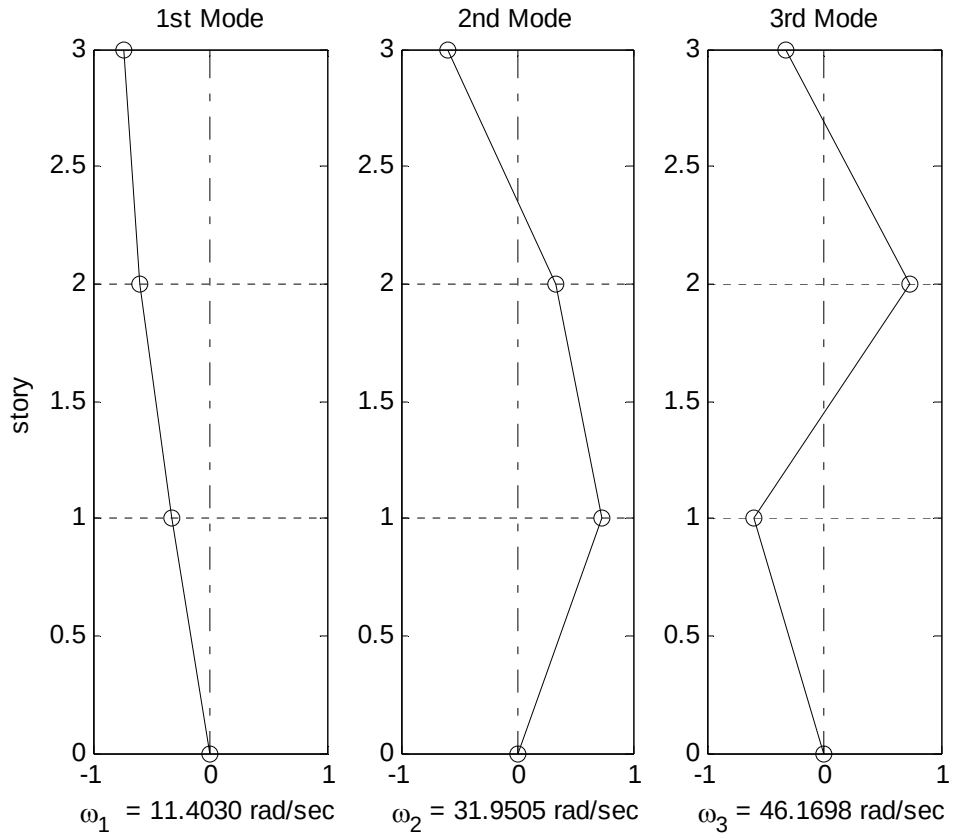

Figure 2.14: Natural frequencies and mode shapes for the structural model

Damping Matrix for the Structural Model

Damping is the mechanism of energy dissipation which is necessary to address the decaying motion of a structure during free vibration [7]. If a structure has a similar damping mechanism throughout the structure, damping can be idealized as classical damping. A common type of classical damping used in most practical analyses of structures is Rayleigh damping [7]:

$$\underline{c} = \alpha_0 \underline{m} + \alpha_1 \underline{k} \tag{2.34}$$

where α_0 and α_1 are the coefficients. The damping ratio for the *n*-th mode is

$$\zeta_n = \frac{\alpha_0}{2}\frac{1}{\omega_n} + \frac{\alpha_1}{2}\omega_n \tag{2.35}$$

The coefficients α_0 and α_1 can be determined from prescribed damping ratios ζ_j and ζ_k for the *j*-th and *k*-th modes. The damping ratios for these two modes are expressed in a matrix form,

$$\frac{1}{2}\begin{bmatrix} 1/\omega_j & \omega_j \\ 1/\omega_k & \omega_k \end{bmatrix}\begin{Bmatrix} \alpha_0 \\ \alpha_1 \end{Bmatrix} = \begin{Bmatrix} \zeta_j \\ \zeta_k \end{Bmatrix} \tag{2.36}$$

This system of equations can be solved to determine α_0 and α_1. With structural properties $\underline{m}$ and $\underline{k}$ and coefficients α_0 and α_1, the damping matrix of system can be computed using Equation (2.34) [7].

For the three-story structural model, the damping ratios of the first and second modes are assumed as 0.05 (5%). Based on the assumption of Rayleigh damping, the damping matrix can be constructed using Equation (2.34). Substituting the natural frequencies ω_1 and ω_2 and the specified ζ_1 and ζ_2, Equation (2.36) has the following solution: $\alpha_0 = 0.8404$ and $\alpha_1 = 0.0023$. The damping matrix of the three-story structural model is evaluated as

$$\underline{c} = \begin{bmatrix} 0.0547 & -0.0214 & 0 \\ -0.0214 & 0.0547 & -0.0214 \\ 0 & -0.0214 & 0.0333 \end{bmatrix} \text{ lb-sec/in} \tag{2.37}$$

2.3.3 Modal Analysis

If structure is a linear system with classical damping such as Rayleigh damping, the total response of an MDOF system is a linear combination of the modal responses. Thus, the dynamic response of linear MDOF systems can be expressed as [7]

$$\underline{x}(t) = \sum_{n=1}^{N_m} \underline{\phi}_n q_n(t) \tag{2.38}$$

where N_m is the total number of modes, $\underline{\phi}_n$ is the mode shape vectors, and $q_n(t)$ is the modal coordinate of the *n*-th mode at time *t*.

Using the transformation of Equation (2.38), the governing equations (2.28) can be written in terms of the modal coordinates *q*, and then premultiplying by $\underline{\Phi}^T$ gives

$$\underline{M}\,\underline{\ddot{q}}(t) + \underline{C}\,\underline{\dot{q}}(t) + \underline{K}\,\underline{q}(t) = -\underline{\Phi}^T\,\underline{m}\,\underline{1}\,a(t) \tag{2.39}$$

where $\underline{M}(=\underline{\Phi}^T\,\underline{m}\,\underline{\Phi})$ is the modal mass matrix, $\underline{C}(=\underline{\Phi}^T\,\underline{c}\,\underline{\Phi})$ is the modal damping matrix, $\underline{K}(=\underline{\Phi}^T\,\underline{k}\,\underline{\Phi})$ is the modal stiffness matrix, and $\underline{\Phi}$ is the mode shape matrix [7]. The modal mass and stiffness matrices are diagonal matrices because of the orthogonality property of the mode shapes. The modal damping matrix is also a diagonal matrix based on the assumption of Rayleigh damping.

Dividing each uncoupled equation in Equation (2.39) by corresponding modal mass M_n gives

$$q_n(t) + 2\zeta_n\omega_n\dot{q}_n(t) + \omega_n{}^2\ddot{q}_n(t) = -\Gamma_n a(t) \tag{2.40}$$

where ζ_n is the damping ratio, ω_n is the natural frequency, and Γ_n is the modal participation factor for the *n*-th mode. The modal participation factor, indicating the contribution of the *n*-th mode to the total response, is given by

$$\Gamma_n = \frac{\underline{\phi}_n{}^T\,\underline{m}\underline{1}}{M_n} \tag{2.41}$$

where $\underline{\phi}_n{}^T$ is the transpose of the mode shape vector, and M_n is the modal mass for the *n*-th mode [7].

Solution Method of Linear Elastic MDOF Systems

Algorithm 2.3 summarizes the procedure to compute the response of MDOF systems using the modal analysis method [7],[14]. With the input parameters, $\underline{m}$, $\underline{k}$, and $\underline{c}$, the modal parameters are computed in step (a). Then uncoupled modal equations can be obtained from the modal parameters ω_n, ζ_n, and Γ_n and the input ground acceleration $a(t)$. Each modal equation can be solved by the Newmak's method (Algorithm 2.2 in Section 2.2.1). The total response is obtained as the sum of the modal contributions as expressed by Equation (2.38).

Algorithm 2.3: Newmark's method: Solution method for linear MDOF systems [7],[14]

Input Parameters: $\underline{m}$, $\underline{k}$, $\underline{c}$, Δt, and $a(t)$
Output Parameters: $\ddot{\underline{x}}(t)$, $\dot{\underline{x}}(t)$, and $\underline{x}(t)$

(a) Calculation for modal parameters
Find ω_n and $\underline{\phi}_n$ from $\underline{m}$ and $\underline{k}$

$$M_n = \underline{\phi}_n^T \underline{m}\ \underline{\phi}_n,\ K_n = \underline{\phi}_n^T \underline{k}\ \underline{\phi}_n,\ \text{and}\ C_n = \underline{\phi}_n^T \underline{c}\ \underline{\phi}_n$$

$$\zeta_n = \frac{C_n}{2\omega_n M_n}\ \text{and}\ \Gamma_n = \frac{\underline{\phi}_n^T \underline{m}\underline{1}}{M_n}$$

(b) Calculation of modal responses using Algorithm 2.2
Input Parameters: ω_n, ζ_n, Δt, and $a(t)$
Output Parameters: $\ddot{q}(t)$, $\dot{q}(t)$, and $q(t)$
(Note: $x(t)$ in Algorithm 2.2 is now $q(t)$)

$$\ddot{q}_n(t) = \Gamma_n \ddot{q}(t),\ \dot{q}_n(t) = \Gamma_n \dot{q}(t),\ \text{and}\ q_n(t) = \Gamma_n q(t)$$

(c) Repeat calculations in step (b) for each mode

(d) Calculation for displacement, velocity, and acceleration

$$\underline{x}(t) = \sum_{n=1}^{N_m} \underline{\phi}_n q_n(t),\ \dot{\underline{x}}(t) = \sum_{n=1}^{N_m} \underline{\phi}_n \dot{q}_n(t),\ \text{and}\ \ddot{\underline{x}}(t) = \sum_{n=1}^{N_m} \underline{\phi}_n \ddot{q}_n(t)$$

2.3.4 Displacement Response of the Structural Model

Using the modal analysis method (Algorithm 2.3), samples of displacement response of each story are calculated under the input ground accelerations produced by a stationary Gaussian process (Section 2.1.4). With the system properties, $\underline{m}$, $\underline{k}$, $\underline{c}$, obtained in Section 2.3.2, the modal parameters of the three-story structure are computed (see Table 2.1). Since the first mode has a considerably large Γ and low K compared to the other modes, it is predictable that the structural response is dominated by the first mode. The contribution of the first mode to the total response is presented in Figure 2.15 which shows the two responses almost coincide with respect to time. Hence, for the three-story structural model, the exact response of the system can be approximated by the first mode.

$$\underline{x}(t) = \sum_{i=1}^{3} \underline{\phi}_i \underline{q}_i(t) \approx \underline{\phi}_1 \underline{q}_1(t) \tag{2.42}$$

Table 2.1: Modal parameters of the three-story structure for n-th mode

Mode	Mode 1	Mode 2	Mode 3
Natural Frequency (rad/sec), ω_n	11.4030	31.9505	46.1698
Mode Shape Vector, $\underline{\phi}_n$	$\begin{Bmatrix} -0.3280 \\ -0.5910 \\ -0.7370 \end{Bmatrix}$	$\begin{Bmatrix} 0.9390 \\ 0.3280 \\ -0.5910 \end{Bmatrix}$	$\begin{Bmatrix} -0.5910 \\ 0.7370 \\ -0.3280 \end{Bmatrix}$
Modal Mass (lb-sec^2/in), M_n	0.0283	0.0283	0.0283
Modal Damping (lb-sec/in), C_n	0.0323	0.0904	0.1629
Modal Stiffness (lb/in), K_n	3.6798	28.8896	60.3256
Modal Participation Factor, Γ_n	-1.6560	0.4740	-0.1820

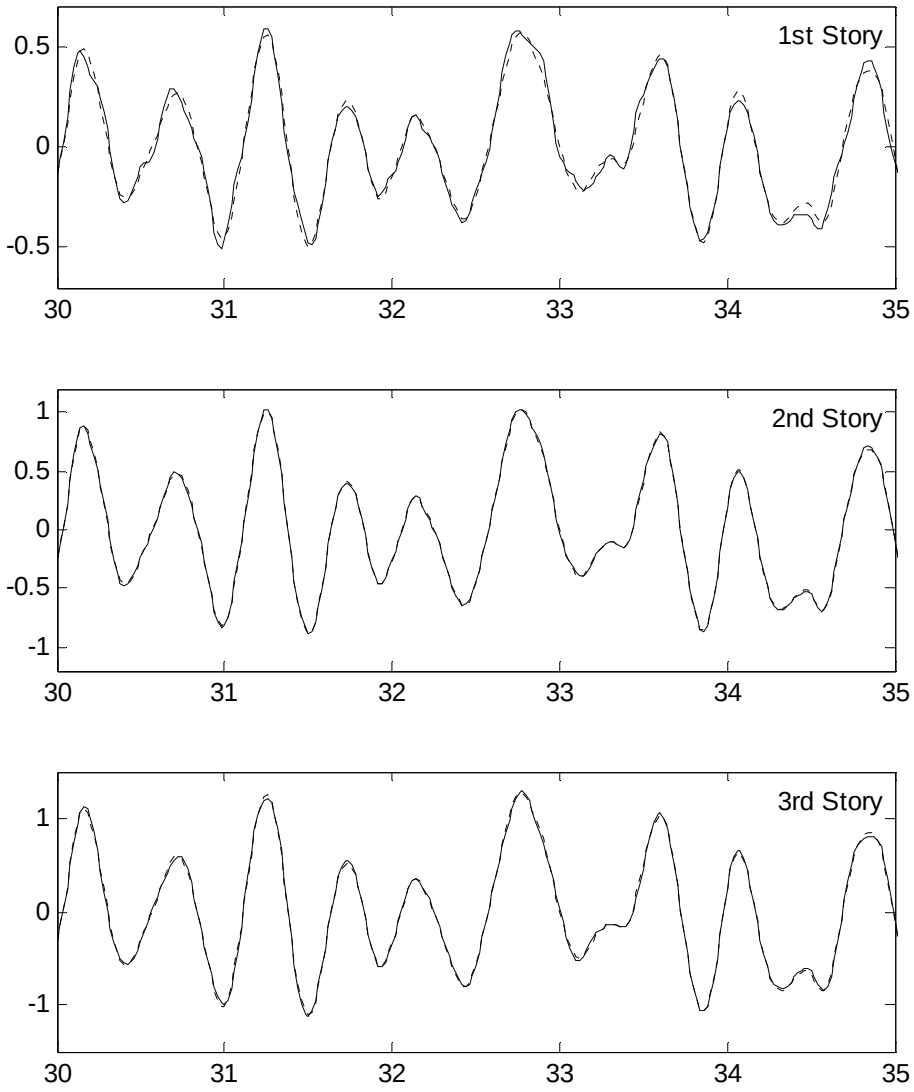

Figure 2.15: Comparison of the total displacement response and displacement response due to the first mode of the three-story structure (solid line: total response; dotted line: response due to the first mode)

2.3.5 Statistical Analysis of Response of MDOF Systems

The SDOF system in Section 2.2.2 shows the simplest type of input-output relations of linear time-invariant system which has single-input and single-output. The basic idea of the input-output relations can be extended to MDOF systems having single-input (ground excitation) and multi-outputs (story displacement responses). If the input

excitation is assumed to be zero-mean stationary Gaussian, the output responses of the linear elastic MDOF systems are also stationary Gaussian processes with zero-mean [10].

(a) Mean of displacement response of the Structural Model

Using the 10,000 samples of displacement response of each *i*-th story, $X_r^{(i)}(t)$ where $r = 1, 2, ..., 10,000$, the mean of $X^{(i)}(t)$ is estimated as

$$E[X^{(i)}(t)] \approx \frac{1}{10,000} \sum_{r=1}^{10,000} X_r^{(i)}(t), \quad i = 1, 2, 3 \tag{2.43}$$

Similar to the result of the SDOF system, the estimated mean of $X^{(i)}(t)$ for each story is approximately zero at any time *t* as shown in Figure 2.16.

(b) Covariance of displacement response of the structural model

The covariance function of displacement responses $X^{(j)}(t)$ and $X^{(k)}(t)$ (where the story numbers $j, k = 1, 2, 3$) is

$$c_{X^{(j)}X^{(k)}}(t, \tau) = E[(X^{(j)}(t-\tau) - \mu_{X^{(j)}(t-\tau)})(X^{(k)}(t) - \mu_{X^{(k)}(t)})] \tag{2.44}$$

where $\mu_{X^{(j)}(t)} = E[X^{(j)}(t)]$ and τ is the lag time. Then scaled covariance function is

$$\xi_{X^{(j)}X^{(k)}}(t, \tau) = \frac{c_{X^{(j)}X^{(k)}}(t, \tau)}{\sigma_{X^{(j)}(t+\tau)} \sigma_{X^{(k)}(t)}} \tag{2.45}$$

Figure 2.17 shows the estimated scaled covariance functions with the corresponding maximum values. Because the displacement responses are stationary, the covariance function only depends on the time lag τ. The scaled covariance functions for all cases have their maximum values at $\tau = 0$, and the amplitudes of the covariance functions decrease as τ increases. It is notable that the maximum values of

the covariance functions between two different story displacements, $X^{(j)}(t)$ and $X^{(k)}(t)$ where $j \neq k$, are also close to one at $\tau = 0$. This shows that there is a strong correlation between two different story displacements [3]. To illustrate the correlation, the story displacements $X^{(j)}(t)$ versus $X^{(k)}(t)$ where $j \neq k$ are presented in Figure 2.18 in which linear relationships are observed.

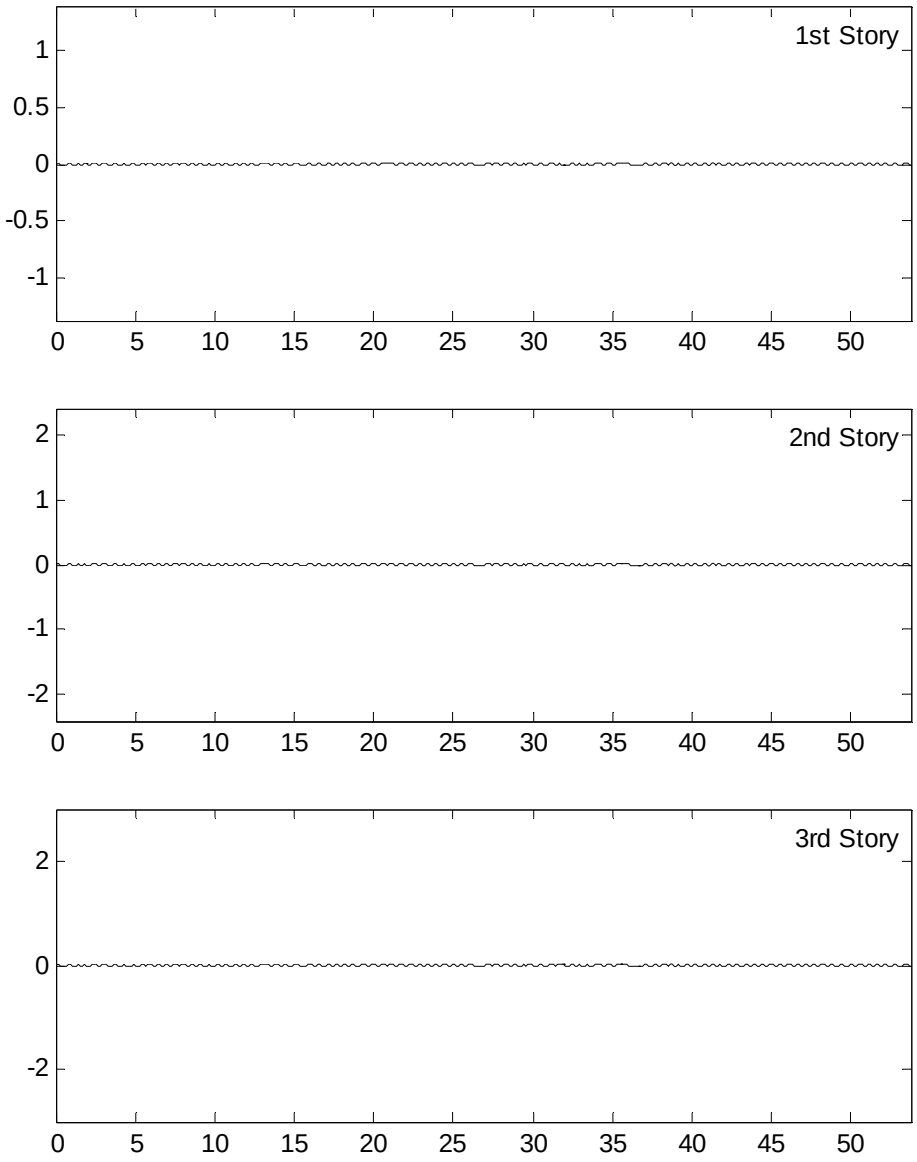

Figure 2.16: Mean of $X^{(i)}(t)$ of the three-story model (maximum and minimum values on the y-axis are set to the average of the peak values of $X_r^{(i)}(t)$)

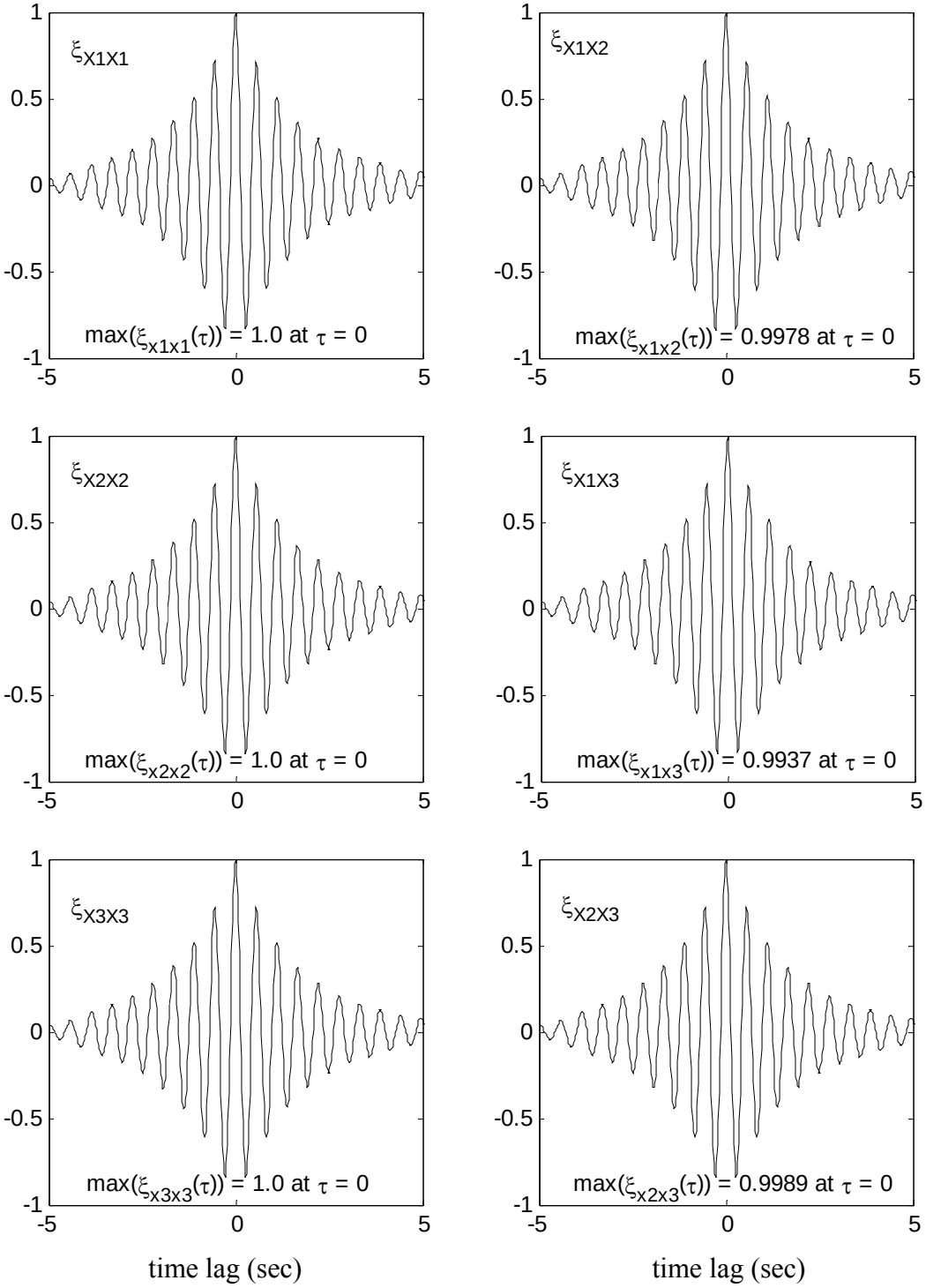

Figure 2.17: Scaled covariance functions of story displacement of the three-story model

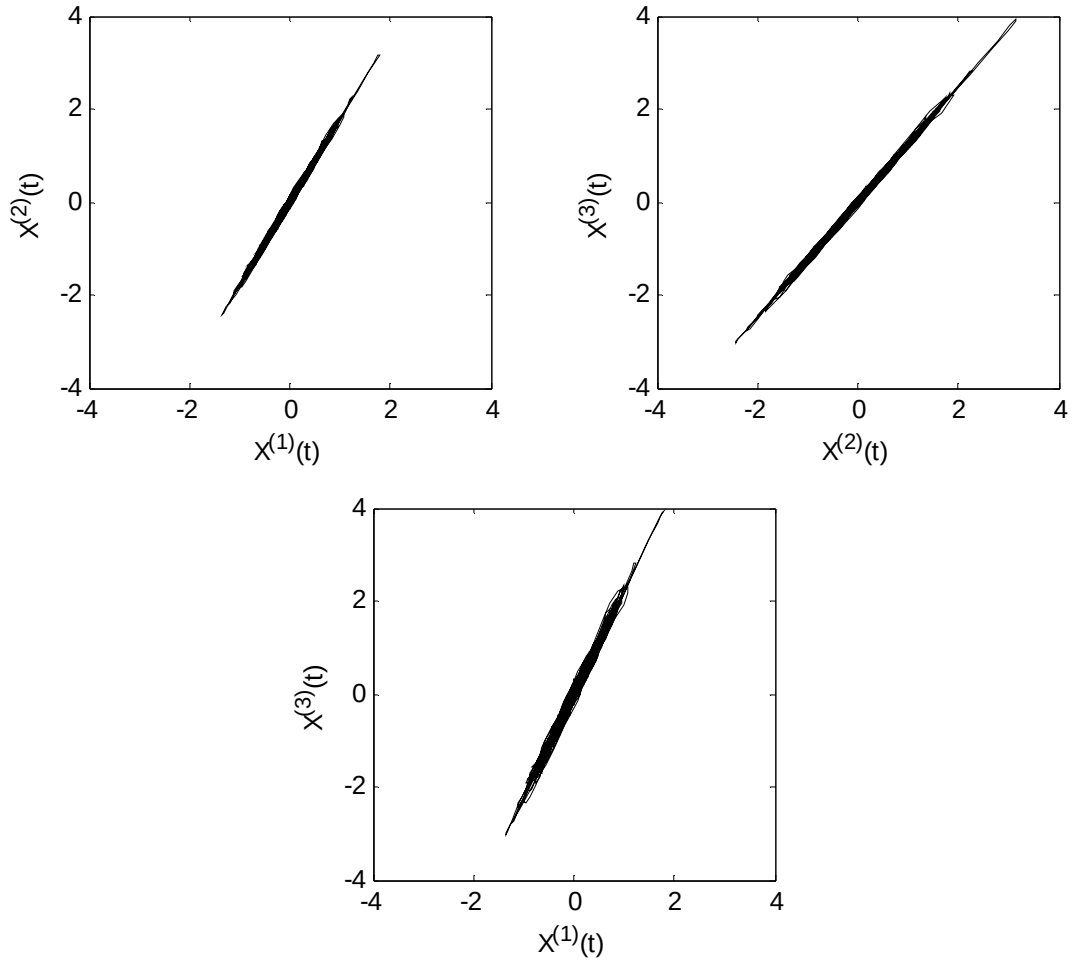

Figure 2.18: Linear relationship between two different story displacements

2.3.6 Failure Rate of MDOF Systems

Failure Rate due to an Earthquake

For MDOF systems, the failure rate can be developed for each story based on interstory displacement $\Delta^{(i)}(t)$ defined by

$$\Delta^{(i)}(t) = \begin{cases} X^{(i)}(t) - X^{(i-1)}(t) & i \geq 2 \\ X^{(i)}(t) & i = 1 \end{cases} \tag{2.46}$$

where $X^{(i)}(t)$ is the displacement response of the *i*-th story. In a similar manner as that developed for SDOF systems in Section 2.2.3, failure rate of each story can be estimated as

$$P_F{}^{(i)} \approx \frac{1}{n_s}\sum_{r=1}^{n_s} 1\left(\max_t |\Delta_r{}^{(i)}(t)| \geq \delta_{cr}\right) \tag{2.47}$$

where $\Delta_r{}^{(i)}(t)$ is the samples of the interstory displacement of the *i*-th story, δ_{cr} is the critical interstory displacement, and n_s is the total number of samples,. Using the 10,000 samples of $\Delta^{(i)}(t)$ of each *i*-th story ($i = 1, 2, 3$), the failure probabilities of the structural model are estimated, and the resulting curves are presented in Figure 2.19 (solid lines).

Lifetime Failure Rate

As introduced in Section 2.1.1, earthquake occurrences can be modeled by a Poisson process. Let n^* be the number of particular earthquakes which cause $\max_t |\Delta(t)| \geq \delta_{cr}$. Then the probability that n^* earthquakes will occur during the lifetime of structure t_s can be expressed as

$$P(N(t_s) = n^*) = \frac{(\lambda_F^*(\delta_{cr})t_s)^{n^*}}{n^*!} e^{-\lambda_F^*(\delta_{cr})t_s} \tag{2.48}$$

where $\lambda_F^*(\delta_{cr})$ is the mean occurrence rate of the particular earthquakes which can be obtained by

$$\begin{aligned} \lambda_F^*(\delta_{cr}) &= \lambda\left(1 - F(\delta_{cr})\right) \\ &= \lambda P_F(\delta_{cr}) \end{aligned} \tag{2.49}$$

where $F(\delta_{cr})$ is the cumulative distribution function (CDF) of the peak interstory displacement and its complement is the failure rate function $P_F(\delta_{cr})$.

Using Equation (2.48), the probability of no occurrence of such earthquakes during the lifetime t_s is

$$P\left(N(t_s)=0\right)=e^{-t_s\lambda_F^*(\delta_{cr})} \tag{2.50}$$

Then lifetime failure probability P_{LF} of a structure can be obtained by

$$P_{LF}=1-P\left(N(t_s)=0\right) \tag{2.51}$$

The lifetime failure probability curves for the structural model are presented in Figure 2.19 (dotted lines) assuming $\lambda=0.6$ quakes/year and $t_s=50$ years.

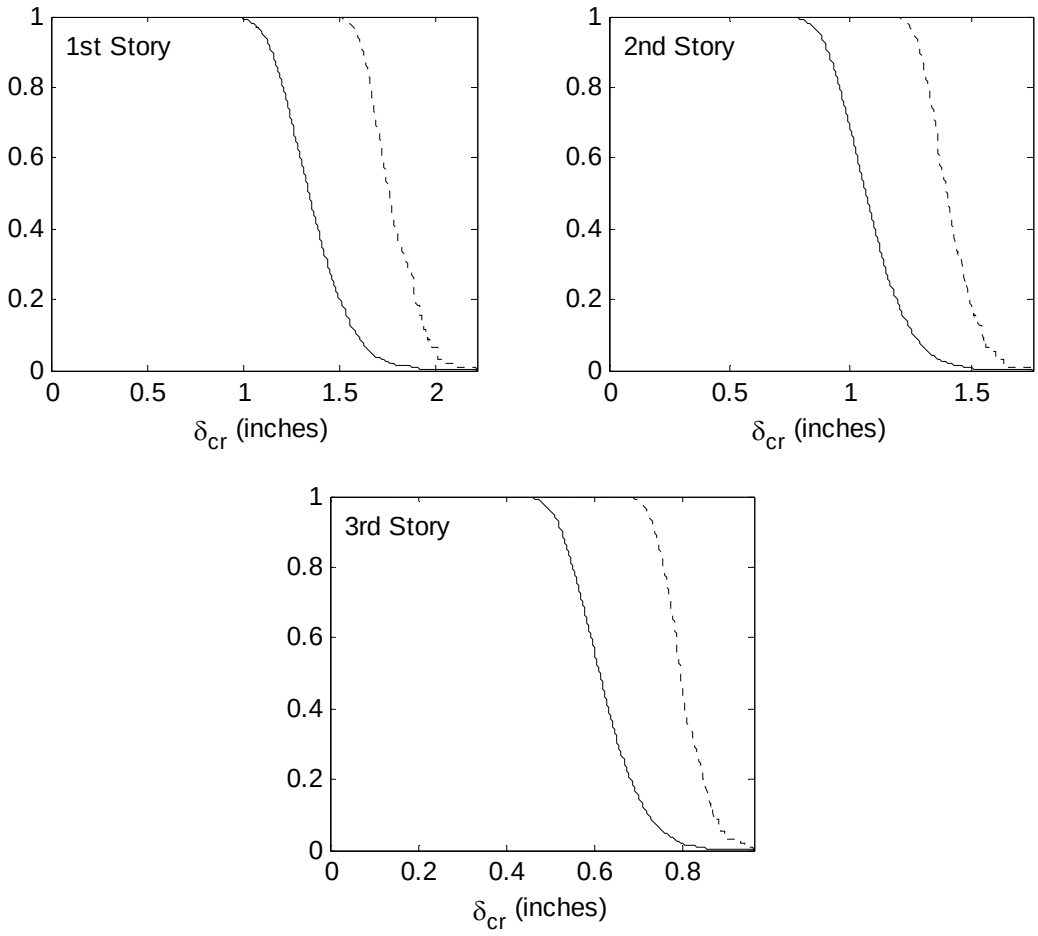

Figure 2.19: Failure rate curves of the three-story structural model (solid lines: failure rate due to an earthquake, dotted lines: lifetime failure rate)

2.3.7 Repair Cost Probability of the Three-Story Model

The repair cost probability, as considered in this section, represents the probability that seismic repair cost equals or exceeds a certain critical repair cost (i.e. an upper bound of the repair cost). The failure rate curve discussed in the previous section can be used to assess the probability of damage level of a structure due to future earthquakes, whereas repair cost probability curve is appropriate for estimating monetary loss because it directly presents the likelihood of future damage costs.

Repair Cost Functions

Based on the assumption that the lateral displacement is a primary basis of measuring seismic damage of a structure [18], repair cost functions can be expressed in terms of interstory displacement. Assuming a repair cost is incurred when the interstory displacement δ is equal to or greater than 0.7 inches, the following two arbitrary functions, $C_1(\delta)$ and $C_2(\delta)$, are used as repair cost functions for the structural model.

$$C_1(\delta) = \begin{cases} 50(\delta - 0.7) & \delta \geq 0.7 \\ 0 & \delta < 0.7 \end{cases} \tag{2.52}$$

$$C_2(\delta) = \begin{cases} 3(e^{2(\delta-0.7)} - 1) & \delta \geq 0.7 \\ 0 & \delta < 0.7 \end{cases} \tag{2.53}$$

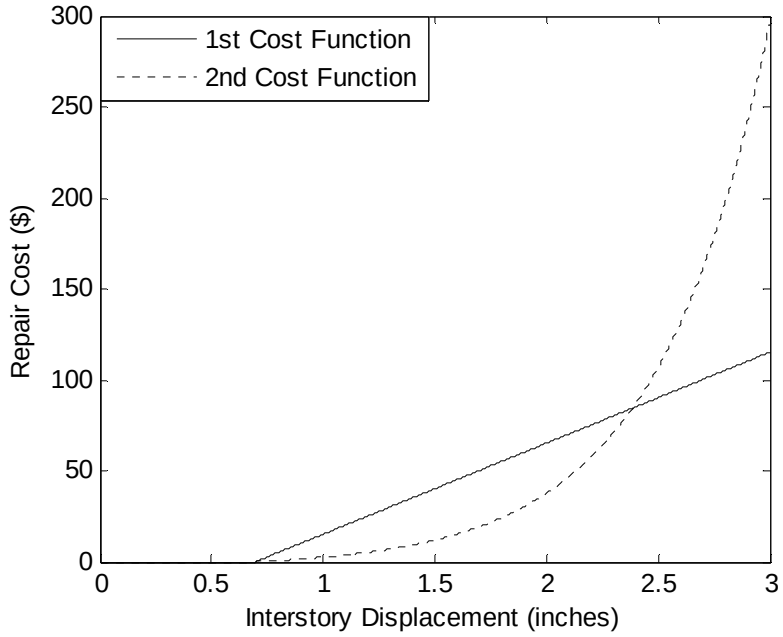

Figure 2.20: Repair cost functions C_1 and C_2 in terms of interstory displacement

Exceedance Probability of Repair Cost

Let C be a random variable denoting repair cost of a structure. Then the exceedance probability of repair costs due to an earthquake is given by

$$\begin{aligned} P_{RC}(C \geq c_{cr}) &= P\left(\max_t |\Delta(t)| \geq C_n^{-1}(c_{cr})\right) \\ &\approx \frac{1}{n_s}\sum_{r=1}^{n_s} 1\left(\max_t |\Delta_r(t)| \geq C_n^{-1}(c_{cr})\right) \end{aligned} \tag{2.54}$$

where c_{cr} is the critical cost, $\max_t |\Delta(t)|$ is the maximum interstory displacement, n_s is the total number of samples, and C_n is the repair cost function, C_1 or C_2. The inverse of repair cost function, $C_n^{-1}(c_{cr})$, yields a interstory displacement inducing the critical repair cost c_{cr}.

Using the 10,000 samples of $\max_t |\Delta^{(i)}(t)|$ of the structural model (where the story number $i = 1, 2, 3$), the exceedance probabilities of the repair costs $P_{RC}{}^{(i)}(C > c_{cr})$

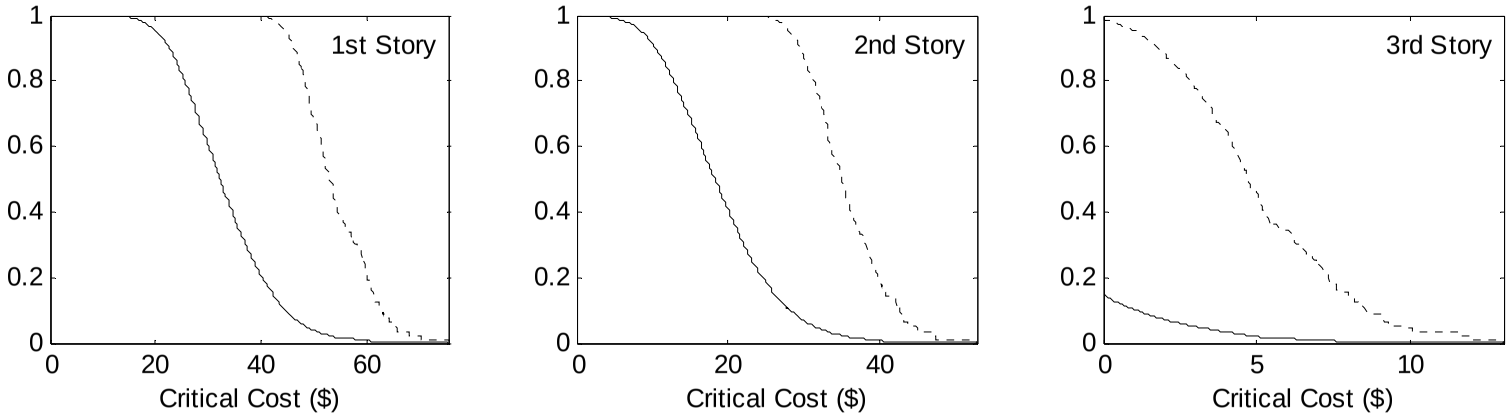

Figure 2.21: Repair cost probability functions using the repair cost function $C_1(\delta)$
(solid lines: repair cost probability due to an earthquake, dotted lines: lifetime repair cost probability)

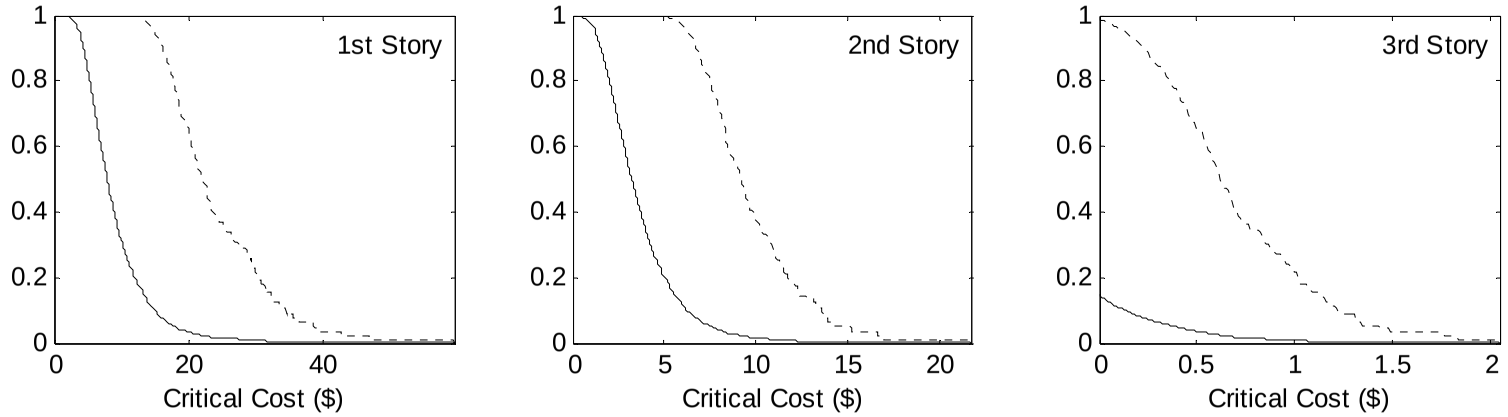

Figure 2.22: Repair cost probability functions using the repair cost function $C_2(\delta)$
(solid lines: repair cost probability due to an earthquake, dotted lines: lifetime repair cost probability)

due to an earthquake are estimated from Equation (2.54). The resulting probability curves are presented in Figures 2.21 and 2.22 with solid lines.

Lifetime repair cost probability is derived in a similar manner as described for the lifetime failure probability in Section 2.3.6. From the probability curves (solid lines) in Figures 2.21 and 2.22, mean arrival rate of particular earthquakes causing $C \geq c_{cr}$ is obtained as

$$\lambda_{RC}^{*}(c_{cr}) = \lambda P_{RC}(C \geq c_{cr}) \tag{2.55}$$

Based on the assumption of a Poisson process for earthquake occurrence, the exceedance probability of the lifetime repair costs is derived as

$$\begin{aligned} P_{LRC}(C > c_{cr}) &= 1 - P\left(N(t_s) = 0\right) \\ &= 1 - e^{-t_s \lambda_{RC}^{*}(c_{cr})} \end{aligned} \tag{2.56}$$

Assuming $\lambda = 0.6$ quakes/year and $t_s = 50$ years, the exceedance probability functions of the lifetime repair costs are presented in Figures 2.21 and 2.22 with dotted lines.

CHAPTER 3

LINEAR ANALYSIS OF EIGHT-STORY BUILDING

In this chapter, seismic analysis of an existing building is performed in order to estimate probable economic loss. The study model is an eight-story residential building located in Los Angeles, southern California where some of the well known faults underlie such as San Andreas, Newport-Inglewood, Whittier, and more. For reliable estimation of seismic structural performance, artificial accelerograms are generated based on ground motion data recorded in the study region. The methods for seismic response analysis of linear MDOF systems have been developed in Chapter 2 with providing essential background in structural dynamics. Utilizing the analysis methods, the procedure to construct fragility curves is developed. The fragility curve represents the probability that building damage exceeds a specified damage state under various levels of ground motion intensity measure. These damage state probabilities are then converted to dollar value of loss related to structural and nonstructural damage and economic aspects of damage.

3.1 Steel Moment Resisting Frame

Steel frames have been used in building construction for more than a century. In some cases, steel frames are designed to support gravity loads with very small capacity of moment resisting, but in the other case, steel frames are designed to have full resistance to lateral loads, called steel moment resisting frames. In general, steel moment frames are more flexible than other lateral resisting systems such as shear walls and braced frames. This low stiffness can produce large interstory displacement that may result relatively greater nonstructural damage [18].

As building codes are developed to require a high level of earthquake resistant design, designers began to design fully restrained connections. In the late 1950's, structural welding which had begun in the shipbuilding industry became widespread in the building industry as a mean of designing stronger and fully restrained connections. Currently, welded steel moment frame (WSMF) construction is commonly used for mid- and high-rise buildings in the United States and around the world [12].

Prior to the 1994 Northridge earthquake, severe damage to WSMF structures had rarely been reported in precedent earthquakes, and no failure of structures constructed in accordance with contemporary practice was reported. Thus, this type of construction was considered as the most ideal structural system for lateral resistance. However, such structural systems were re-evaluated after the Northridge earthquake because of the widespread reports of structural damage [12].

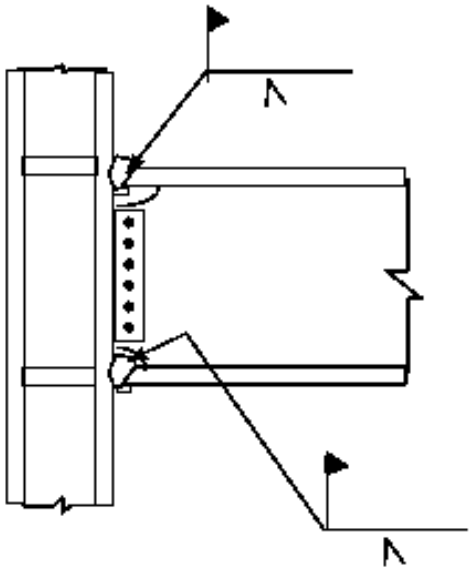

Figure 3.1: Typical welded moment resisting connection prior to 1994 [12]

The typical connection of WSMF prior to the Northridge earthquake shown in Figure 3.1 was expected to have large plastic capacity to remain ductile after reaching its yield capacity. However, investigation of structural damage due to the Northridge earthquake showed brittle fractures developed at much lower level of plastic demand than originally intended. Thus, significant modifications were made to improve the moment connection.

Special moment resisting frames, moment frames after the Northridge earthquake, were developed to have maximum flexural demand. In one case, the frame is designed to have plastic deformation at pre-determined locations within the beam span by reducing the flange width for plastic hinging (Refer to Figure 3.2) [11],[12].

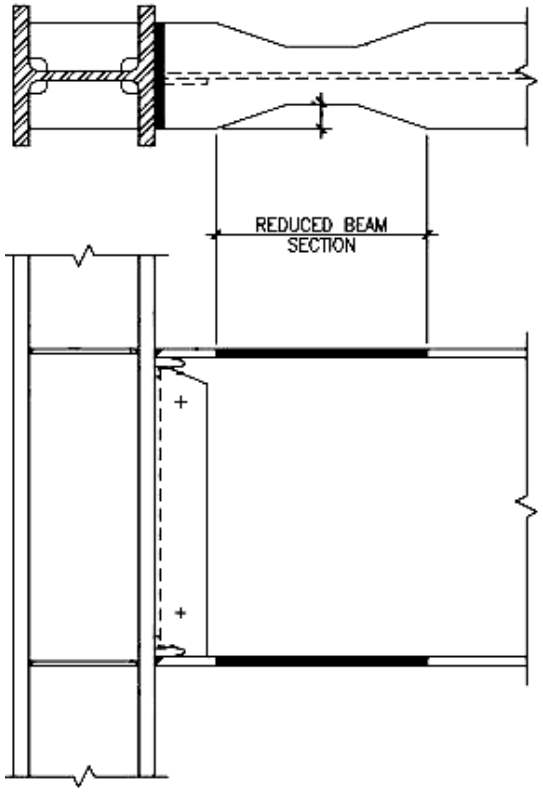

Figure 3.2: Reduced Beam Section (RBS) connection [11]

3.2 Building Description

An eight-story residential building located in Los Angeles, California is used to perform seismic damage analysis. The lateral load resisting system of the building is composed of steel moment frames designed per UBC 97 [35], and the structural steel conforms to ASTM A992 with a minimum yield stress of 50 ksi. Figure 3.3 shows the layout of moment frames in the plan view (shown as ►—◄) and an elevation view of the N-S moment frames.

The structure has a typical floor area of 8,775 ft^2; each floor is occupied by a residential use (7905 ft^2) and corridor (870 ft^2). A typical story height is 10.25 ft, except for the first story which has a story height of 10 ft. The design dead loads are as follows: 45 psf for roof and 91 psf for typical floor. The live loads are determined in accordance with UBC 97 [35]; 20 psf for roof, 40 psf for residence area, 100 psf for corridor, and 100 psf for stairs.

The seismic response analysis is performed with ground motion applied along the N-S direction. In the analysis, the eight-story building is simplified to a lumped mass linear elastic model in which each concentrated mass has one degree-of-freedom representing the lateral displacement of the story. The gravity frames, having negligible capacity of lateral force resistance, are not taken into account in story stiffness.

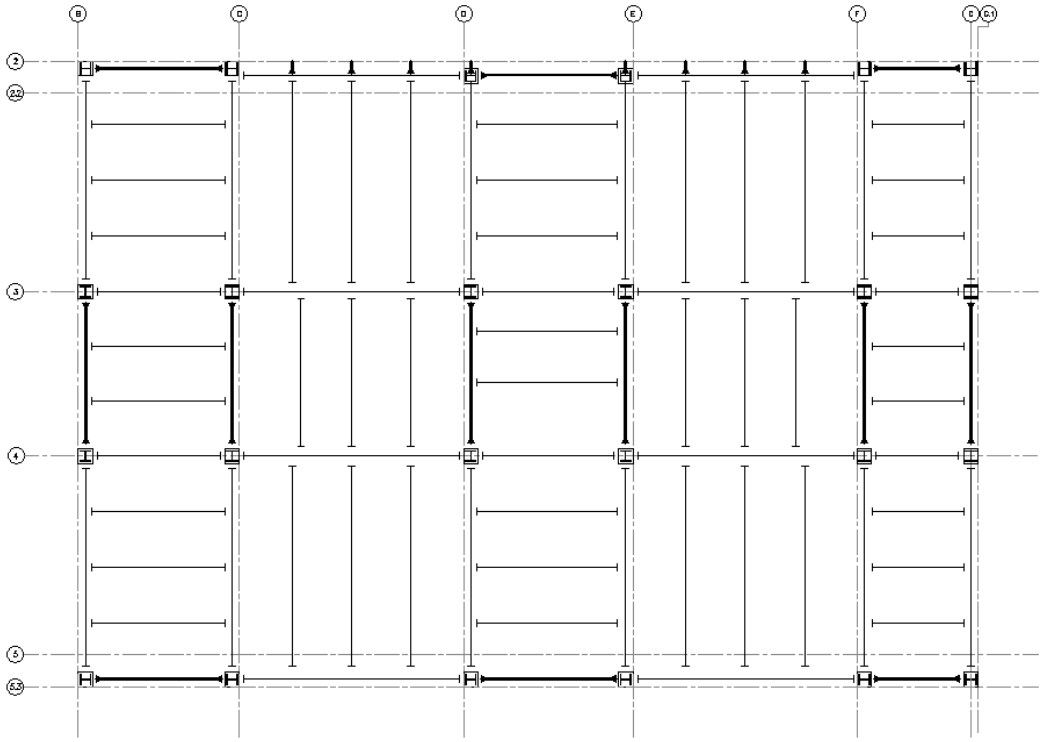

(a) Building plan (moment frames are symbolized as ►—◄)

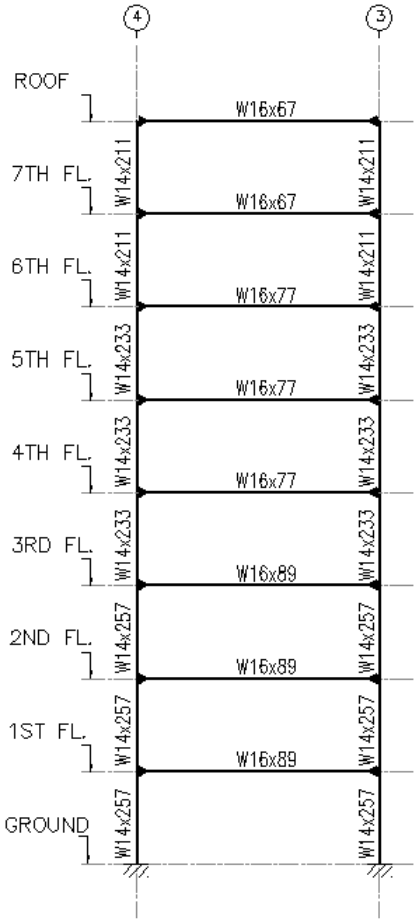

(b) Moment frames in the N-S direction

Figure 3.3: Plan view of the eight-story building and elevation view of the N-S moment frame

3.3 Seismic Response Analysis of the Eight-Story Building

To evaluate the seismic reliability of the eight-story building, a large number of ground motions are generated that represent possible future earthquakes in the region. Earthquake ground motions are modeled by a stationary Gaussian process based on the recorded accelerogram of the 1994 Northridge earthquake. Under the ground motions generated, the response samples of the building are obtained by implementing the dynamic analysis method of linear MDOF systems (Section 2.3).

3.3.1 Generation of Stationary Ground Motion

Because recorded accelerograms are generally limited at a site, it is necessary to generate artificial earthquake ground motions for a proper estimation of building performance [22]. Thus, ground motion acceleration in the study region is modeled by a stationary Gaussian process based on the time history record of the 1994 Northridge earthquake (component: 360 deg) measured at UCLA Grounds (Station #: 24688) at Los Angeles (Refer to Figure 3.4) [9].

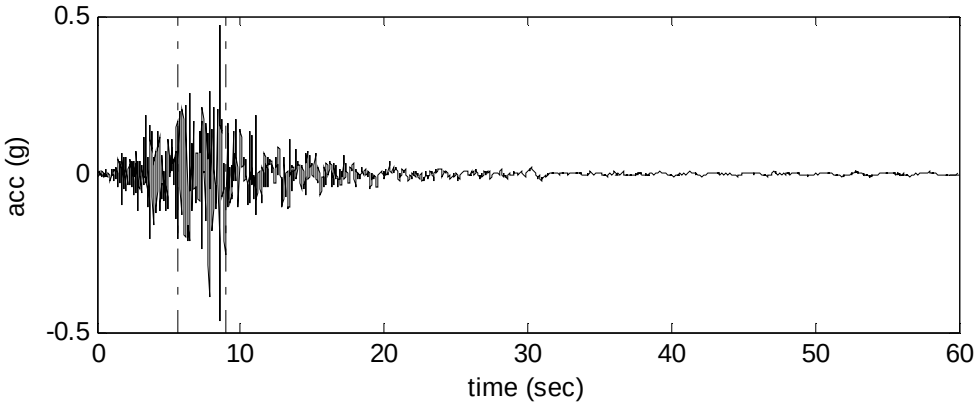

Figure 3.4: Ground motion acceleration of the 1994 Northridge earthquake (component: 360 deg) recorded at UCLA station (Ground motion data was obtained from Cosmos Virtual Data Center website [9])

Following the procedure for modeling stationary ground motion described in Section 2.1.4, the strong ground motion portion corresponding to the time range of 5.7 to 9.0 seconds is assumed as a sample of a stationary first-order Gaussian Markov process $A_s(t)$ with zero-mean and the autocorrelation function, $r(\tau) = \sigma^2 e^{-\kappa|\tau|}$. Thus the one-sided spectral density of $A_s(t)$ is $g(\nu) = 2\sigma^2\kappa / \pi(\nu^2 + \kappa^2)$. Using the reference ground motion record of $A_s(t)$, the variance σ^2 and positive constant κ are estimated as $\hat{\sigma}^2 = 0.0201$ and $\hat{\kappa} = 39.60$, and accordingly, the estimated functions of $r(\tau)$ and $g(\nu)$ are shown in Figure 3.5. From the one-sided spectral density function $g(\nu)$, see Figure 3.5(b), the cutoff frequency ν_c' is set to 500 rad/sec. Then 10,000 samples of input ground acceleration are generated using Equation (2.11) with 10,000 non-overlapping intervals, i.e. $\Delta\nu_k = 0.05$ rad/sec [23],[34]. Figure 3.6 shows a sample of the stationary ground acceleration.

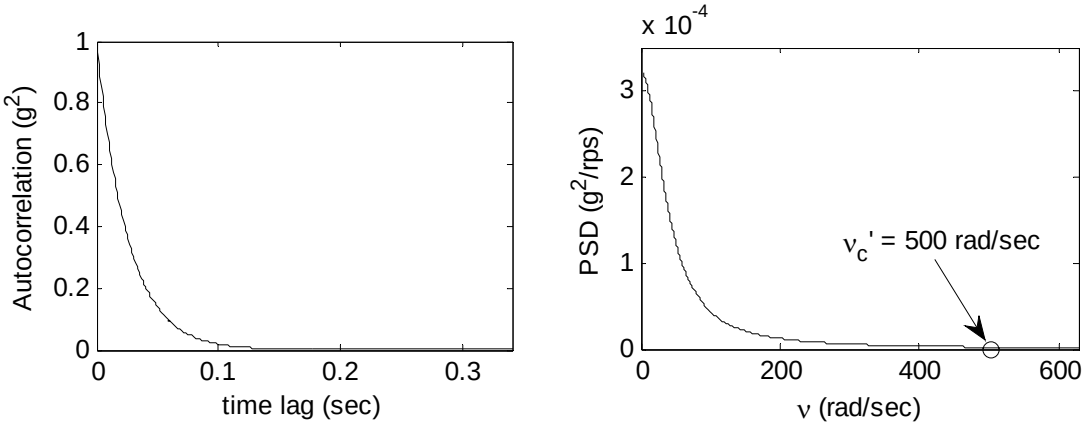

(a) Normalized Autocorrelation Function (b) One-sided Power Spectral Density

Figure 3.5: Normalized autocorrelation function and one-sided PSD of the 1994 Northridge earthquake

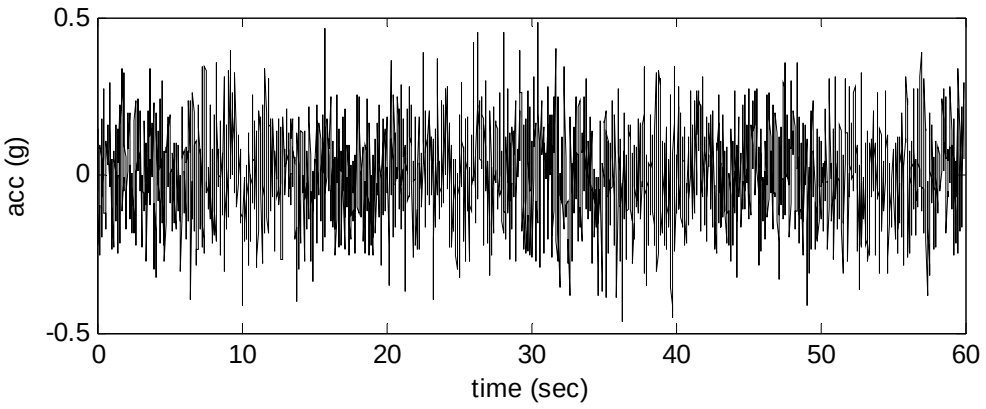

Figure 3.6: A sample of ground motion acceleration modeled by a stationary Gaussian process based on the time history record of the 1994 Northridge earthquake

3.3.2 System Properties of the Eight-Story Building

For the eight-story building subjected to earthquake-induced ground motion, the equations of motion can be written as $\underline{m}\ddot{\underline{x}}(t)+\underline{c}\dot{\underline{x}}(t)+\underline{k}\,\underline{x}(t)=-\underline{m}\,\underline{1}a(t)$ (Repeat of Equation (2.28)) where $\underline{m}$ is the mass matrix, $\underline{c}$ is the damping matrix, $\underline{k}$ is the stiffness matrix, $\underline{x}(t)$ is the vector of relative displacements, and $a(t)$ is the earthquake-induced ground acceleration [7].

Mass Matrix

The eight-story building is idealized as a lumped mass system with the mass m_i which is determined from the sum of the dead and live loads at the *i*-th floor level. The lumped mass at a typical floor (1st through 7th) is $m_1=\ldots=m_7=3113$ lb-sec^2/in , and $m_8=1658$ lb-sec^2/in for the roof (8th). The mass matrix of the eight-story building is

$$\underline{m}=\begin{bmatrix} m_1 & 0 & \cdots & 0 \\ 0 & \ddots & \ddots & \vdots \\ \vdots & \ddots & \ddots & 0 \\ 0 & \cdots & 0 & m_8 \end{bmatrix} \tag{3.1}$$

Stiffness Matrix

The story stiffness k_i is the sum of the lateral stiffness of all frames in the *i*-th story. If shear deformations in structural elements are neglected, k_i can be written as

$$k_i = \sum k_{frame} = \sum \frac{24EI_c}{h_i^3} \frac{12\rho + 1}{12\rho + 4} \tag{3.2}$$

where h_i is the story height, E=29,000 ksi, $\rho = I_b / 4I_c$ is the beam-column stiffness ratio, and I_b and I_c are the moment of inertia of beam and column [7].

Table 3.1: Moment of inertia of the N-S moment frame elements [1]

Story	Height (ft)	Column Size	I_c (in^4)	Beam Size	I_b (in^4)
1	10.00	W14×257	3400	W16×89	1310
2-3	10.25	W14×257	3400	W16×89	1310
4-6	10.25	W14×233	3010	W16×77	1120
7-8	10.25	W14×211	2660	W16×67	970

The story stiffnesses are as follows: k_1 = 3,435,720 lb/in, $k_2 = k_3$ = 3,190,407 lb/in, $k_4 = k_5 = k_6$ = 2,794,025 lb/in, and $k_7 = k_8$ =2,453,820 lb/in. Thus the stiffness matrix of the structure is

$$\underline{k} = \begin{bmatrix} k_1 + k_2 & -k_2 & 0 & \cdots & 0 \\ -k_2 & \ddots & \ddots & \ddots & \vdots \\ 0 & \ddots & \ddots & \ddots & 0 \\ \vdots & \ddots & \ddots & \ddots & -k_8 \\ 0 & \cdots & 0 & -k_8 & k_8 \end{bmatrix} \tag{3.3}$$

Natural Frequencies and Mode Shapes

Determined by solving the eigenvalue problem in Equation (2.33), the natural frequencies ω_n and mode shapes $\underline{\phi}_n$ of the structure are presented in Figure 3.7, with the corresponding modal participation factors Γ_n.

Regarding the dynamic analysis of multi-mode structural systems, it is common that the first few modes contribute significantly to the total displacement response of buildings while higher-mode contributions are negligible [7]. For the eight-story building the contribution of the first mode is the largest, and the modal contributions to the response decrease for higher modes (see Figure 3.7). Therefore, the total response is mainly dominated by the first mode.

Damping Matrix

For a typical steel building, the suggested value of the elastic damping ratio is in between 5 to 7% [17]. In this study, the damping ratios of the eight-story structure are assumed as 5% for the first and second modes. Assuming Rayleigh damping, the damping matrix $\underline{c}$ is expressed as a linear combination of the mass and stiffness matrices with two coefficients α_0 and α_1 as given in Equation (2.34). Using the natural frequencies, ω_1 and ω_2, and the specified damping ratios, ζ_1 and ζ_2, the two coefficients are computed as $\alpha_0 = 2.9279$ and $\alpha_1 = 0.0009$ using Equation (2.36). Then the damping matrix is

$$\underline{c} = 2.9279\underline{m} + 0.0009\underline{k} \tag{3.4}$$

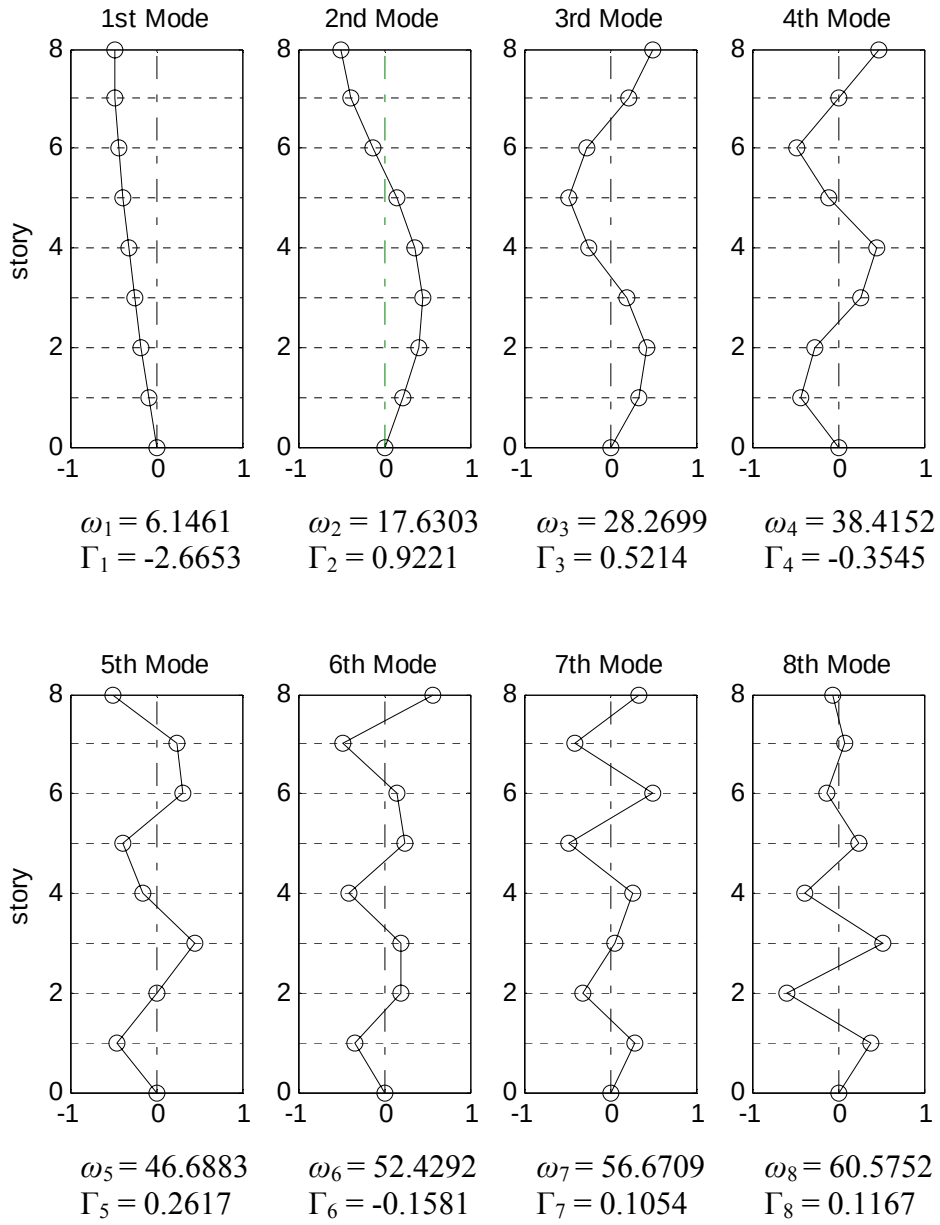

Figure 3.7: Modes of the eight-story building

3.3.3 Statistical Analysis of Responses and Evaluation of the Dominant Mode

Input-Output Relations

Using the samples of a zero-mean stationary Gaussian ground acceleration $A_s(t)$ generated in Section 3.3.1, samples of the building responses, i.e. story displacement and acceleration, are obtained by the modal analysis method, see Algorithm 2.3. Since the system is assumed to be linear elastic, the displacement and acceleration responses of each story, $X^{(i)}(t)$ and $\ddot{X}^{(i)}(t)$ where $i = 1, 2, \ldots, 8$, are zero-mean stationary Gaussian processes [10],[13].

(a) Mean values of the building responses, $X^{(i)}(t)$ and $\ddot{X}^{(i)}(t)$

Figure 3.8 shows the estimated mean values of $X^{(i)}(t)$ and $\ddot{X}^{(i)}(t)$ of the odd-numbered floors ($i = 1, 3, 5, 7$). The figure illustrates that the mean of the response samples is very close to zero at any time *t* as that of the samples of ground acceleration.

(b) Covariance functions of the building responses, $X^{(i)}(t)$ and $\ddot{X}^{(i)}(t)$

The covariance is employed to show the statistical relation between two random variables. In Figure 3.9, the maximum covariances between two different story displacements, $X^{(j)}(t)$ and $X^{(k)}(t)$ where $j \neq k$, are observed at lag time $\tau \approx 0$. Thus, it is predictable that the two different story displacements have a strong correlation, and the first mode is dominant in the story displacement response. However, the scaled covariance functions between two different story accelerations, $\ddot{X}^{(j)}(t)$ and $\ddot{X}^{(k)}(t)$ where $j \neq k$, do not show a strong dependency at $\tau = 0$, see Figure 3.10.

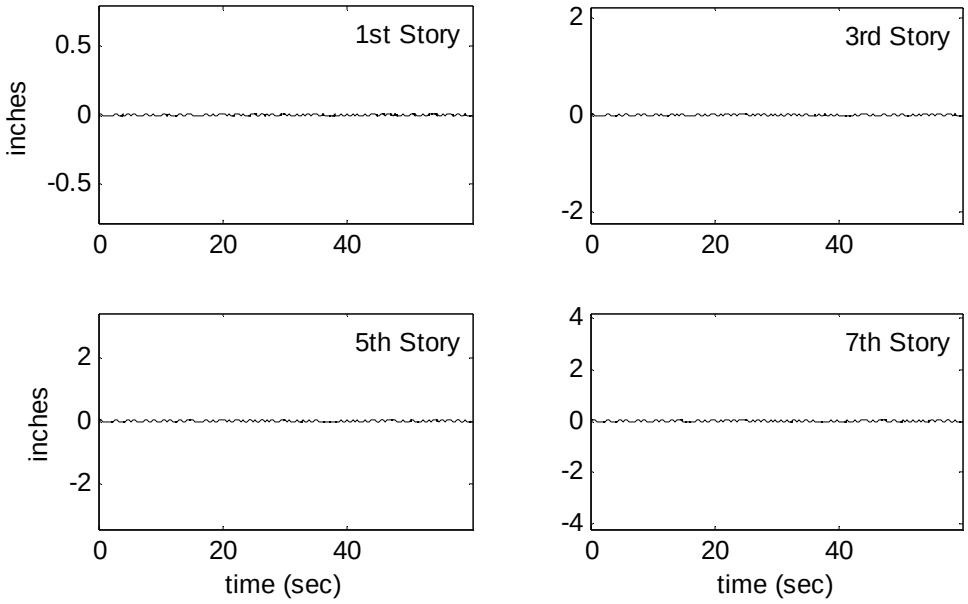

(a) Mean of story displacement for the eight-story building

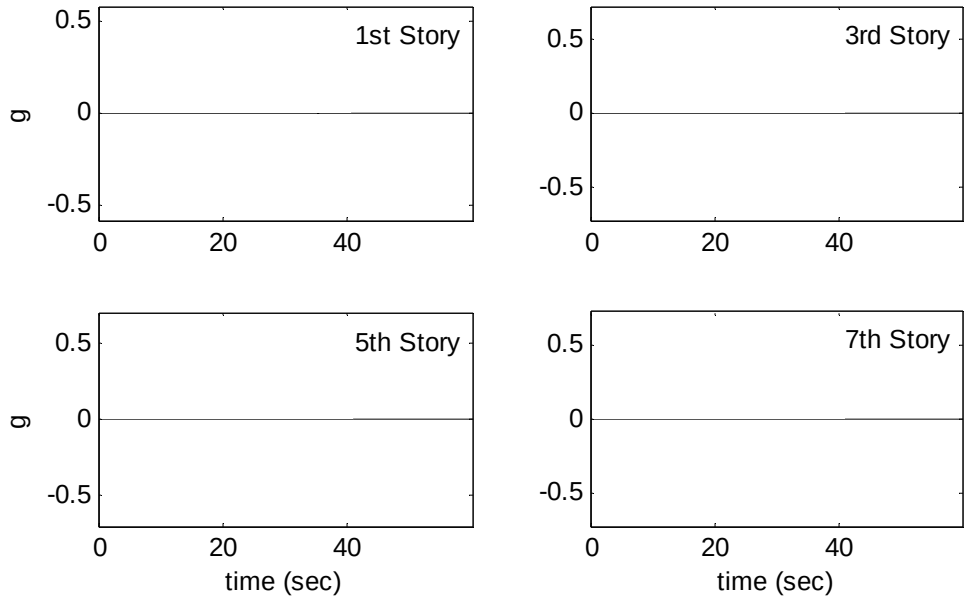

(b) Mean of story acceleration for the eight-story building

Figure 3.8: Mean of the responses for the eight-story building

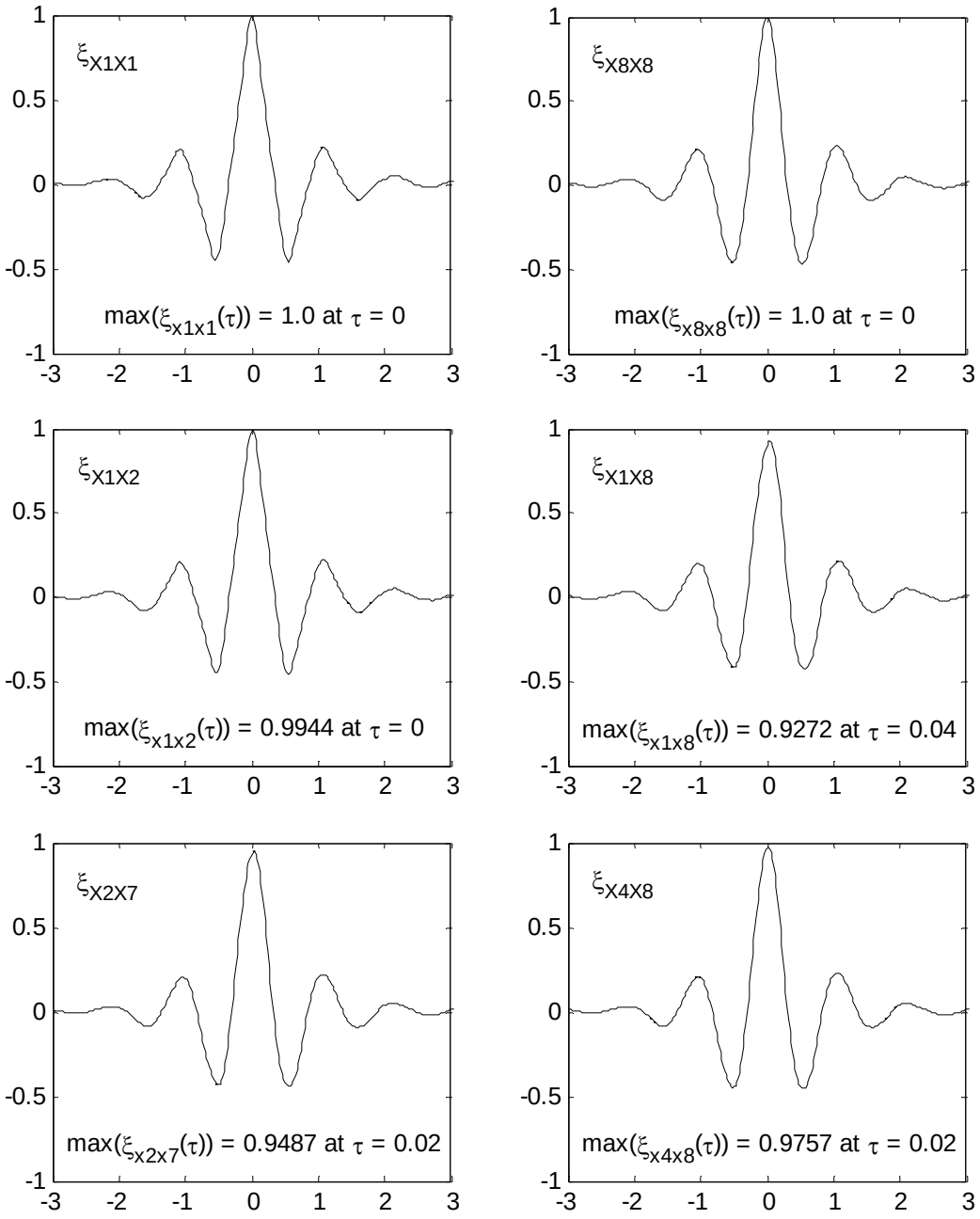

Figure 3.9: Scaled covariance of story displacement of the eight-story building

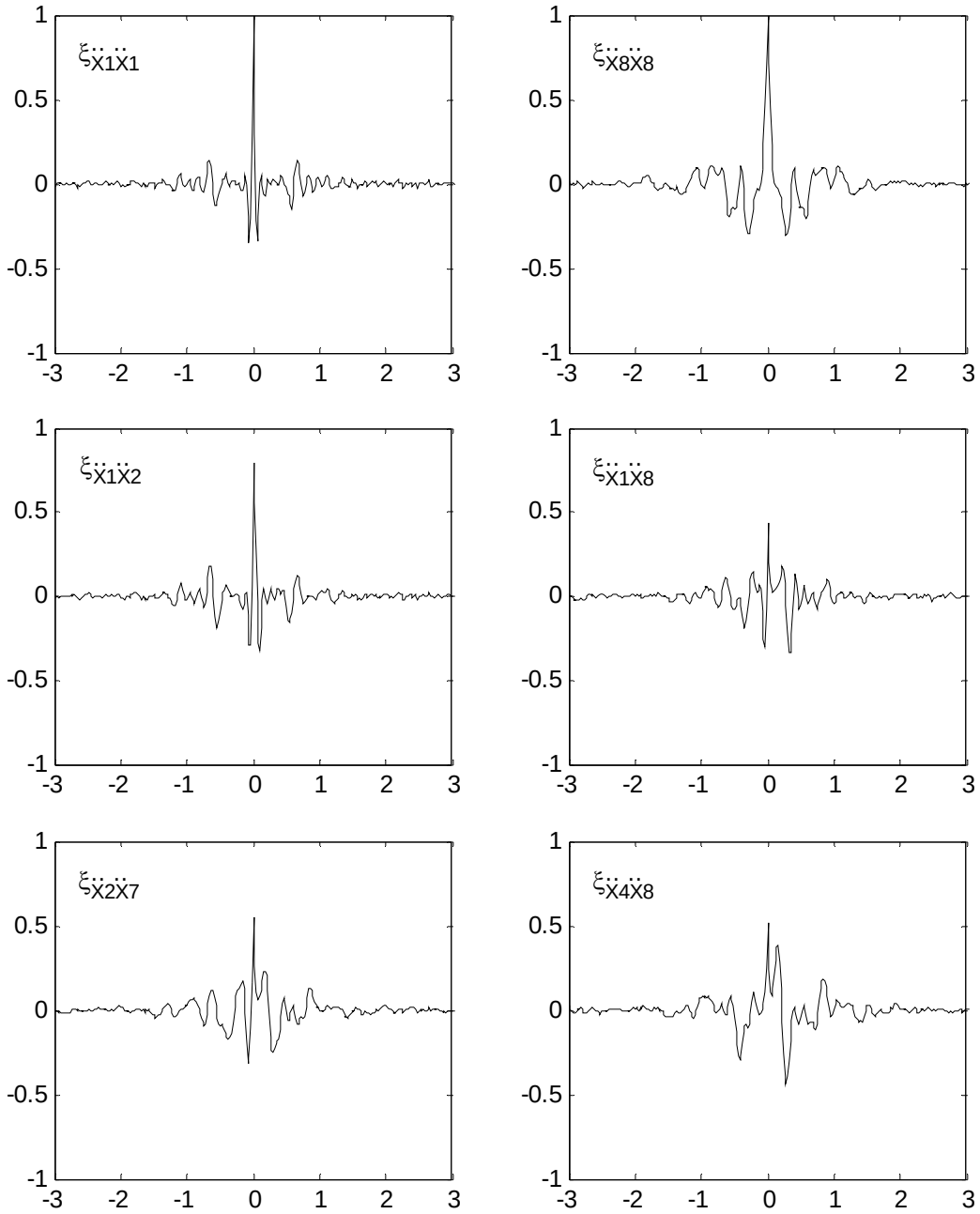

Figure 3.10: Scaled covariance of story acceleration of the eight-story building

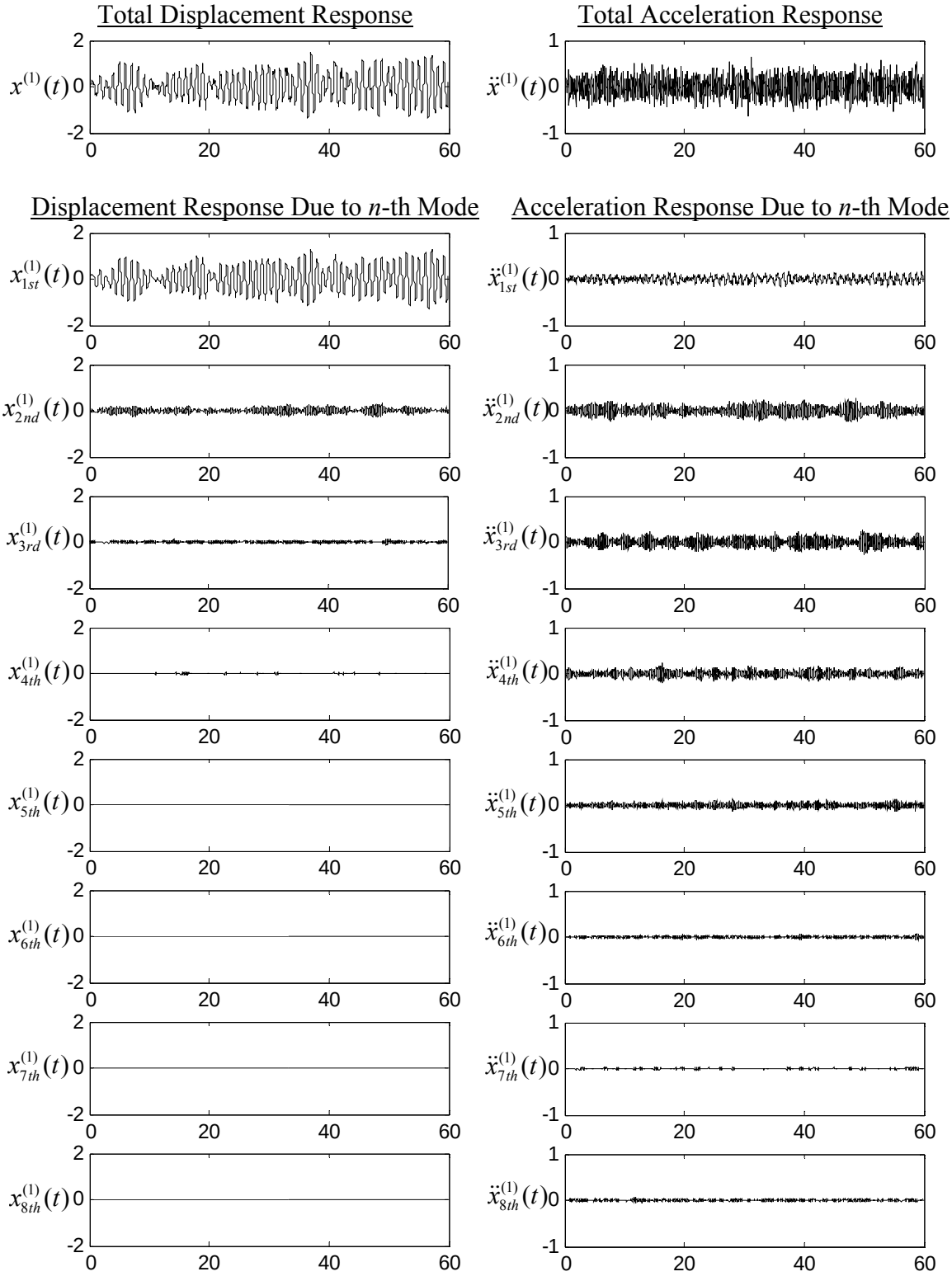

Figure 3.11: Exact solutions and responses due to *n*-th mode of the 1st story

Evaluation of the Dominant Mode

The exact solutions for the first story responses $x^{(1)}(t)$ and $\ddot{x}^{(1)}(t)$, obtained from a combination of the modal contributions according to Equation (2.38), are shown in Figure 3.11 (top). In the same figure, the first story responses due to the *n*-th mode, $x_{n-th}^{(1)}(t)$ and $\ddot{x}_{n-th}^{(1)}(t)$ where $n = 1, 2, \ldots, 8$, are presented to show the contributions of the various modes. The total displacement response is significantly dominated by the first mode while the contributions of higher modes decrease progressively. However, the total acceleration response is largely influenced by the acceleration responses due to the first five modes. The responses of the other stories also follow the similar pattern as the first story; that is, displacement responses are dominated by the first mode, and acceleration responses are governed by a combination of several modal responses.

3.4 Failure Rate of the Eight-Story Building

Buildings are composed of both structural (load-carrying) and nonstructural components (e.g. architectural, mechanical, electrical, and plumbing components). Damage to the structural system is primarily a function of interstory drift, and damage to nonstructural components is a function of interstory drift or floor acceleration [18]. In this study, maximum interstory drift ratio and floor acceleration, $\max_t |\Delta_R^{(i)}(t)|$ and $\max_t |A_f^{(i)}(t)|$, are considered as damage indicators for the estimation of failure probability. Interstory drift ratio $\Delta_R^{(i)}(t)$ of the *i*-th story is defined by

$$\Delta_R^{(i)}(t) = \begin{cases} \left(X^{(i)}(t) - X^{(i-1)}(t)\right)/h^{(i)}, & i \geq 2 \\ X^{(i)}(t)/h^{(i)}, & i = 1 \end{cases} \tag{3.5}$$

where $h^{(i)}$ is the height of the story, and floor acceleration $A_f^{(i)}(t)$ of the *i*-th floor can be computed from

$$A_f^{(i)}(t) = a(t) + \ddot{X}^{(i)}(t) \tag{3.6}$$

in which $a(t)$ is the input ground acceleration and $\ddot{X}^{(i)}(t)$ is the acceleration response of the *i*-th story which can be determined by the modal analysis method [7].

Then the failure probability of the *i*-th story is estimated as

$$P_F^{(i)} \approx \frac{1}{10,000} \sum_{j=1}^{10,000} 1(DM_j^{(i)} \geq dm_{cr}), \quad i = 1, 2, \ldots, 8 \tag{3.7}$$

where $DM_j^{(i)}$ is the sample of Damage Measure, i.e. $(\max_t |\Delta_R^{(i)}(t)|)_j$ or $(\max_t |A_f^{(i)}(t)|)_j$, and dm_{cr} is the critical value of the damage measure, i.e. the critical interstory drift ratio $\delta_{R,cr}$ or floor acceleration $a_{f,cr}$.

Lifetime Failure Probability

Based on the assumption of a Poisson process for the occurrence of earthquakes, the lifetime failure probability of the building can be developed from the failure probability due to an earthquake (refer to the procedure described in Section 2.3.6).

In this study, the lifetime of the eight-story structure is assumed to be 75 years. To estimate the mean occurrence rate of earthquakes, the table of Significant Los Angeles Area Earthquakes provided by USGS [37] is employed, see Table 3.2. The table shows that 19 earthquakes, ranging in magnitude from 4.8 to 6.7, have been recorded since 1920. Thus, the mean occurrence rate of earthquakes is estimated as $\hat{\lambda} = 0.2159$ quakes/year. Then the mean occurrence rate $\lambda_F^{*(i)}(dm_{cr})$ of particular earthquakes causing $DM^{(i)} \geq dm_{cr}$ is obtained by

$$\lambda_F^{*(i)}(dm_{cr}) = 0.2159 P_F^{(i)}(dm_{cr}) \tag{3.8}$$

where $P_F^{(i)}(dm_{cr})$ is the failure rate of the *i*-th story at given dm_{cr}. Using Equations (2.50) and (2.51), the lifetime failure probabilities are estimated as

$$P_{LF}^{(i)} = 1 - e^{-75\lambda_F^{*(i)}(dm_{cr})} \tag{3.9}$$

The resulting failure probability curves are presented in Figures 3.12 and 3.13.

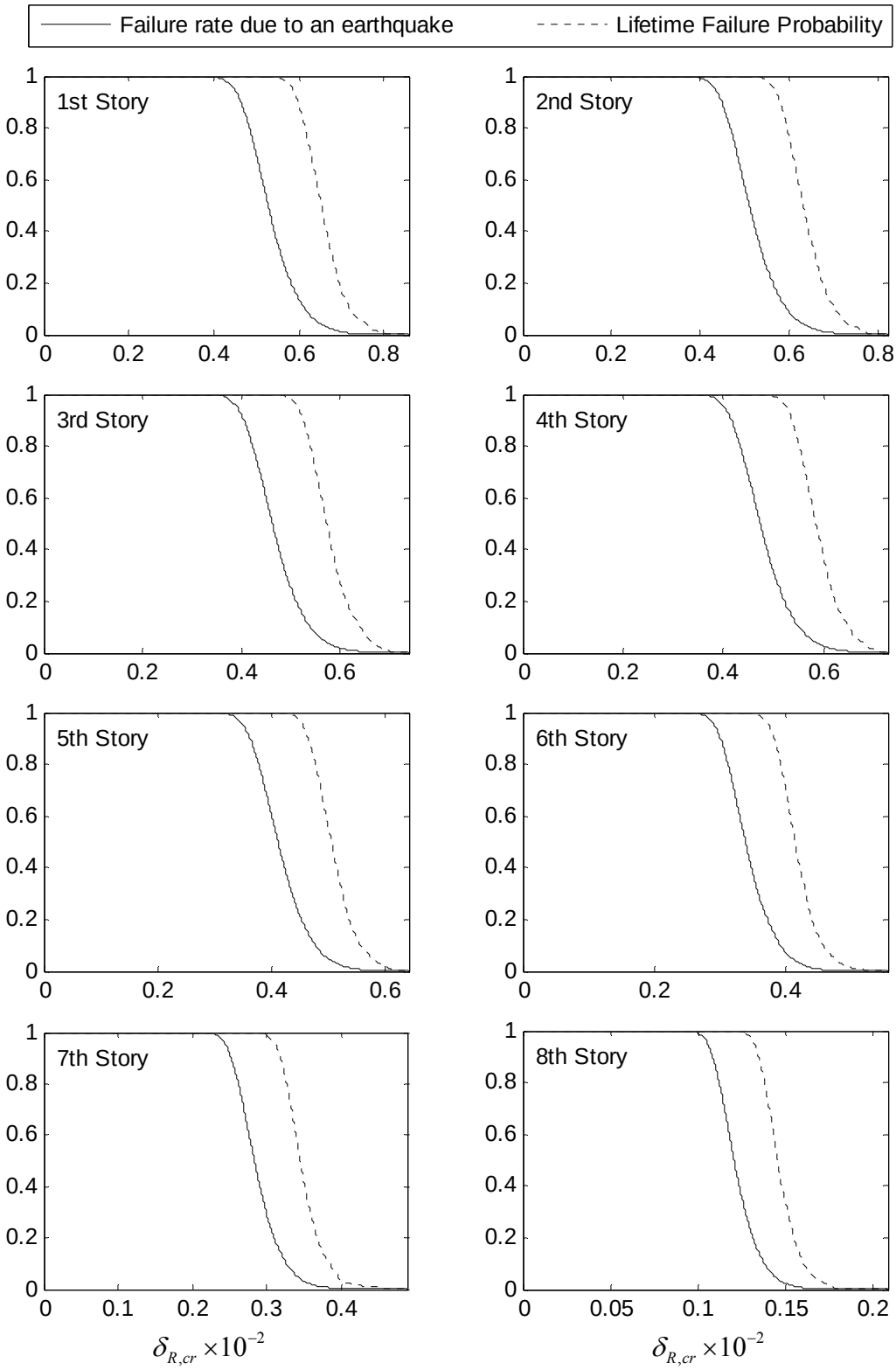

Figure 3.12: Failure rates of the eight-story building in terms of interstory drift ratio

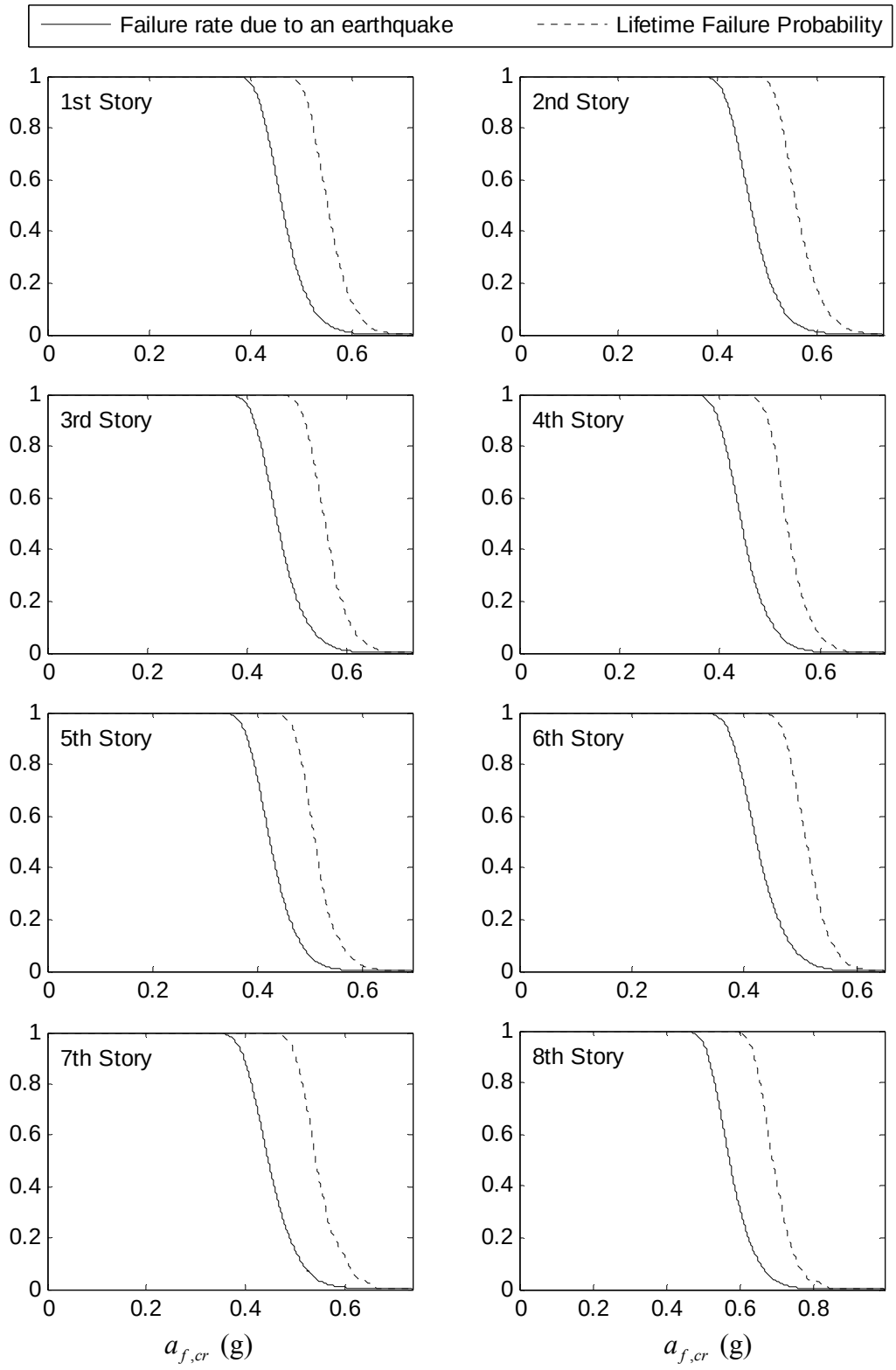

Figure 3.13: Failure rates of the eight-story building in terms of floor acceleration

Table 3.2: Significant Los Angeles Earthquakes [37]

YEAR	MN	DY	HR MIN SECC	LATITUTE		LONGITUDE		MAG	DEPTH	NAME
1920								m1=4.9		
1930								m1=5.2		
1933	3	11	01 54 07.80	33°	37.00′	-177°	58.00′	m1=6.4	0.00	Long Beach
1938	5	31	08 34 55.41	33°	41.93′	-177°	30.64′	m1=5.2	10.00	
1941	10	22	06 57 18.50	33°	49.00′	-118°	13.00′	m1=4.8	0.00	
1941	11	14	08 41 36.30	33°	47.00′	-118°	15.00′	m1=4.8	0.00	
1952	8	23	10 09 07.15	34°	31.16′	-118°	11.89′	m1=5.2	13.10	
1969	10	24	08 29 12.11	33°	17.46′	-118°	11.56′	m1=5.1	10.00	
1970	9	12	14 30 52.98	34°	16.19′	-119°	32.40′	m1=5.2	8.00	Lytle Creek
1971	2	9	14 00 41.83	34°	24.67′	-117°	24.04′	m1=6.7	8.40	San Fernando (Sylmar)
1973	2	21	14 45 57.30	34°	3.89′	-118°	2.10′	m1=5.9	8.00	Point Mugu
1979	1	1	23 14 38.94	34°	56.66′	-119°	40.88′	m1=5.2	11.28	Malibu
1981			15 50 50.13	33°	39.09′	-118°	5.58′	m1=6.0	6.00	Santa Babara Island
1957			14 42 20.02	34°	3.68′	-119°	4.71′	m1=5.9	9.53	Whittier Narrows
1988			11 38 26.44	34°	9.06′	-118°	7.81′	m1=5.0	14.27	Pasadena
1989			06 53 28.84	33°	55.12′	-118°	37.65′	m1=5.0	11.86	Malibu
1990			23 43 36.75	34°	8.62′	-117°	41.84′	m1=5.3	4.49	Upland
1991			14 43 54.66	34°	16.19′	-117°	59.58′	m1=5.8	9.15	Sierra Madre
1994			12 30 55.39	34°	12.80′	-118°	32.22′	m1=6.7	18.40	Northridge

3.5 Fragility Curves

Failure rate curves discussed in the previous section in essence represent the probability of exceedance of peak building response whereas fragility curves show the conditional probability of reaching or exceeding a particular damage state as a function of earthquake intensity measure. Fragility curves are often represented by lognormal distribution functions with two parameters.

In this section, the procedure to develop fragility curves is described and applied to the eight-story building as a mean of evaluating its seismic vulnerability.

3.5.1 Damage of Structural and Nonstructural Components

Buildings are composed of both structural (load-carrying) and nonstructural components (e.g., architectural, mechanical, electrical, and plumbing components). For fragility analysis, these components are treated separately and their damage levels are classified in terms of one of four damage states: Slight, Moderate, Extensive, and Complete [18].

Structural Damage

To assess structural damage of steel moment frame buildings, maximum interstory drift is the basic parameter used because it is assumed to be about the same as the drift angle demand on nearby beam-column connections [12]. General descriptions of the four damage states for the steel moment frame are provided below [18]:

> **Slight Structural Damage:** Minor deformations in connections or hairline cracks in few welds.
> **Moderate Structural Damage:** Some steel members have yielded exhibiting observable permanent rotations at connections; few welded connections may exhibit major cracks through welds or few bolted connections may exhibit broken bolts or enlarged bolt holes.
> **Extensive Structural Damage:** Most steel members have exceeded their

yield capacity, resulting in significant permanent lateral deformation of the structure. Some of the structural members or connections may have exceeded their ultimate capacity exhibited by major permanent member rotations at connections, buckled flanges and failed connections. Partial collapse of portions of structure is possible due to failed critical elements and/or connections.
Complete Structural Damage: Significant portion of the structural elements have exceeded their ultimate capacities or some critical structural elements or connections have failed resulting in dangerous permanent lateral displacement, partial collapse or collapse of the building. Approximately 8%(low-rise), 5%(mid-rise) or 3%(high-rise) of the total area of [steel moment frame] buildings with Complete damage is expected to be collapsed.

Based on building type and seismic design level of the eight-story building, high-rise steel moment frame building designed to high seismic standards, the threshold values of damage to structural components are summarized in Table 3.3 [18].

Table 3.3: Threshold of moment frames for structural damage [18]

Damage States	Slight	Moderate	Extensive	Complete
Structural Component (Interstory Drift Ratio)	0.003	0.006	0.015	0.040

Nonstructural Damage

Typical nonstructural components are architectural, mechanical, electrical, and plumbing components. These nonstructural components are grouped into two categories–drift-sensitive and acceleration-sensitive components–because it is impractical to assess damage for individual nonstructural component. Damage to drift-sensitive nonstructural components is primarily a function of interstory drift, and damage to acceleration-sensitive nonstructural components is a function of floor acceleration [18]. The following table summarizes the threshold values of damage to nonstructural components.

Table 3.4: Thresholds of moment frames for nonstructural damage [18]

Damage States	Slight	Moderate	Extensive	Complete
Nonstructural Drift-sensitive Component (Interstory Drift Ratio)	0.004	0.008	0.025	0.050
Nonstructural Acceleration-sensitive Component (Floor Acceleration, g)	0.30	0.6	1.20	2.40

3.5.2 Fragility Curves by a Linear Dynamic Analysis Method

Damage prediction can be expressed in terms of the probability of a building being in or exceeding any of the four damage states [18],[21]. The step-by-step procedure for estimating damage probability of a building is described below and applied to the eight-story building.

Step 1: Incremental Dynamic Analysis

Incremental dynamic analysis (IDA) is a parametric analysis method to estimate structural performance under several earthquake ground motions [38]. The IDA provides prediction of the relationship between seismic demand and capacity [2],[39]. The IDA method involves producing curves of damage measure versus intensity measure under the effect of ground motions, each scaled to several levels of intensity measure [21],[38].

In this study, peak structural response (maximum interstory drift ratio $\max_t |\Delta_R^{(i)}(t)|$ or floor acceleration $\max_t |A_f^{(i)}(t)|$ in which *i* is the story level) is used as a parameter for estimating Damage Measure *DM*, and first mode spectral displacement $S_d(T_1,\zeta_1)$ or acceleration $S_a(T_1,\zeta_1)$ is used as Intensity Measure *IM* of ground motion. The *IM* indicators $S_d(T_1,\zeta_1)$ and $S_a(T_1,\zeta_1)$, corresponding to the first mode period T_1 and damping ratio ζ_1, are defined by [7]

$$S_d(T_1,\zeta_1) \equiv \max_t |x(t,T_1,\zeta_1)| \quad \text{and}$$
$$S_a(T_1,\zeta_1) \equiv \max_t |a_f(t,T_1,\zeta_1)| \tag{3.10}$$

in which

$$a_f(t,T_1,\zeta_1) = a(t) + \ddot{x}(t,T_1,\zeta_1) \tag{3.11}$$

where $a(t)$ is the ground acceleration; the displacement and acceleration response of the first mode, $x(t,T_1,\zeta_1)$ and $\ddot{x}(t,T_1,\zeta_1)$, can be calculated by Algorithm 2.2.

The procedure to construct IDA curves is summarized in Algorithm 3.1. For convenience of notation, $S_d(T_1,\zeta_1)$, $S_a(T_1,\zeta_1)$, $\max_t |\Delta_R{}^{(i)}(t)|$, and $\max_t |A_f{}^{(i)}(t)|$ are symbolized hereon by S_{d1}, S_{a1}, $\Delta^{(i)}_{R,\max}$, and $A^{(i)}_{f,\max}$, respectively.

Algorithm 3.1: Construction of IDA Curves [4],[38],[39]

Step 1-1: Generate an accelerogram for the study area

Step 1-2: Scale the accelerogram by a Scale Factor (SF), where $SF \in (0,+\infty]$

Step 1-3: (a) Obtain *IM* of the scaled accelerogram by dynamic response analysis of the first mode (by Algorithm 2.2 and Equation (3.10))
i.e. S_{d1} and S_{a1} in this study
(b) Obtain *DM* of each story by dynamic response analysis of the structural model (by Algorithm 2.3 and Equations (3.5) and (3.6))
i.e. $\Delta^{(i)}_{R,\max}$ and $A^{(i)}_{f,\max}$ in this study

Step 1-4: Record each vector of (*DM*,*IM*) for plotting an IDA curve
i.e. $\left(\Delta^{(i)}_{R,\max}, S_{d1}\right)$ and $\left(A^{(i)}_{f,\max}, S_{a1}\right)$ in this study

Step 1-5: Repeat *Step 1-2* through *1-4* with higher *SF*s until *IM* reaches to predetermined value.
Note: *SF* must be small enough to minimize error in the interpolation process in *Step 1-6*.

Step 1-6: Plot IDA curves using the recorded vectors of (*DM*,*IM*)
Note: A Spline interpolation can be used for smooth IDA curves

Step 1-7: Repeat *Step 1-1* through *1-6* until obtaining sufficient information to estimate seismic demand and capacity relationship

IDA Curves for the Eight-Story Building

Using the 10,000 samples of artificial ground acceleration (generated in Section 3.3.1), the total of 10,000 IDA curves are generated for the eight-story building of which the fundamental period and damping ratio are $T_1 = 1.0223$ sec and $\zeta_1 = 0.05$.

In Step 1-2 of Algorithm 3.1, a sample of the generated ground accelerograms is scaled with $SF = 0.05g$ in peak ground acceleration (PGA). Then two sets of discrete points for each *i*-th story, i.e. $(\Delta^{(i)}_{R,\max}, S_{d1})$ and $(A^{(i)}_{f,\max}, S_{a1})$, are obtained by dynamic analysis, see Step 1-3 and 1-4. Increasing the scale factor by a constant value of $0.05g$, Steps 1-2 through 1-5 are repeated until reaching sufficiently large *IM* (in this study, the limits of *IM*s are set to 40 inches for S_{d1} and 3.0 g for S_{a1}). Then the entire IDA curve for each story is developed by a spline interpolation of the discrete points which is performed using a MATLAB function called *interp1* [28]. Hence, *DM* values can be obtained at any level of *IM* [39].

Figure 3.14 shows twenty IDA curves for the 1st and 5th stories. Because the eight-story building is assumed as a linear system, a linear relationship between maximum building response and earthquake intensity measure is observed [21].

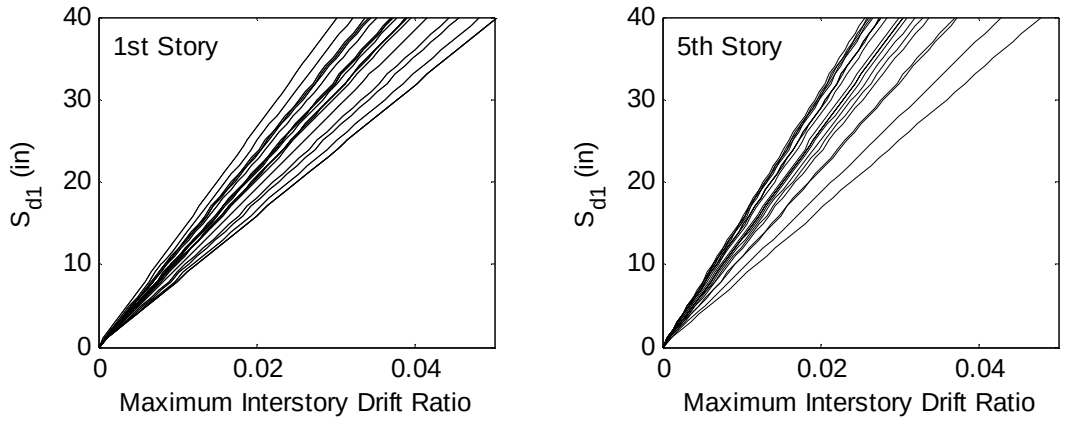

(a) Twenty IDA curves as a function of spectral displacement

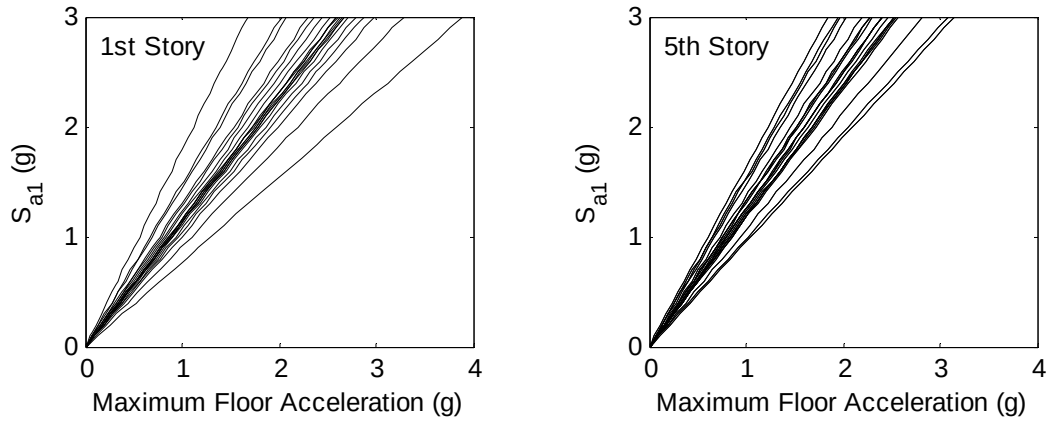

(b) Twenty IDA curves as a function of spectral acceleration

Figure 3.14: Twenty IDA curves for the 1st and 5th stories

Step 2: Construction of Fragility Curves

From IDA results a fragility curve can be developed by first determining the conditional probability of reaching or exceeding a damage state *ds* for various levels of intensity measure. For a given level of *IM*, the probability of being in or exceeding a particular damage state can be determined by counting the number of times that maximum structural responses equal to or exceed a damage state threshold value, $\delta_{R,ds}$ or $a_{f,ds}$, and dividing by the total number of trials *n* [8]. Then it is formulated as follow

$$P_C[ds \mid IM] = \frac{1}{n}\sum_{j=1}^{n} 1\left(DM_j^{IM} \geq dm_{ds}\right) \tag{3.12}$$

where IM is the intensity measure, i.e. S_{d1} or S_{a1}, $DM_j^{IM}(t)$ is the samples of damage measures at a given IM, i.e. $(\Delta_{R,\max}^{S_{d1}})_j$ or $(A_{f,\max}^{S_{a1}})_j$, and dm_{ds} is the threshold of a damage state *ds*, i.e. $\delta_{R,ds}$ or $a_{f,ds}$ (see Tables 3.3 and 3.4).

As an illustrative example, simple fragility curves are constructed for structural damage in the 1st story using the twenty IDA curves in Figure 3.15 (repeat of Figure 3.14(a)). Twenty-one levels of intensity $S_{d1} = 0, 2, \cdots, 40$ inches are used for this evaluation, and the threshold value for each structural damage state is summarized in Table 3.3. For each given intensity of S_{d1}, the probability of reaching or exceeding each damage state is evaluated using Equation (3.12) (see Table 3.5 for values), and accordingly, a simple example of fragility curves is presented in Figure 3.16.

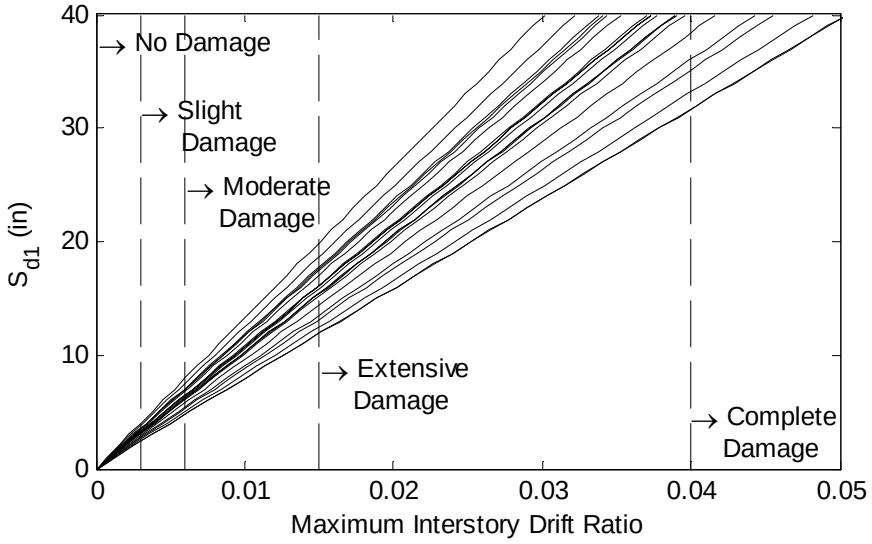

Figure 3.15: Twenty IDA curves of the 1st story

Table 3.5: Cumulative damage state probabilities for the example

S_{d1} (inches)	$P[ds \mid S_{d1}]$			
	Slight	Moderate	Extensive	Complete
0	0.00	0.00	0.00	0.00
2	0.00	0.00	0.00	0.00
4	1.00	0.00	0.00	0.00
6	1.00	0.30	0.00	0.00
8	1.00	1.00	0.00	0.00
10	1.00	1.00	0.00	0.00
12	1.00	1.00	0.10	0.00
14	1.00	1.00	0.25	0.00
16	1.00	1.00	0.55	0.00
18	1.00	1.00	0.90	0.00
20	1.00	1.00	1.00	0.00
22	1.00	1.00	1.00	0.00
24	1.00	1.00	1.00	0.00
26	1.00	1.00	1.00	0.00
28	1.00	1.00	1.00	0.00
30	1.00	1.00	1.00	0.00
32	1.00	1.00	1.00	0.10
34	1.00	1.00	1.00	0.15
36	1.00	1.00	1.00	0.20
38	1.00	1.00	1.00	0.25
40	1.00	1.00	1.00	0.30

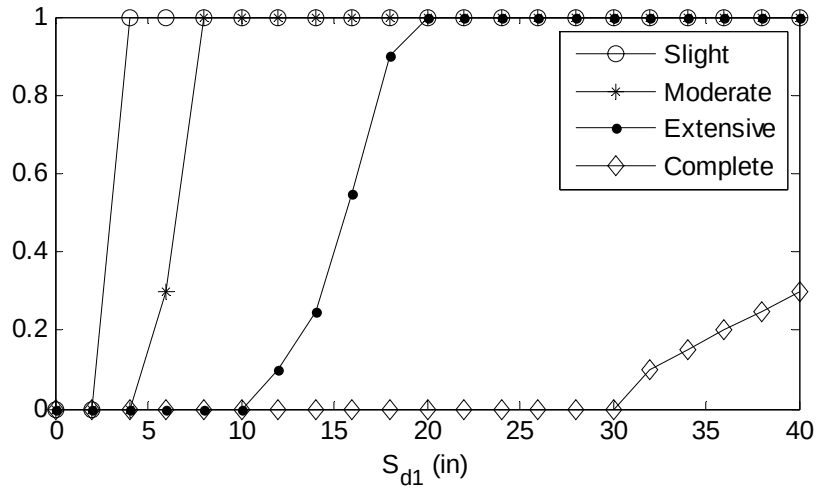

Figure 3.16: A simple example of fragility curves

Analytical Fragility Curves for the Eight-Story Building

In real application, fragility curves are developed for various levels of seismic intensity measure. Following the procedure illustrated by a simple example above, the fragility curves for the 1st and 5th stories are plotted in Figure 3.19 (dotted lines).

Step 3: Fragility Function (lognormal CDF)

Generally, the fragility curves can be expressed using two-parameter lognormal distribution functions. Then the cumulative probability of reaching or exceeding a damage state for a given ground motion intensity measure is expressed as [24],[29]

$$P_C[ds \mid IM] = \Phi\left[\frac{1}{\beta_{ds}} \ln\left(\frac{IM}{\overline{IM}_{ds}}\right)\right] \tag{3.13}$$

where $\overline{IM}_{ds}$ is the median value of intensity measure (i.e. $\overline{S}_{d1,ds}$ or $\overline{S}_{a1,ds}$) at which the building reaches the threshold of damage state, β_{ds} is the standard deviation of $\ln IM$ of damage state, and Φ is the standard normal cumulative distribution function [12],[18].

The estimation of the two parameters, median $\overline{IM}_{ds}$ and log standard deviation β_{ds}, is performed in the following manner: If samples are lognormally distributed, the geometric mean is a logical estimator of the median. Thus, in this study, the median value in Equation (3.13) is defined as the geometric mean of IM [24],[31]. Since IM is a lognormal random variable, $\ln IM$ is normal with mean $\mu_{\ln IM}$ and standard deviation $\sigma_{\ln IM}$. Thus the following relationship can be obtained

$$\Phi(s) = \Phi\left(\frac{\ln IM - \mu_{\ln IM}}{\sigma_{\ln IM}}\right) \tag{3.14}$$

where s is the standard normal variable [21]. From Equation (3.14), the relationship between s and $\ln IM$ can be expressed as

$$\ln IM = \sigma_{\ln IM} s + \mu_{\ln IM} \tag{3.15}$$

Using a set of points $(s, \ln IM)$ obtained from a fragility curve, $\mu_{\ln IM}$ and $\sigma_{\ln IM}$ can be estimated by linear regression analysis [21]. Then the two parameters in Equation (3.13) are estimated as

$$\begin{aligned} \overline{IM}_{ds} &= \exp(\mu_{\ln IM}) \quad \text{and} \\ \beta_{ds} &= \sigma_{\ln IM} \end{aligned} \tag{3.16}$$

To illustrate the procedure described above, consider the fragility curve for Extensive damage to structural components in the 1st story, see Figure 3.16 (repeated in Figure 3.18). The standard normal random variables *s* corresponding to the intensity measures S_{d1} are estimated as $s = \Phi^{-1}(P_C[ds \geq E \mid S_{d1}])$ where *E* denotes Extensive damage, then the set of points $(s, \ln S_{d1})$ are obtained (see Table 3.6). Using these points, $\mu_{\ln S_{d1}}$ and $\sigma_{\ln S_{d1}}$ are estimated as shown in Figure 3.17 which is the lognormal probability plot of *s* versus $\ln S_{d1}$. The linear regression analysis is performed using a MATLAB function, *polyfit* [28]. Figure 3.18 compares the fragility curves constructed using data from the IDA curves and lognormal fit.

Table 3.6: A set of data points obtained to estimate two parameters of lognormal CDF

Fragility Curve		Lognormal Probability Plot	
$P_C[ds \geq E \mid S_{d1}]$	S_{d1}	$s = \Phi^{-1}(P_C[ds \geq E \mid S_{d1}])$	$\ln S_{d1}$
0.10	12	-1.2816	2.4849
0.25	14	-0.6745	2.6391
0.55	16	0.1257	2.7726
0.90	18	1.2816	2.8904

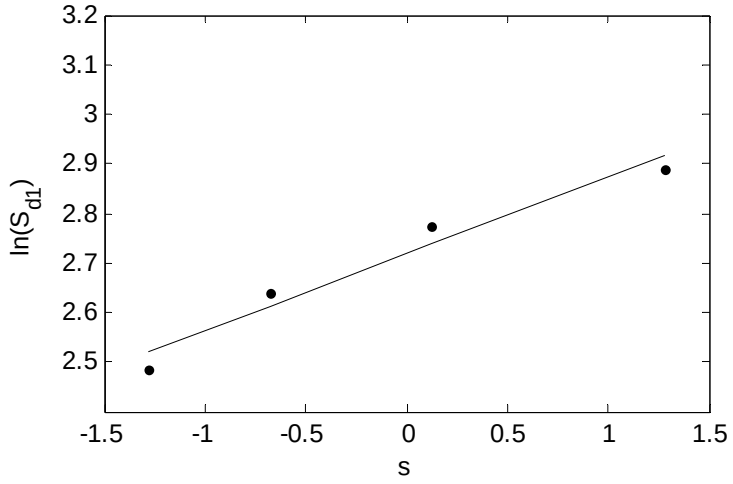

Figure 3.17: Example of linear regression method to estimate the two parameters of lognormal CDF

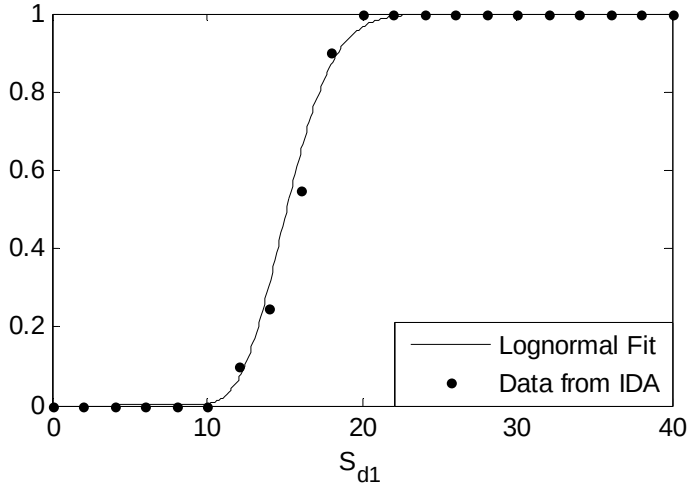

Figure 3.18: Comparison of fragility curves constructed from IDA data and lognormal CDF

Table 3.7: Estimated parameters of fragility function for the eight-story building

(a) Structural fragility curve parameters

Story	Slight		Moderate		Extensive		Complete	
	median	*beta*	*median*	*beta*	*median*	*beta*	*median*	*beta*
1	3.0095	0.1411	6.0440	0.1413	15.0995	0.1423	40.9201	0.1519
2	3.1179	0.1408	6.2507	0.1403	15.6405	0.1384	42.2833	0.1478
3	3.4652	0.1356	6.9078	0.1321	17.2531	0.1350	46.7094	0.1453
4	3.3899	0.1348	6.7637	0.1369	16.8671	0.1353	45.2180	0.1392
5	3.8806	0.1385	7.7647	0.1391	19.3818	0.1376	51.5016	0.1410
6	4.6847	0.1458	9.3819	0.1454	23.4733	0.1449	53.3200	0.0963
7	5.6536	0.1561	11.2933	0.1572	28.2625	0.1565	–	–
8	13.2639	0.1609	26.5236	0.1593	55.4189	0.1092	–	–

(b) Nonstructural drift-sensitive fragility curve parameters

Story	Slight		Moderate		Extensive		Complete	
	median	*beta*	*median*	*beta*	*median*	*beta*	*median*	*beta*
1	4.0555	0.1445	8.0768	0.1436	25.2262	0.1434	52.1933	0.1594
2	4.1875	0.1393	8.3458	0.1407	26.0648	0.1401	54.2832	0.1583
3	4.6013	0.1350	9.2168	0.1344	28.8538	0.1395	58.3936	0.1461
4	4.4806	0.1324	9.0021	0.1331	28.2141	0.1381	53.2363	0.1199
5	5.1795	0.1384	10.3386	0.1385	32.5133	0.1441	54.1186	0.0881
6	6.2557	0.1462	12.5215	0.1461	39.4974	0.1523	–	–
7	7.5337	0.1565	15.0461	0.1564	48.0939	0.1676	–	–
8	17.6879	0.1601	35.5139	0.1630	–	–	–	–

(c) Nonstructural acceleration -sensitive fragility curve parameters

Story	Slight		Moderate		Extensive		Complete	
	median	*beta*	*median*	*beta*	*median*	*beta*	*median*	*beta*
1	0.3428	0.1668	0.6860	0.1680	1.3727	0.1702	2.7372	0.1674
2	0.3442	0.1657	0.6848	0.1668	1.3645	0.1679	2.7126	0.1630
3	0.3386	0.1648	0.6791	0.1647	1.3558	0.1679	2.7554	0.1790
4	0.3517	0.1661	0.7071	0.1639	1.4161	0.1616	2.8759	0.1705
5	0.3729	0.1471	0.7470	0.1467	1.4982	0.1452	2.9615	0.1422
6	0.3745	0.1420	0.7462	0.1461	1.4960	0.1456	3.0089	0.1498
7	0.3530	0.1514	0.7074	0.1539	1.4153	0.1518	2.8411	0.1532
8	0.2752	0.1555	0.5473	0.1570	1.0991	0.1577	2.2068	0.1592

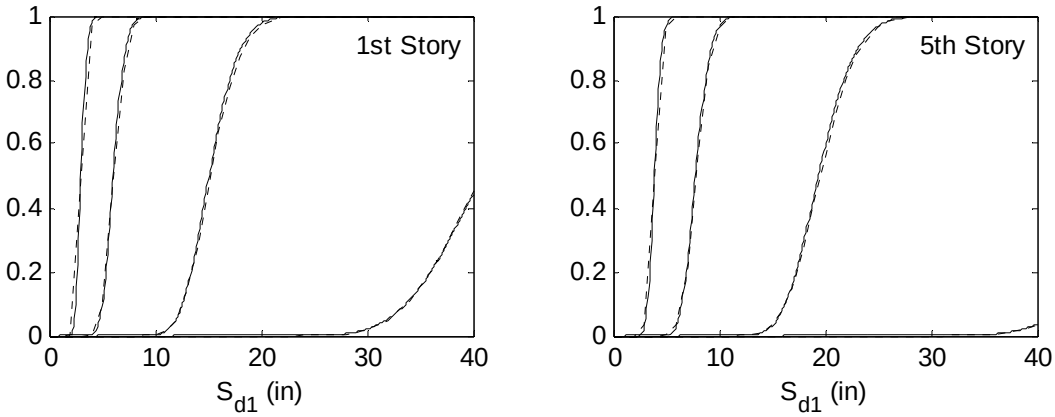

(a) Fragility curves of structural components

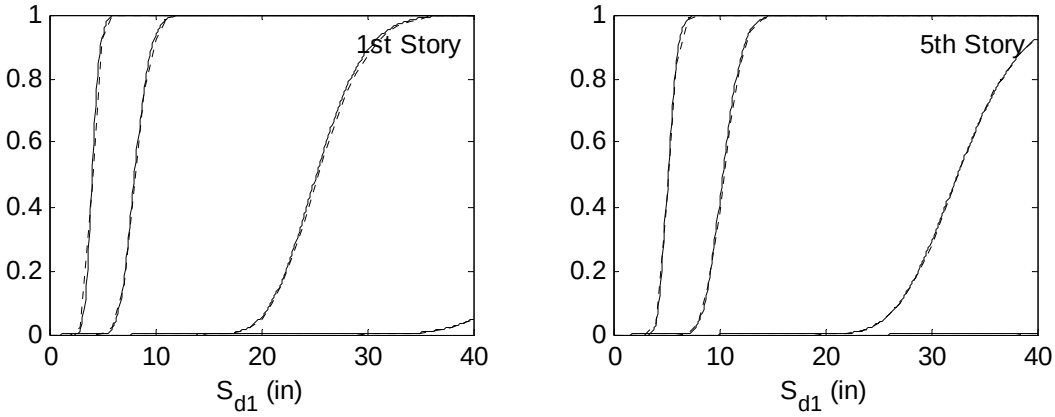

(b) Fragility curves of nonstructural components (drift-sensitive)

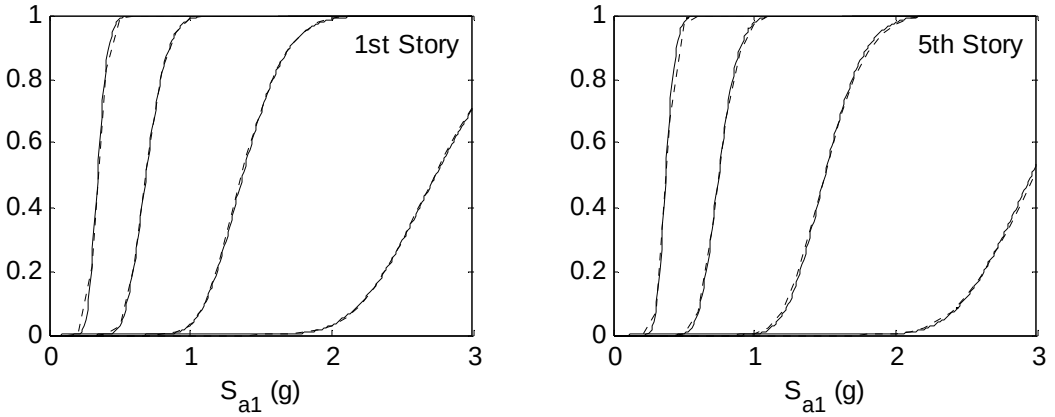

(c) Fragility curves of nonstructural components (acceleration-sensitive)

Figure 3.19: Fragility curves for the 1st and 5th stories of the eight-story building (dotted lines: by IDA data, solid lines: by a lognormal fit)

Analytical Fragility Curves of the Eight-Story Building

Table 3.7 summarizes estimated parameters of fragility functions for the eight-story building. If the conditional probability of a particular damage state is always zero within the predetermined *IM* limits (i.e. 40 inches for S_{d1} and 3.0 g for S_{a1}), lognormal curve fitting is not applicable. Thus, some of the parameters in severe damage states are not available.

Using the estimated parameters, the fragility functions for the 1st and 5th stories are shown in Figure 3.19 (solid lines). Comparing to the fragility curves developed directly from IDA results (dotted lines), it is observed that a lognormal CDF is a good fit for a fragility curve.

3.6 Cost Functions for the Eight-Story Building

This section describes the development of loss functions that are used to estimate economic losses as a function of ground motion intensity measure. The economic losses can be caused by either one or both of two cases: direct damage (e.g. structural and nonstructural damage and monetary losses during replacement time) and induced damage after effects of earthquakes (e.g. inundation, fires, and hazardous materials release) [18]. In this study, only direct damage is considered to estimate the dollar loss. For development of direct economic cost functions, HAZUS and FEMA are used as major references which provide a probabilistic approach to estimate mean economic loss using fragility curves. Figure 3.20 illustrates the basic scheme for developing cost functions.

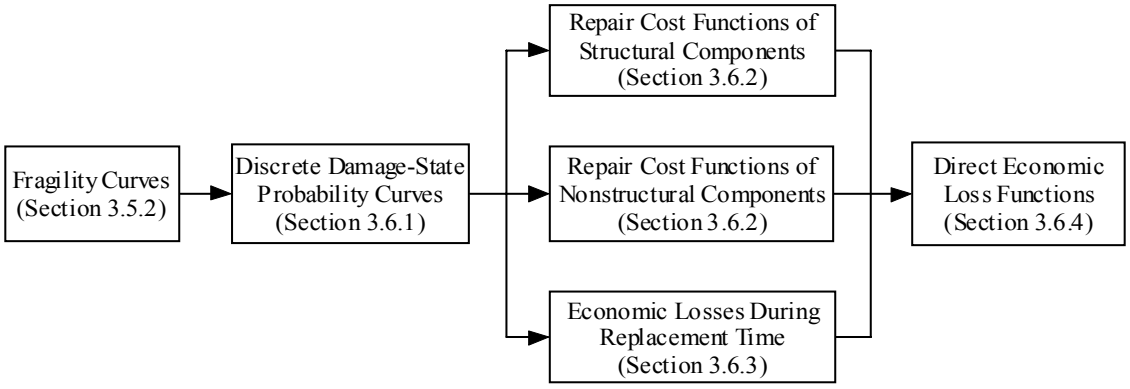

Figure 3.20: Flowchart for developing the direct economic loss functions

3.6.1 Discrete Damage-State Probability Curves

In order to estimate seismic damage in terms of dollar value, discrete damage-state probability curves are first constructed. These curves are calculated by taking the difference in probability between adjacent damage-state fragility curves [12]. Thus, discrete damage-state probabilities at a given Intensity Measure IM (i.e. S_{d1} or S_{a1}) are defined as

$$\begin{aligned} P_D[ds_i \mid IM] &= 1 - P_C[ds_{i+1} \mid IM] && i = 0 \\ P_D[ds_i \mid IM] &= P_C[ds_i \mid IM] - P_C[ds_{i+1} \mid IM] && i = 1,2,3 \\ P_D[ds_i \mid IM] &= P_C[ds_i \mid IM] && i = 4 \end{aligned} \tag{3.17}$$

where the damage state ds_i is defined as ds_0 = No damage, ds_1 = Slight, ds_2 = Moderate, ds_3 = Extensive, and ds_4 = Complete damage. The sum of $P_D[ds_i \mid IM]$ at any value of intensity measure equals to one. Figure 3.21 shows the discrete damage-state probability curves for structural and nonstructural components (drift-sensitive and acceleration-sensitive) of the 1st and 5th stories. The overlap of discrete damage curves in the figure indicates the degree of uncertainty in prediction of damage state at a given level of earthquake intensity measure [12].

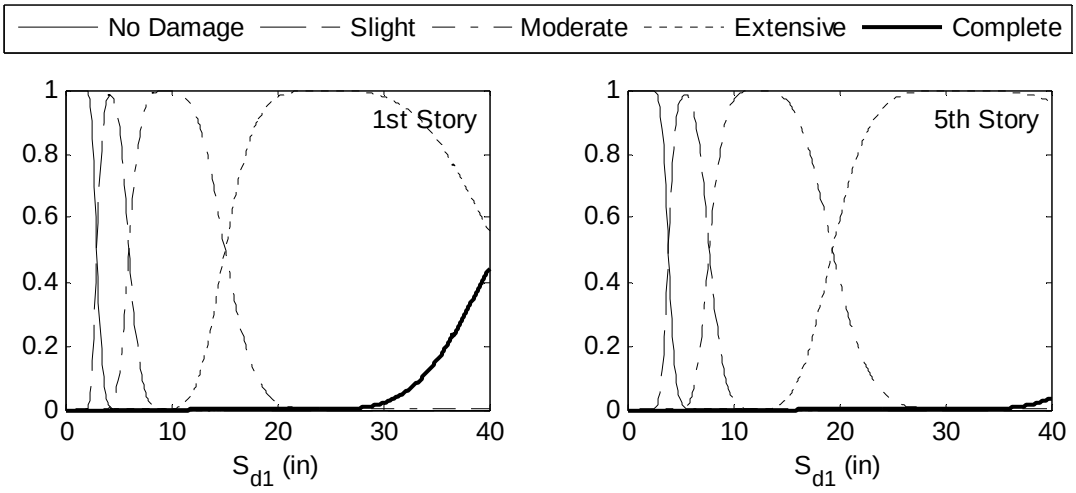

(a) Discrete damage probability curves of structural components

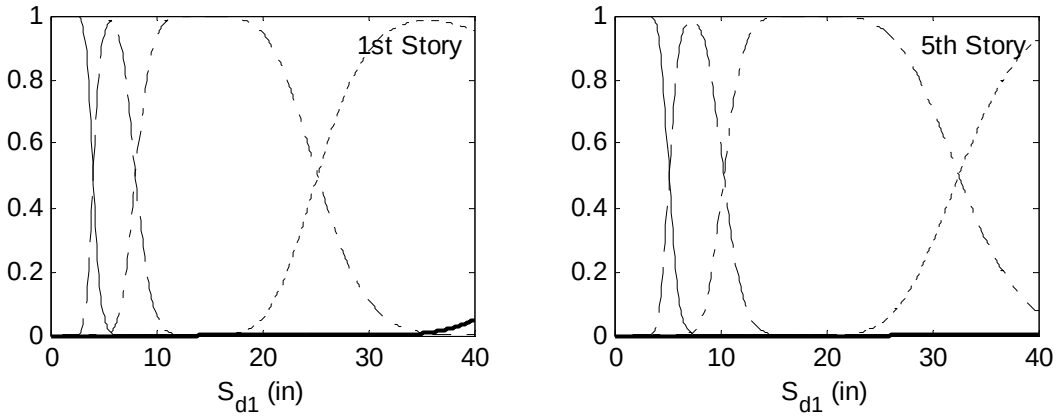

(b) Discrete damage probability curves of nonstructural components (drift-sensitive)

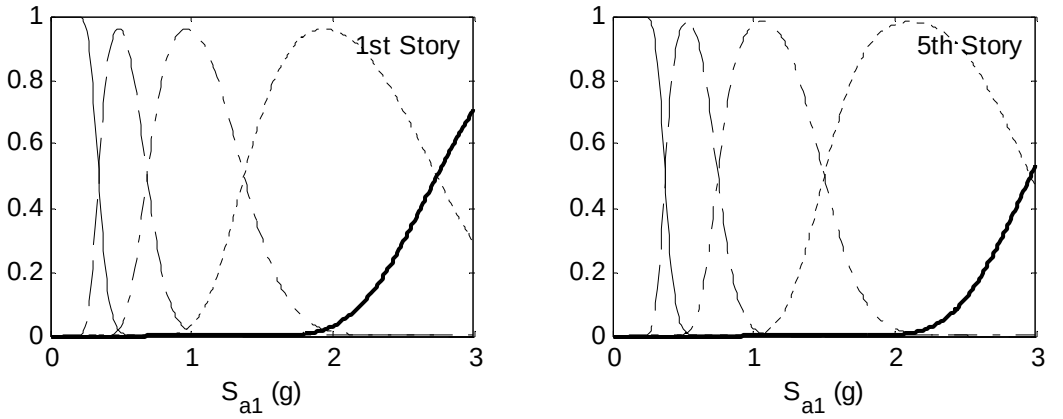

(c) Discrete damage probability curves of nonstructural components (acceleration-sensitive)

Figure 3.21: Discrete damage-state probability curves for the 1st and 5th stories

3.6.2 Repair Cost Functions for Structural and Nonstructural Damage

To develop repair cost functions, damage state costs of the structural system and nonstructural components are determined. Two basic parameters involved in the damage state cost are replacement cost of building per floor and repair cost ratio corresponding to each damage state.

For the eight-story building, the replacement cost of the building per square foot is evaluated reflecting building perimeter, story height, and location adjustment factors in R. S. Means 2007 [5], and it is estimated to be $\$142.55/ft^2$. Multiplying the replacement cost per square foot by a typical floor area of 8775 ft^2, the replacement costs of the building per floor is estimated as $1,250,876 (per floor).

Repair cost ratios are expressed as a percentage of building repair value related to occupancy classifications, and these ratios are obtained from HAZUS. Based on occupancy classification of the eight-story building, "Residential Multi Family Dwelling" (labeled as "RES3") [18], the repair cost ratio for each damage state of structural and nonstructural components are presented in Table 3.8.

Then damage state cost is defined as the product of the replacement costs of the building per floor and repair cost ratio corresponding to each damage state (Refer to Table 3.8).

Table 3.8: Repair cost ratios and damage state costs of the eight-story building [18]

(a) Structural components

Damage State	Slight	Moderate	Extensive	Complete
Repair Cost Ratio (%)	0.3	1.4	6.9	13.8
Damage State Cost ($/floor)	3,753	17,512	86,310	172,621

(b) Drift-sensitive nonstructural components

Damage State	Slight	Moderate	Extensive	Complete
Repair Cost Ratio (%)	0.9	4.3	21.3	42.5
Damage State Cost ($/floor)	11,258	53,788	266,437	531,622

(c) Acceleration-sensitive nonstructural components

Damage State	Slight	Moderate	Extensive	Complete
Repair Cost Ratio (%)	0.8	4.3	13.1	43.7
Damage State Cost ($/floor)	10,007	53,788	163,865	546,633

Structural Repair Costs

Repair cost of structural damage for damage state ds_i can be estimated as the product of structural damage state cost for ds_i and discrete probability of structural components in ds_i.

$$RCS_{ds_i}(S_{d1}) = DSC_S(ds_i) \times P_{D,S}[ds_i \mid S_{d1}] \tag{3.18}$$

where $DSC_S(ds_i)$ is the damage state cost for structural damage state ds_i (Table 3.8a) and $P_{D,S}[ds_i \mid S_{d1}]$ is the discrete probability of structural components for damage state (see Figure 3.22a in Section 3.6.1). Then repair cost for structural damage at a given intensity measure $RCS(S_{d1})$ is the sum of the products for each damage state.

$$RCS(S_{d1}) = \sum_{i=1}^{4} RCS_{ds_i}(S_{d1}) \tag{3.19}$$

The repair costs for structural damage in the 1st and 5th stories are shown in Figure 3.22 as a function of S_{d1}.

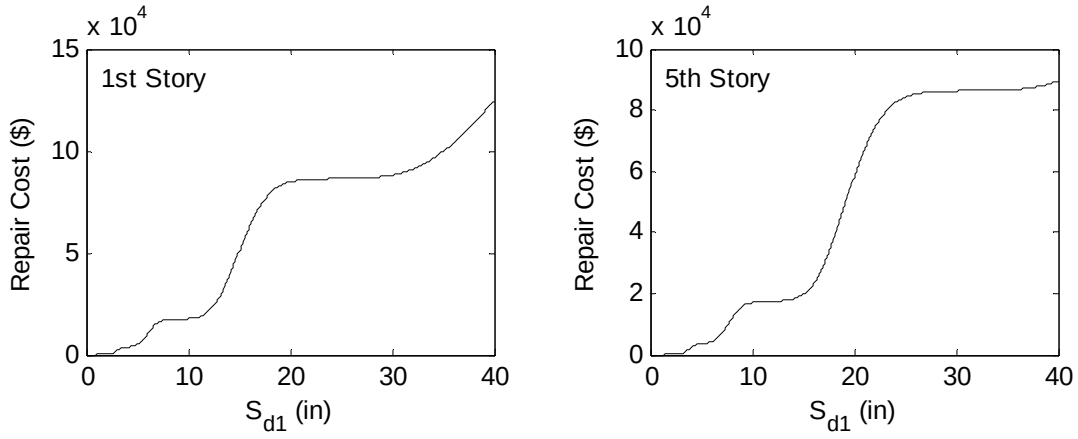

Figure 3.22: Repair cost functions for structural damage in the 1st and 5th stories

Nonstructural Repair Costs

A similar calculation is made for nonstructural damage which is subdivided into drift-sensitive and acceleration-sensitive damage. Repair cost of drift-sensitive nonstructural damage is

$$RCNSD(S_{d1}) = \sum_{i=1}^{4} RCNSD_{ds_i}(S_{d1}) = \sum_{i=1}^{4} DSC_{NSD}(ds_i) \times P_{D,NSD}[ds_i \mid S_{d1}] \qquad (3.20)$$

where $RCNSD_{ds_i}(S_{d1})$ is the repair cost of drift-sensitive nonstructural damage for damage state ds_i at a given intensity measure S_{d1}, $DSC_{NSD}(ds_i)$ is the damage state cost of drift-sensitive nonstructural damage for ds_i (Table 3.8b), and $P_{D,NSD}[ds_i \mid S_{d1}]$ is the discrete probability of drift-sensitive nonstructural damage for ds_i (Figure 3.23a).

Similarly, repair cost of acceleration-sensitive nonstructural damage is

$$RCNSA(S_{a1}) = \sum_{i=1}^{4} RCNSA_{ds_i}(S_{a1}) = \sum_{i=1}^{4} DSC_{NSA}(ds_i) \times P_{D,NSA}[ds_i \mid S_{a1}] \qquad (3.21)$$

where $RCNSA_{ds_i}(S_{a1})$ is the repair cost of acceleration-sensitive nonstructural damage for damage state ds_i at a given intensity measure S_{a1}, $DSC_{NSA}(ds_i)$ is the damage

state cost of acceleration-sensitive nonstructural damage for ds_i (Table 3.8c), and $P_{D,NSA}[ds_i \mid S_{a1}]$ is the discrete probability of acceleration-sensitive nonstructural damage for ds_i (Figure 3.23b). The repair costs for nonstructural damage in the 1st and 5th stories are shown in Figure 3.23 as a function of IM (S_{d1} or S_{a1}).

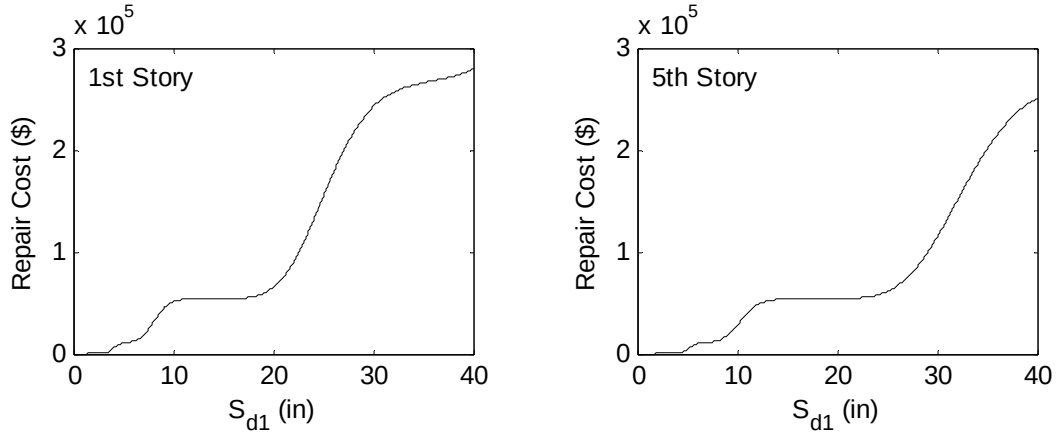

(a) Repair cost functions for drift-sensitive nonstructural damage

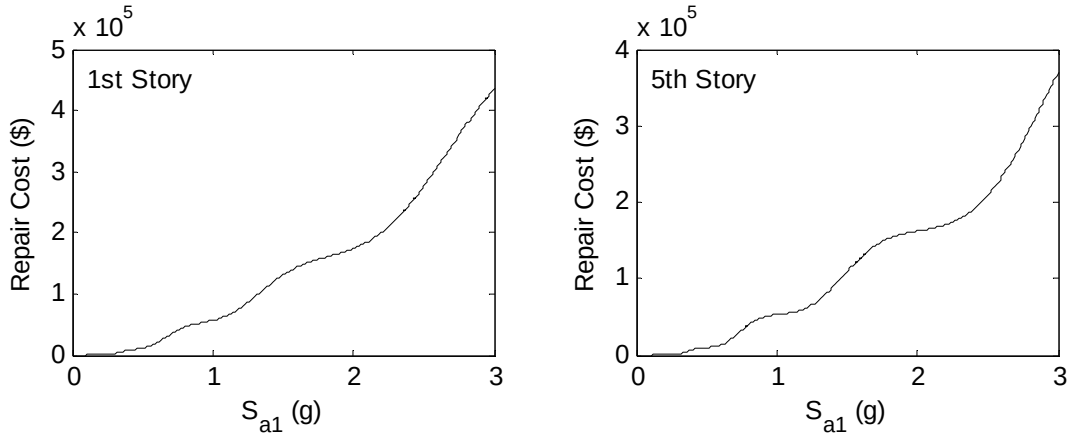

(b) Repair cost functions for acceleration-sensitive nonstructural damage

Figure 3.23: Repair cost functions for nonstructural damage in the 1st and 5th stories

The total repair costs of nonstructural damage $RCNS(S_{a1}, S_{d1})$ is estimated as the sum of Equations (3.20) and (3.21).

$$RCNS(S_{a1}, S_{d1}) = RCNSD(S_{d1}) + RCNSA(S_{a1}) \tag{3.22}$$

3.6.3 Monetary Losses during the Recovery time

Monetary losses during the restoring time are also included for estimating the direct economic losses. The monetary losses may be incurred when a building or portion of a building is closed during the recovery time. In the study, only the amount of rental income loss and relocation costs such as the costs of shifting and transferring and the rental of temporary space are considered as the monetary losses [18]. It is assumed that these losses are unlikely to incur when the building is in damage states ds_0 or ds_1 (No damage or Slight damage) [18]. The non-residential roof floor is excluded in the evaluation of these losses.

The relocation cost $REL(S_{d1})$ at a given intensity level S_{d1} is

$$REL(S_{d1}) = FA \times \begin{bmatrix} (1-\%OO) \times \sum_{i=2}^{4} \left(P_{D,S}[ds_i \mid S_{d1}] \times DC \right) + \\ \%OO \times \sum_{i=2}^{4} \left(P_{D,S}[ds_i \mid S_{d1}] \times \left(DC + RENT \times RT(ds_i) \right) \right) \end{bmatrix} \quad (3.23)$$

, and the rental income loss $RY(S_{d1})$ is given by

$$RY(S_{d1}) = (1-\%OO) \times FA \times RENT \times \sum_{i=2}^{4} \left(P_{D,S}[ds_i \mid S_{d1}] \times RT(ds_i) \right) \quad (3.24)$$

where FA is the floor area (8,775 ft^2), $P_{D,S}[ds_i \mid S_{d1}]$ is the discrete probability of the structural components for damage state ds_i at given S_{d1}, DC is the disruption cost (\$/ft^2), $RT(ds_i)$ is the recovery time for ds_i, $\%OO$ is the percent owner occupied, and $RENT$ is the rental cost (\$/ft^2/day) [18]. Thus, monetary loss $ML(S_{d1})$ during recovery time is estimated as the sum of the relocation cost and rental income loss

$$ML(S_{d1}) = REL(S_{d1}) + RY(S_{d1}) \quad (3.25)$$

The recovery time $RT(ds_i)$ in Equation (3.24) includes not only actual repair time but also other additional delays related to decision-making, negotiation,

inspection, and contract. The recovery time for buildings in the damage states slight or moderate will be close to the actual repair time, but for buildings in the damage states extensive or complete will be longer than the actual repair time due to additional tasks which must be carried out [18]. HAZUS provides the recovery times for a "RES3" building: 10, 120, 480, and 960 days for Slight, Moderate, Extensive, and Complete damage, respectively.

In HAZUS, the default values of the rental costs $RENT$ and disruption costs DC for a "RES3" building are given by \$0.02/ft^2/day and \$0.73/ft^2 which are given in 1994 US dollars [18]. To address an advance in prices from 1994 to the present, the price index history table provided by U.S. Department of Labor [36] is employed in this study. Hence, the rental and disruption cost are adjusted to be \$0.03/ft^2/day and \$1.06/ft^2. The monetary loss functions during the recovery time for the 1st and 5th stories are plotted in Figure 3.24.

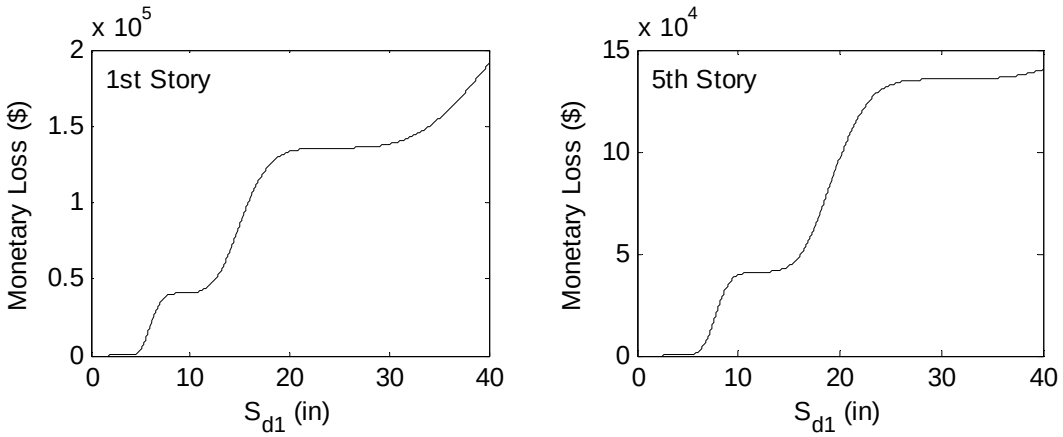

Figure 3.24: Monetary loss functions during the recovery time for the 1st and 5th stories

3.6.4 Direct Economic Cost Functions

The direct economic cost is the sum of costs induced by damaged structural and nonstructural (acceleration-sensitive and drift-sensitive) components and monetary

loss during the recovery time–the sum of Equations (3.19), (3.22), and (3.25). The direct economic cost function $DEC(S_{d1}, S_{a1})$ is formulated in terms of S_{d1} and S_{a1} as below

$$DEC(S_{d1}, S_{a1}) = RCS(S_{d1}) + RCNS(S_{d1}, S_{a1}) + ML(S_{d1}) \tag{3.26}$$

in which $RCS(S_{d1})$ is the repair cost of structural damage given by Equation (3.19), $RCNS(S_{d1}, S_{a1})$ is the repair cost of nonstructural damage given by Equation (3.22), and *ML* is the monetary loss during replacement time given by Equation (3.25).

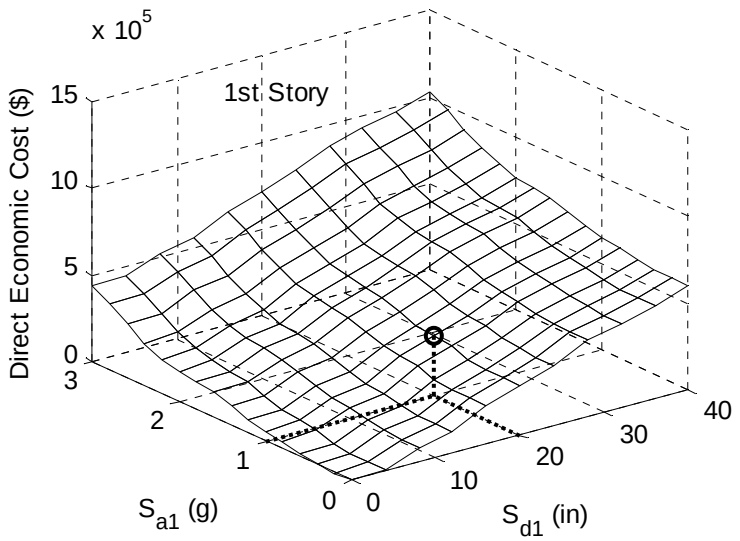

Figure 3.25: Direct economic cost function for the 1st story

As an example, Figure 3.25 shows the direct economic cost function for the 1st story. If the building is subjected to an earthquake having Intensity Measure of $S_{d1} = 20$ inches and $S_{a1} = 1.0$ g, the direct economic cost of the 1st story can be estimated at $DCE(20\text{ in}, 1.0\text{g})$ of Equation (3.26) that gives the estimation of $340,000.

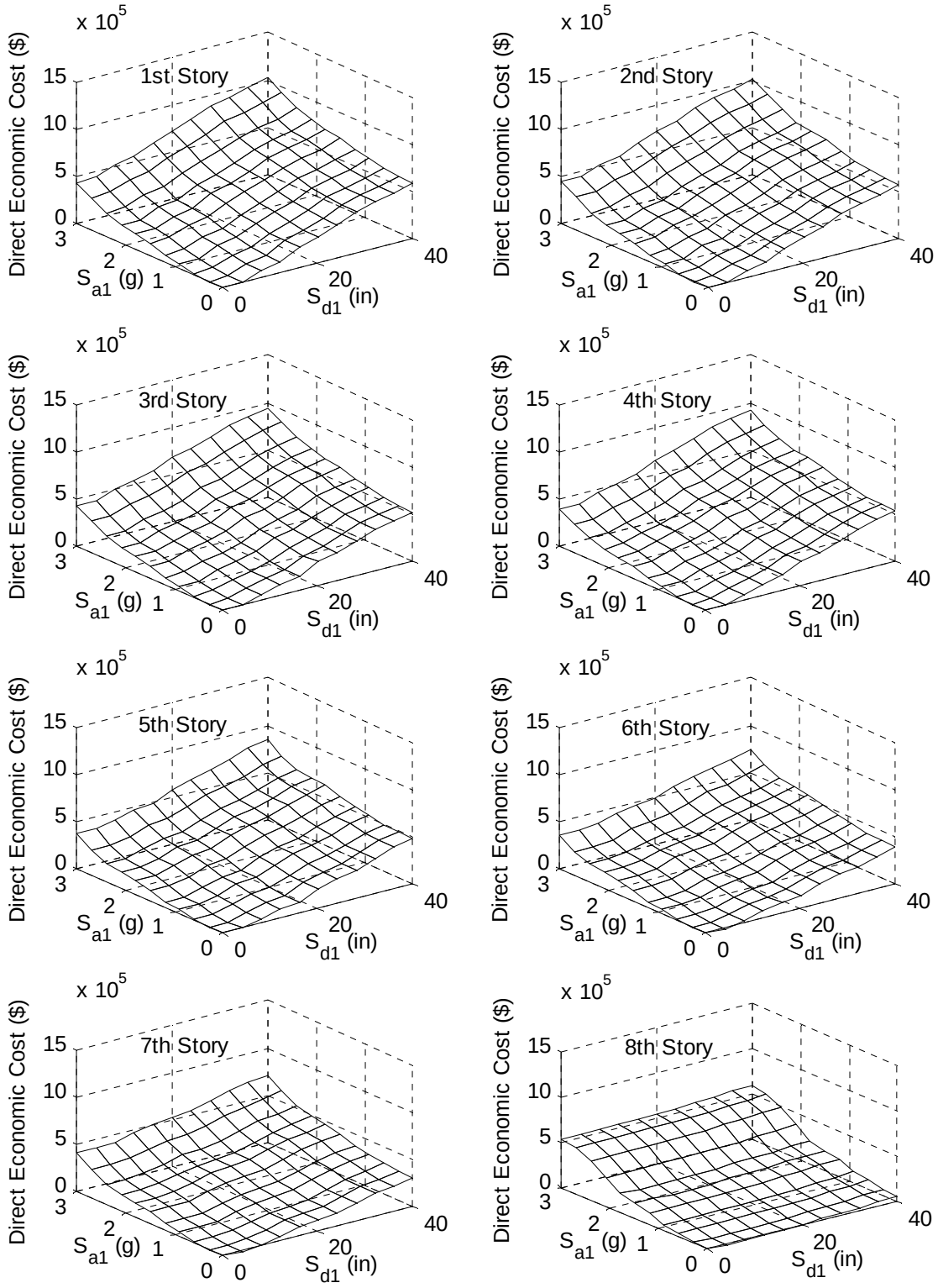

Figure 3.26: Direct economic cost functions for the eight-story building

The direct economic cost function for each story of the eight-story building is shown in Figure 3.26. In the lower stories, where the interstory displacement is much larger then the upper region (Refer to the failure rate curves in Figure 3.12), the cost is significantly influenced by drift-sensitive damage. In the 8th story, the direct economic cost is mainly influenced by acceleration-sensitive damage because monetary losses (relocation expenses and rental income loss) are not incurred in the non-residential area and interstory displacement is relatively small.

3.7 Exceedance Probability of Direct Economic Cost

The intensity measures, i.e. S_{d1} and S_{a1}, of the 10,000 samples of ground acceleration are measured, and they are assumed as samples of possible Intensity Measures *IM*s for an earthquake occurrence. As shown in Figure 3.27, in which the distribution of *IMs* is presented, the maximum values of the possible intensities are 9.3680 inches in spectral displacement and 0.9204 g in spectral acceleration. Thus, the direct economic cost functions developed in the previous section has sufficiently large ranges of *IM*s, i.e. [0, 40] inches of S_{d1} and [0, 3] g of S_{a1}, for damage cost analysis of the building.

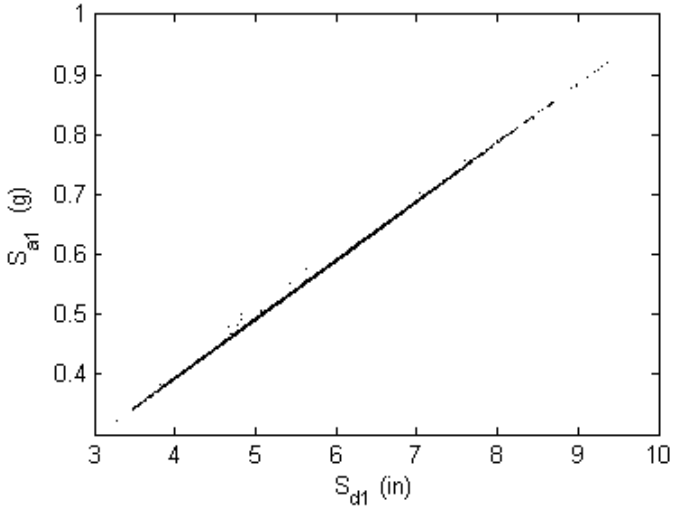

Figure 3.27: Distribution of intensity measures for an earthquake occurrence obtained from 10,000 samples of stationary ground motion (Section 3.3.1)

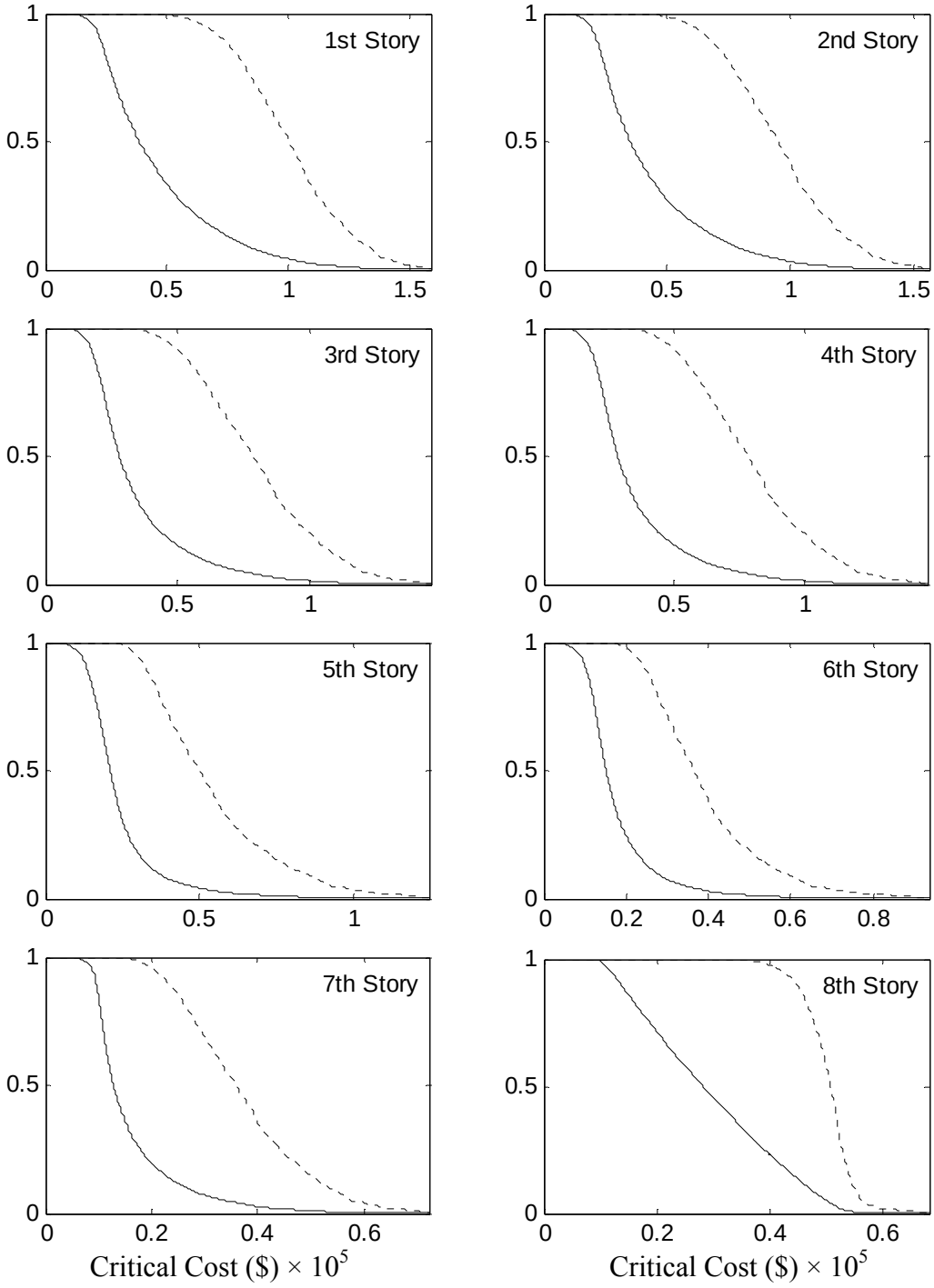

Figure 3.28: Probability curves of the direct economic cost for each story (solid line: probability due to an earthquake; dotted line: lifetime probability)

Applying the *IM* samples (S_{d1}, S_{a1}) in Figure 3.27 to Equation (3.26), 10,000 samples of direct economic cost, $C_j^{(i)}$, for each *i*-th story are obtained (where $j = 1,\ 2,\ \cdots,\ 10,000$). Then the exceedance probability of the direct economic cost $P_{EC}(C^{(i)} > c_{cr})$ due to an earthquake can be estimated by counting the number of times that the samples $C_j^{(i)}$ equal or exceed a critical cost c_{cr} and then dividing it by the total number of the samples.

$$P_{EC}(C^{(i)} \geq c_{cr}) \approx \frac{1}{10,000} \sum_{j=1}^{10,000} 1(C_j^{(i)} \geq c_{cr}) \tag{3.27}$$

The resulting probability curves are presented in Figures 3.28 with solid lines.

Assuming that earthquake occurrence is a Poisson process, the probabilities of lifetime cost are derived based on the estimated mean arrival rate $\hat{\lambda} = 0.2159$ quakes/year (see Section 3.3.5). The mean arrival rate $\nu_{EC}^{*(i)}(c_{cr})$ of particular earthquakes causing $C^{(i)} \geq c_{cr}$ is obtained as

$$\nu_{EC}^{*(i)}(c_{cr}) = 0.2159 P(C^{(i)} \geq c_{cr}) \tag{3.28}$$

Then the exceedance probabilities during the lifetime can be obtained by

$$P_{LEC}(C^{(i)} > c_{cr}) = 1 - e^{-75\nu_{EC}^{*(i)}(c_{cr})} \tag{3.29}$$

where $e^{-75\nu_{EC}^{*(i)}(c_{cr})}$ is the probability of no earthquake occurrence which causes $C^{(i)} \geq c_{cr}$ during the lifetime of 75 years. The resulting probability curves are presented in Figures 3.28 with dotted lines.

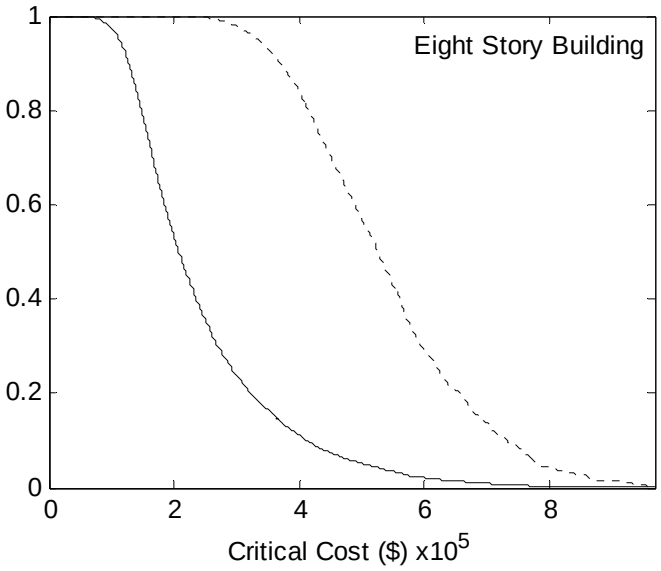

Figure 3.29: Probability curves of the direct economic cost for the eight-story building (solid line: probability due to an earthquake; dotted line: lifetime probability)

To evaluate the exceedance probability for the entire structure, the 10,000 samples of total direct economic cost C_j^T of the building is obtained as

$$C_j^T = \sum_{i=1}^{8} C_j^{(i)}, \quad j = 1,\ 2,\ \cdots,\ 10,000 \tag{3.30}$$

, and then following the procedure used to develop the cost probability curves for each story, the direct economic cost probability curves for the entire structure are presented in Figure 3.29.

CHAPTER 4

NONLINEAR ANALYSIS OF EIGHT-STORY BUILDING

Most buildings experience inelastic deformations caused by yielding of structural components under severe earthquake loads. Therefore, nonlinear analysis is essential to provide a more reliable estimation of structural performance. In contrast to Chapter 3, which describes the procedure for the linear analysis of the eight-story building subjected to stationary ground motion, this chapter introduces nonlinear analysis of the building with the effects of non-stationary properties of real earthquake ground motions.

The input ground motions are modeled as a non-stationary Gaussian process based on the time history record of the 1994 Northridge earthquake. The equations of motion for linear elastic MDOF systems are modified to recognize the effects of both geometric and material nonlinearities. Subsequently, methodology for solving these equations is introduced. Based on the nonlinear analysis, failure rate curves and fragility curves for the eight-story building are developed following the procedure in Section 3.5. Using fragility curves, the damage state probabilities are converted to dollar value of loss to estimate probable direct economic loss.

4.1 Generation of Non-stationary Ground Motion

Samples of ground motion are modeled as a non-stationary Gaussian process using a deterministic modulating envelope function $w(t)$ [6],[8].

$$A^*(t) = w(t)A_s(t) \tag{4.1}$$

where $A_s(t)$ is the sample of stationary Gaussian process with zero-mean (Refer to Section 3.3.1) and $A^*(t)$ is the sample of non-stationary Gaussian process. For the

envelope function $w(t)$, which is used to control the process amplitude level [19], the following window function found by Saragoni and Hart [30] is utilized.

$$w(t) = at^b e^{-ct} H(t) \tag{4.2}$$

where $H(t)$ is the unit-step function. The shape parameters b and c are defined as

$$b = -\varepsilon \ln \eta / \left[1 + \varepsilon\left(\ln \varepsilon - 1\right)\right] \tag{4.3}$$

$$c = b / \varepsilon T_w \tag{4.4}$$

The normalizing factor a is

$$a = \left(e / \varepsilon T_w\right)^b \tag{4.5}$$

in which $T_w = 2T_d$, T_d is the duration of strong ground shaking, which is defined as the time interval between the 5 and 95 percent levels of the cumulative integral of squared acceleration, ε is the ratio between the time of the peak of the envelope function and T_w, and η is the ratio of the amplitude at time T_w to the maximum amplitude [6],[30].

From the acceleration time history record of the Northridge earthquake (see Figure 4.1), the maximum amplitude is observed at t = 8.58 seconds. Thus, it is assumed that the peak of envelope function is at t = 8.58 seconds. Table 4.1 summarizes the parameters involved in the envelope function which is presented in Figure 4.3. Then 10,000 samples of non-stationary acceleration time history $A^*(t)$ are produced using Equation (4.1) with the 10,000 samples of $A_s(t)$ generated in Section 3.3.1.

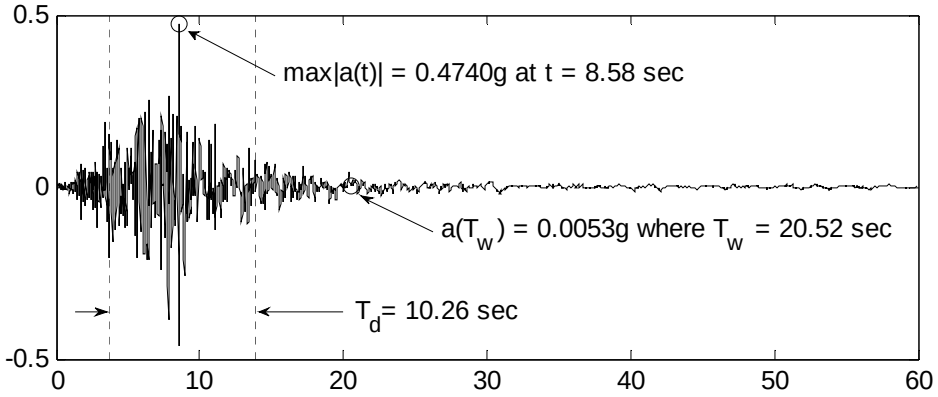

Figure 4.1: Acceleration time history of the 1994 Northridge earthquake
(Ground motion data was obtained from Cosmos Virtual Data Center website [9])

Table 4.1: Parameters of the envelope function $w(t)$

T_d	T_w	ε	η	a	b	c
10.2600	20.5200	0.4181	0.0113	4.89×10^{-5}	8.6352	1.0064

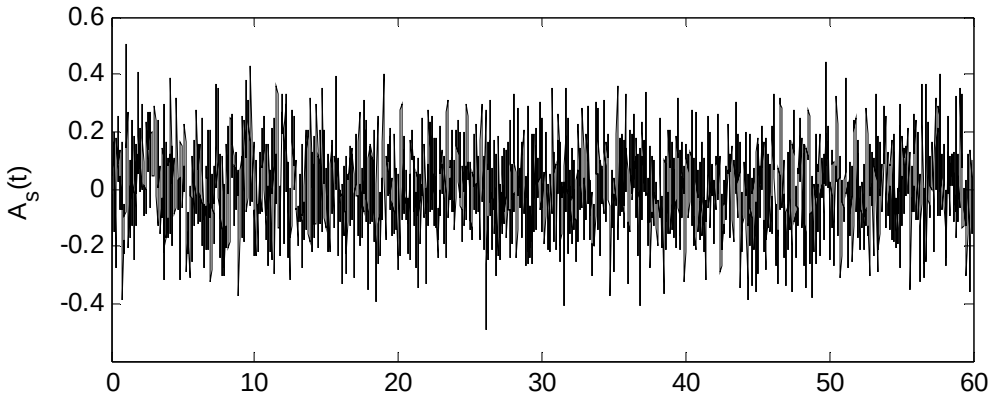

Figure 4.2: A sample of stationary ground acceleration

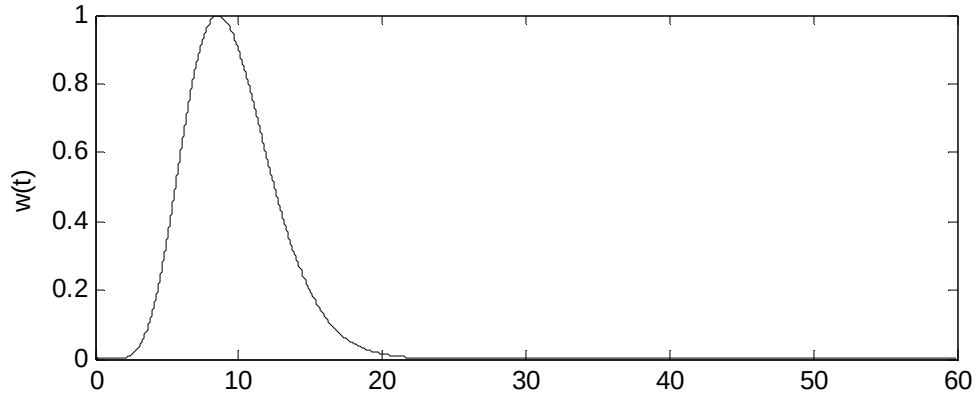

Figure 4.3: Deterministic modulate envelope function $w(t)$

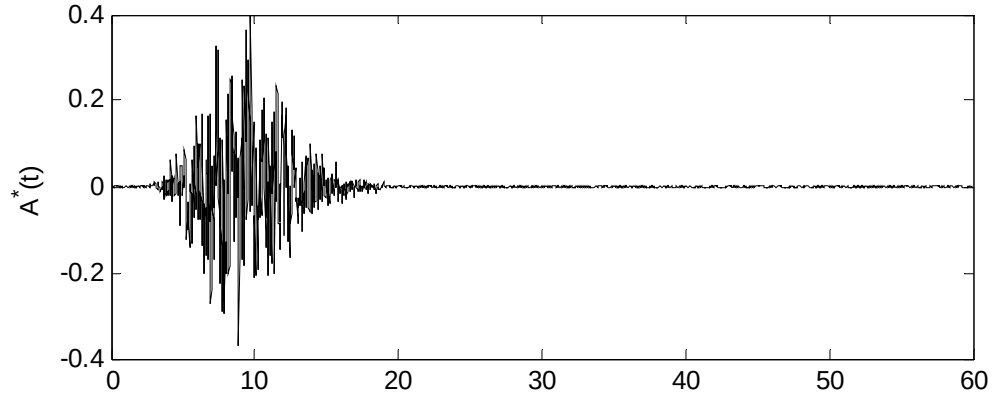

Figure 4.4: A sample of non-stationary ground acceleration

Same as in the previous chapter, the ground motion intensity levels are measured by first mode spectral displacement S_{d1} and acceleration S_{a1} of the eight-story building. Figure 4.5 shows the distribution of possible ground motion intensity levels which are obtained from the 10,000 samples of non-stationary ground motion. These values of the intensity measures will be used as input values of the direct economic cost function to obtain samples of the direct economic cost (Refer to Section 4.7).

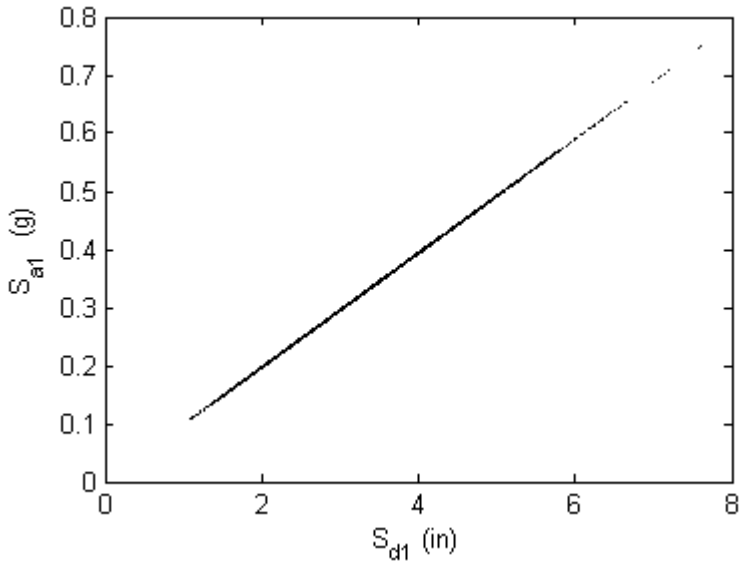

Figure 4.5: Distribution of possible intensity measures obtained from the 10,000 samples of non-stationary ground acceleration

4.2 Theoretical Background of Nonlinear Dynamic Analysis

During strong earthquakes, most structures undergo inelastic deformation. Thus, the nonlinear analysis is essential for a reliable prediction of structural performance. This section provides a brief discussion of geometric and material nonlinearities. Subsequently, the governing equations of motion are developed for nonlinear MDOF systems including the effects of both geometric and material nonlinearities.

4.2.1 Geometric and Material Nonlinearities

Geometric Nonlinearity

Structures may experience substantial lateral displacement under severe ground motion. If this is the case, the responses of structure are significantly influenced by P-Δ effects–the second-order moment effects of the gravity loads acting on the laterally deformed structure [7].

For building-type structures of which the total displacement can be assumed to be very small compared to the structural dimensions, the P-Δ effects can be implemented into a *direct and exact* solution method without iteration process for nonlinear dynamic analysis [40]. For example, consider the structural model in Figure 4.6.

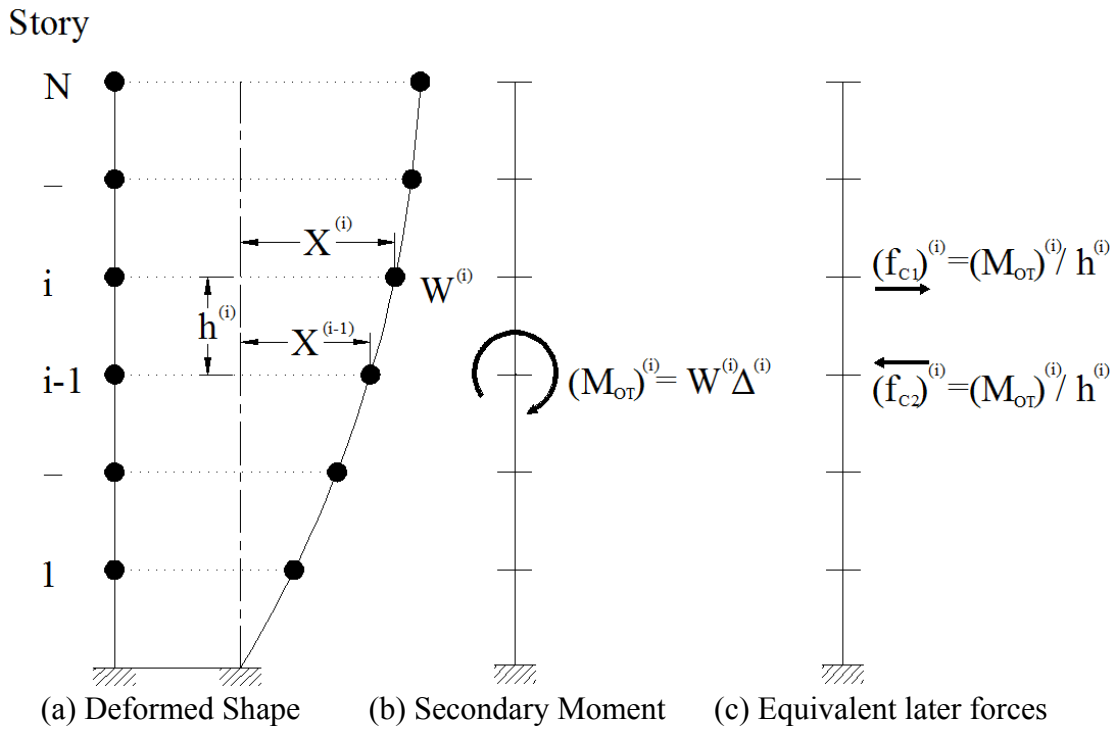

Figure 4.6: P-Δ effects on a structural model

Due to the weight above the *i*-th story $W^{(i)}$ acting on the deformed shape, the secondary overturning moment $M_{OT}{}^{(i)} = W^{(i)}\Delta^{(i)}$ where $\Delta^{(i)} = x^{(i)} - x^{(i-1)}$ is produced, see Figure 4.1(b). The moment can be resolved into two equivalent lateral forces $f_{C1}{}^{(i)}$ and $f_{C2}{}^{(i)}$ with the distance $h^{(i)}$, the height of the *i*-th story, as shown in Figure 4.1(c) [40].

$$\begin{aligned} f_{C1}{}^{(i)} &= W^{(i)}\Delta^{(i)} / h^{(i)} \quad \text{and} \\ f_{C2}{}^{(i)} &= -f_{C1}{}^{(i)} \end{aligned} \tag{4.6}$$

, or in terms of matrix notation

$$\begin{Bmatrix} f_{C1}{}^{(i)} \\ f_{C2}{}^{(i)} \end{Bmatrix} = \frac{W^{(i)}}{h^{(i)}} \begin{bmatrix} 1.0 & -1.0 \\ -1.0 & 1.0 \end{bmatrix} \begin{Bmatrix} x^{(i)} \\ x^{(i-1)} \end{Bmatrix} \tag{4.7}$$

Note that the matrix which contains $W^{(i)} / h^{(i)}$ factor is the geometric stiffness matrix for an element including axial force effects only [40]. Let $k_g^{(i)} = W^{(i)} / h^{(i)}$, then the geometric stiffness matrix of the *i*-th story can be rewritten as

$$\underline{k}_g^{(i)} = \begin{bmatrix} k_g^{(i)} & -k_g^{(i)} \\ -k_g^{(i)} & k_g^{(i)} \end{bmatrix} \tag{4.8}$$

In a manner similar to the above, lateral forces can be evaluated for all story levels, and the resulting lateral forces $\underline{k}_g \underline{x}(t)$ can be added to known external forces $\underline{p}_{ext}(t)$ acting on building [40],[41]. Then the total forces $\underline{p}(t)$ acting on the system is

$$\underline{p}(t) = \underline{p}_{ext}(t) + \underline{k}_g \underline{x}(t) \tag{4.9}$$

where $\underline{k}_g$ is the global geometric stiffness matrix of an *n*-story building

$$\underline{k}_g = \begin{bmatrix} k_g^{(1)} & -k_g^{(1)} & 0 & \cdots & 0 \\ -k_g^{(1)} & k_g^{(1)} + k_g^{(2)} & -k_g^{(2)} & & \vdots \\ 0 & & \ddots & & 0 \\ \vdots & & -k_g^{(n-1)} & k_g^{(n-1)} + k_g^{(n)} & -k_g^{(n)} \\ 0 & \cdots & 0 & -k_g^{(n)} & k_g^{(n)} \end{bmatrix} \tag{4.10}$$

Material Nonlinearity

In the previous two chapters, under the assumption that systems behave in a linear elastic range, lateral resisting forces $\underline{f_s}$ and displacements $\underline{x}(t)$ have a linear relationship; that is, $\underline{f_s} = \underline{k}\,\underline{x}(t)$ in which $\underline{k}$ is a constant stiffness matrix (in Equation (2.26)). Buildings, however, are expected to deform into the inelastic range, i.e. perform in a ductile manner, when subjected to strong ground motion. The force-deformation relation for structural elements of inelastic system is nonlinear and hysteretic [7]; thus, the stiffness term representing dynamic inelastic behavior can be expressed as

$$\underline{f_s}(t) = \underline{f_s}\left(\underline{x}(t), \dot{\underline{x}}(t)\right) \tag{4.11}$$

4.2.2 Equations of Motion for Nonlinear Inelastic MDOF Systems

General equations of motion for a nonlinear MDOF system can be written as

$$\underline{m}\,\ddot{\underline{x}}(t) + \underline{c}\,\dot{\underline{x}}(t) + \underline{f_s}(t) = \underline{p}(t) \tag{4.12}$$

where $\underline{m}$ is the mass matrix, $\underline{c}$ is the damping matrix, and $\underline{p}(t)$ is the vector of external forces. Substituting Equations (4.9) and (4.11) into Equation (4.12) gives the equations of motion including both geometric and material nonlinearities [7],[41].

$$\underline{m}\,\ddot{\underline{x}}(t) + \underline{c}\,\dot{\underline{x}}(t) + \underline{f_s}\left(\underline{x}(t), \dot{\underline{x}}(t)\right) = \underline{p}_{ext}(t) + \underline{\mathrm{k}}_{\mathrm{g}}\,\underline{x}(t) \tag{4.13}$$

4.3 Solution Method for Nonlinear Systems

Unlike the case of a linear elastic MDOF system (see Section 2.3), a modal superposition method is not applicable for nonlinear system. Therefore, the equations of motion (Equation (4.13)) for such systems responding into their nonlinear range need to be solved by a direct method.

In this study, Wilson's theta method is used to compute the nonlinear response of the eight-story building. The method is unconditionally stable, and its accuracy and stability depend on value of θ [7]. Chopra states that optimal accuracy can be achieved with $\theta = 1.42$ [7]. The procedure of Wilson's method is summarized in Algorithm 4.1 in which the input parameters are defined as: $\underline{m}_s$ is the vector of story mass, $\underline{k}_s$ is the vector of elastic story stiffness, $\underline{c}$ is the damping matrix, Δt is the time step of integration, and $a(t)$ is the input ground acceleration.

Algorithm 4.1 includes modified Newton-Raphson iteration method to minimize the error within each constant time step Δt. In the modified Newton-Raphson method (see Algorithm 4.2), the tangent stiffness matrix $\hat{\underline{k}}_T$, constructed at the beginning of the time step, is used throughout the iteration process. The iteration process continues until the incremental story displacements $\Delta \underline{x}_{(j)}$ in the j-th iteration becomes small enough to be considered as convergence [7].

Algorithm 4.1: Wilson's Method: Solution method for nonlinear MDOF systems [7]

Input Parameters: $\underline{m}_s$, $\underline{k}_s$, $\underline{c}$, Δt, θ and $a(t)$

Output Parameters: $\ddot{\underline{x}}(t)$, $\dot{\underline{x}}(t)$, and $\underline{x}(t)$

(a) Initial conditions

$\underline{x}_0 = \underline{0}$ and $\dot{\underline{x}}_0 = \underline{0}$

(b) Initial calculation

Construct $\underline{m}$ and $\underline{k}$ from $\underline{m}_s$ and $\underline{k}_s$

$(\underline{f}_s)_0 = \underline{k}\underline{x}_0$

$\underline{p}_{ext}(t) = -\underline{m}\underline{1}a(t)$

Solve $\ddot{\underline{x}}_0$ from $\underline{m}\ddot{\underline{x}}_0 = \underline{p}_0 - \underline{c}\dot{\underline{x}}_0 - (\underline{f}_s)_0$

$A = \frac{6}{\theta\Delta t}\underline{m} + 3\underline{c}$ and $B = 3\underline{m} + \frac{\theta\Delta t}{2}\underline{c}$

(c) Repeat calculations for each time step i

Implement $P-\Delta$ effects into the incremental forces

$\Delta\underline{p} = \underline{p}_{ext}(t_i) - \underline{p}_{ext}(t_{i-1}) + \underline{k}_g\Delta\underline{x}$ (see Section 4.2)

$\delta\hat{\underline{p}} = \theta(\Delta\underline{p}) + A\dot{\underline{x}}_{i-1} + B\ddot{\underline{x}}_{i-1}$

Determine the tangent stiffness matrix $\underline{k}_t$

(see Algorithm 4.3 in Section 4.2.2 for the eight-story structure or Algorithm 4.4 in Section 4.4.2 for the alternative structure)

$\hat{\underline{k}} = \underline{k}_t + \frac{3}{\theta\Delta t}\underline{c} + \frac{6}{(\theta\Delta t)^2}\underline{m}$

Solve for $\delta\underline{x}$ from $\hat{\underline{k}}$ and $\delta\hat{\underline{p}}$ using modified Newton-Raphson Method (see Algorithm 4.2)

$\delta\ddot{\underline{x}} = \frac{6}{(\theta\Delta t)^2}\delta\underline{x} - \frac{6}{\theta\Delta t}\dot{\underline{x}}_{i-1} - 3\ddot{\underline{x}}_{i-1}$

$\Delta\ddot{\underline{x}} = \frac{1}{\theta}\delta\ddot{\underline{x}}$

$\Delta\dot{\underline{x}} = (\Delta t)\ddot{\underline{x}}_{i-1} + \frac{\Delta t}{2}\Delta\ddot{\underline{x}}$

$\Delta\underline{x} = (\Delta t)\dot{\underline{x}}_{i-1} + \frac{(\Delta t)^2}{2}\ddot{\underline{x}}_{i-1} + \frac{(\Delta t)^2}{6}\Delta\ddot{\underline{x}}$

$\underline{x}_i = \underline{x}_{i-1} + \Delta\underline{x}$, $\dot{\underline{x}}_i = \dot{\underline{x}}_{i-1} + \Delta\dot{\underline{x}}$, and $\ddot{\underline{x}}_i = \ddot{\underline{x}}_{i-1} + \Delta\ddot{\underline{x}}$

Algorithm 4.2: Modified Newton-Raphson Iteration [7]

Input Parameters: $\underline{f_s}(t_i)$, $\delta\underline{\hat{p}}$, $\underline{k}_e$, $\underline{f_y}$, and $\hat{\underline{k}}$

Output Parameters: $\delta\underline{x}$ and $\underline{f_s}(t_{i+1})$

(a) Initialize data

$\underline{f_s}_{(0)} = \underline{f_s}(t_i)$, $\delta\underline{x}_{(0)} = 0$, $\hat{\underline{k}}_T = \hat{\underline{k}}$ and $\Delta R_{(1)} = \delta\underline{\hat{p}}$

(b) Repeat calculations for each iteration step j

Solve $\Delta\underline{x}$ from $\hat{\underline{k}}_T \Delta\underline{x}_{(j)} = \Delta R_{(j)}$

$$\underline{f_s}_{(j)} = \underline{f_s}_{(j-1)} + \underline{k}_{(j)}\Delta\underline{x}_{(j)}$$

$$\Delta\underline{f}_{(j)} = \underline{f_s}_{(j)} - \underline{f_s}_{(j-1)} + (\hat{\underline{k}}_T - \underline{k}_t)\Delta\underline{x}_{(j)}$$

$$\Delta\underline{R}_{(j+1)} = \Delta\underline{R}_{(j)} - \Delta\underline{f}_{(j)}$$

$$\delta\underline{x}_{(j)} = \delta\underline{x}_{(j-1)} + \Delta\underline{x}_{(j)}$$

4.4 Nonlinear Analysis of the Eight-Story Building

Nonlinear dynamic analysis of the eight-story building is performed under the following assumptions: (1) the building is subjected to ground acceleration in the N-S direction, (2) the building is simplified into a lumped-mass model, and (3) the gravity frames are not taken into account in story stiffness.

In nonlinear analysis, both geometric and material nonlinearities are considered. To illustrate the influence of the P-Δ effects and material inelasticity on the building response, the response time history of the eight-story building is presented for three cases: linear elastic and nonlinear inelastic with or without P-Δ effects. Failure rate curves are then obtained by nonlinear dynamic analysis. These curves provide more accurate prediction about seismic vulnerability of the eight-story building compared with those obtained by linear analysis.

4.4.1 Force–Displacement Relations

To determine tangent stiffness matrix in the solution method, see Step (c) of Algorithm 4.1, force-displacement relationship of frames needs to be characterized. The fore-displacement relationship of frames is found using a structural analysis program, MASTAN 2 [27]. The procedure is illustrated with the following numerical example using a moment frame in the 2nd story.

The moment frame in the 2nd story is modeled in MASTAN 2 as shown in Figure 4.7 in accordance to the section and material properties provided in Section 3.2. The modeling of the frame involves defining a set of lateral forces which are applied as a static load to nonlinear model of the frame (in this case, 0.5kips at each node N2 and N3). Then 1st-order inelastic analysis is performed with a load increment of 0.1 kips until the frame becomes fully plastic. Accordingly, at the applied load of 535.0 kips, two plastic hinges are developed at the beam ends, and additional plastic hinges at lower end of columns occur at 536.9 kips, and then the frame is fully plastic, see Figure 4.8.

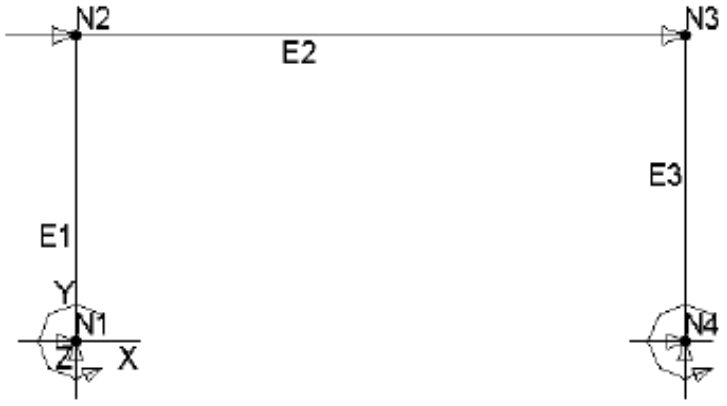

Figure 4.7: A moment frame in the 2nd story modeled in MASTAN2

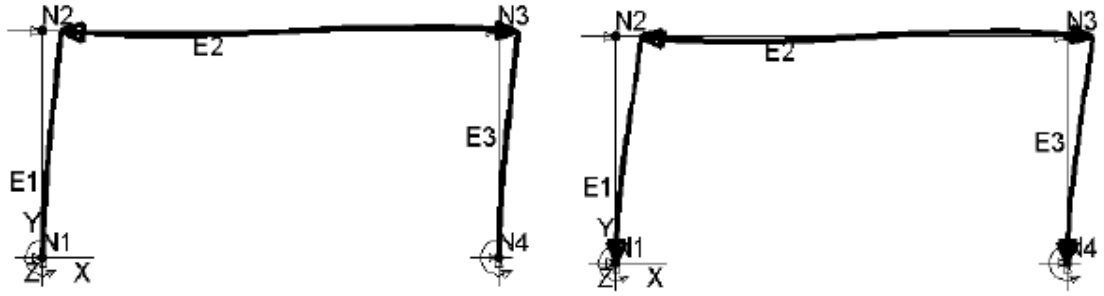

(a) Two plastic hinges at beam ends (b) Total four plastic hinges in the frame

Figure 4.8: Plastic hinges on deflected shape of the 2nd story moment frame

The deflection at the top of the frame against the total applied shear is plotted in Figure 4.9 which shows a bilinear relationship. A bilinear stiffness curve can be characterized by pre-yield stiffness (the slope of the first line), post-yield stiffness (the slope of the second line), and yield strength. The pre-yield stiffness was computed in Section 3.3.2 analytically. From the figure, yielding strength is estimated to be 536.9 kips, and post-yield stiffness is calculated as the slope of the second linear line which is almost zero, i.e. elastic-perfectly plastic behavior.

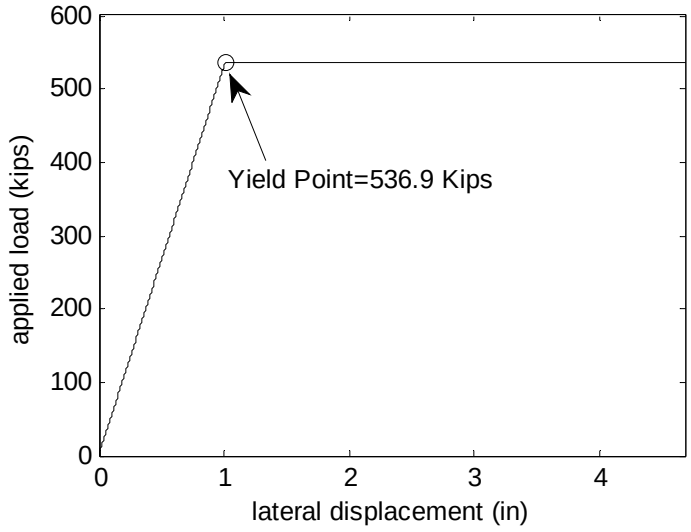

Figure 4.9: Force and displacement relationship of the 2nd story moment frame

The sum of the yield strength of each story frame in the direction of the seismic force is equivalent to the yield shear force of a story [2]. Thus, the yield shear force of the 2nd story is six times the yield force of the story frame (six identical moment frames in N-S direction, see Figure 3.3). In a similar manner, story stiffness is the sum of the lateral stiffness of all frames parallel to the seismic force. Table 4.2 summarizes the yield forces F_y and pre- and post-yield stiffness k_{s1} and k_{s2} of each story.

Table 4.2: Yield forces and lateral stiffness of the eight-story building

Story	Yield Force (kips)	Story Stiffness (kips/inches)	
	F_y	k_{s1}	k_{s2}
1	3301.8	3,435.720	0.0
2	3221.4	3,190.407	0.0
3	3221.4	3,190.407	0.0
4	2853.0	2,794.025	0.0
5	2853.0	2,794.025	0.0
6	2853.0	2,794.025	0.0
7	2532.6	2,453.820	0.0
8	2532.6	2,453.820	0.0

For a bilinear force-displacement model, a method to construct the tangent stiffness matrix is developed in Algorithm 4.3. In step (b) of the algorithm, when frames in the *n*-th story are loaded beyond their elastic limits, story stiffness equals $k_{s2}^{(n)}$, and then during unloading conditions, the frames are elastically unloaded, i.e. story stiffness equals its elastic story stiffness $k_{s1}^{(n)}$. The transition time from loading to unloading is determined by the change in sign of story velocity $\underline{\dot{x}}_i$ that indicates the change in direction of story displacement [7]. Once all story stiffnesses at time t_i are

determined, tangent stiffness matrix $\underline{k}_t$ can be constructed by Equation (3.3). This algorithm can directly be implemented to Wilson's theta method (Algorithm 4.1(c)).

Algorithm 4.3: Tangent stiffness matrix for moment frames

Input Parameters: $\underline{k}_{s1}$, $\underline{k}_{s2}$, $(\underline{F_s})_{i-1}$, $\Delta\underline{x}$, and $\dot{\underline{x}}_i$
Output Parameters: $\underline{k}_t$ and $(\underline{F_s})_i$

(a) Calculate shear forces $(F_s^{(n)})_i$ of the n-th story frames at time t_i
$(\underline{F_s})_i = (\underline{F_s})_{i-1} + \underline{k}_e \Delta\underline{x}$
for n = 1:8
if $|(F_s^{(n)})_i| > F_y^{(n)}$,
then $(F_s^{(n)})_i = sign((F_s^{(n)})_i) \cdot F_y^{(n)}$

(b) Determine stiffness $k^{(n)}$ of the n-th story at time t_i
for n = 1:8
if $|(F_s^{(n)})_i| < F_y^{(n)}$,
then $k^{(n)} = k_{s1}^{(n)}$
else if $sign(\dot{x}_i^{(n)}) \neq sign(\dot{x}_{i-1}^{(n)})$,
then $k^{(n)} = k_{s1}^{(n)}$
else, then $k^{(n)} = k_{s2}^{(n)}$

(c) Construct tangent stiffness matrix $\underline{k}_t$ using $k^{(n)}$

4.4.2 Nonlinear Responses of the Building

Using the 10,000 samples of non-stationary ground acceleration generated in Section 4.1, the responses of the eight-story building are obtained by Wilson's method (Algorithm 4.1). The structural properties of the eight-story building, $\underline{m}_e$, $\underline{k}_e$, and $\underline{c}$, are provided in Section 3.3.2, and the other input parameters are chosen as $\theta = 1.42$

and $\Delta t = 0.01$ seconds. Figure 4.10 shows a sample of the displacement response of the 1st story (solid line).

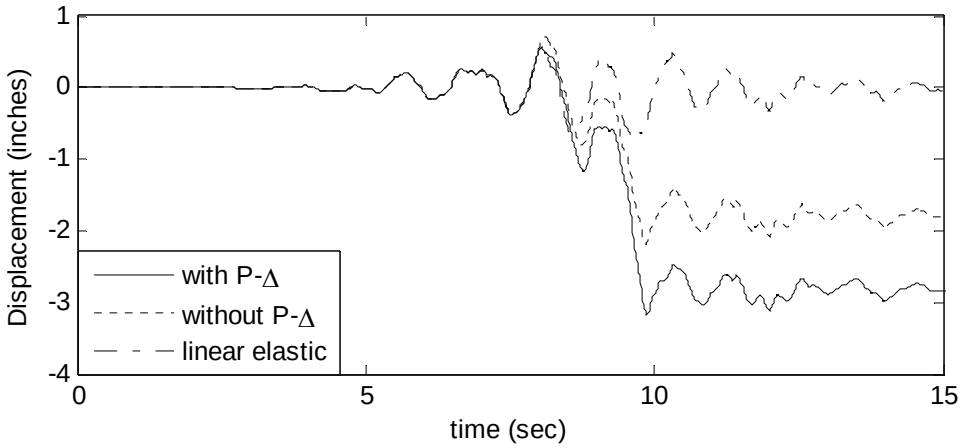

Figure 4.10: Comparison of the different cases of structural analysis

In general, nonlinear analysis is a more accurate method to predict response of buildings subjected to strong ground motion. Besides, the P-Δ effects may be critical in the seismic performance of steel moment frame buildings, which are relatively flexible structure and may be subjected to large lateral displacement [12].

Figure 4.10 is presented for comparison of the dynamic responses obtained by different analysis methods. Under the ground motion presented in Figure 4.5, the displacement response of the 1st story is obtained for three cases: (1) linear elastic analysis, (2) nonlinear analysis excluding P-Δ effects, and (3) nonlinear analysis including P-Δ effects. The displacement responses are very close while the building remains elastic, but significant differences are observed when strong motion starts at $t \approx 8$ seconds, see Figure 4.5. Also, the figure shows that P-Δ effects have a significant influence on the post-yield response [7]. These differences in the post-yield behavior of the building suggest that it is essential to include P-Δ effects in predicting the seismic response of the building.

4.4.3 Failure Rate

Failure rate curves of the eight-story building are developed by nonlinear dynamic analysis. The failure rate curve represents exceedance probability of damage to building (i.e. plot of peak building response versus exceedance probability in this study). Similar to the method discussed in Section 3.4, damage of the building is measured by maximum interstory drift ratio $\max_t |\Delta_R^{(i)}(t)|$ and floor acceleration $\max_t |A_f^{(i)}(t)|$ in which $\Delta_R^{(i)}(t)$ and $A_f^{(i)}(t)$ are defined in Equations (3.5) and (3.6).

Using the samples of nonlinear responses obtained in the previous section, the two damage indicators are calculated for each of the samples. Then the failure probabilities due to an earthquake are estimated using Equation (3.7). Lifetime failure probabilities are also evaluated under the assumption of a Poisson process for the occurrence of earthquakes with the estimated mean occurrence rate of $\hat{\lambda} = 0.2159$ quakes/year (Refer to Section 3.4 for detailed procedure). The resulting failure probability curves are presented in Figures 4.11 and 4.12.

Comparison is made with the failure curves obtained by linear analysis, see Figures 3.12 and 3.13. Base on the failure rate curves developed in terms of interstory drift ratio (Figures 3.12 and 4.11), much higher failure rate is observed in the lower stories where the frames are likely to be deformed beyond their yield points. However, the failure rates developed in terms of floor acceleration do not show a large difference from those of the linear elastic system (compare Figures 3.13 and 4.12).

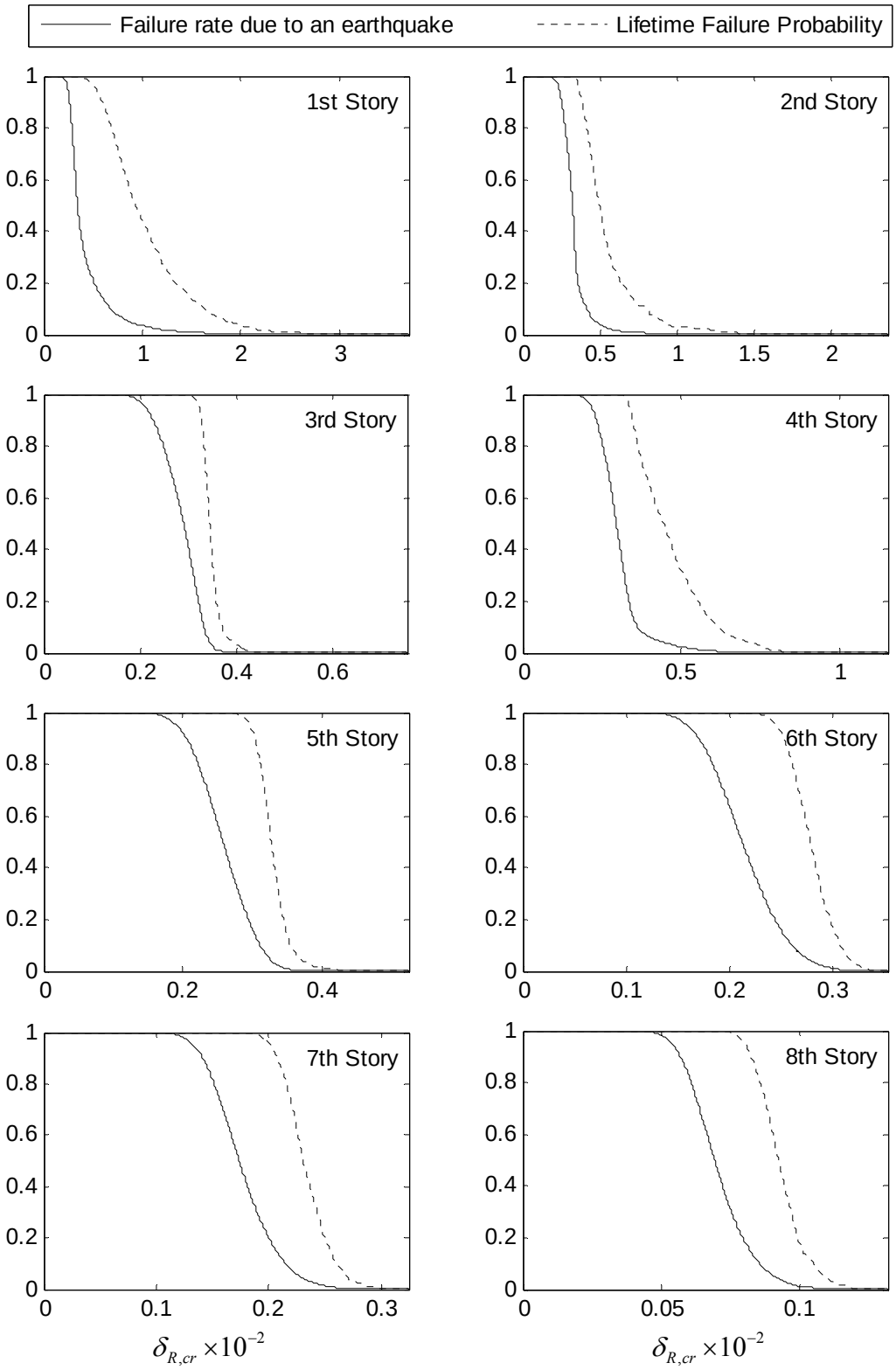

Figure 4.11: Failure rates of the eight-story building in terms of interstory drift ratio

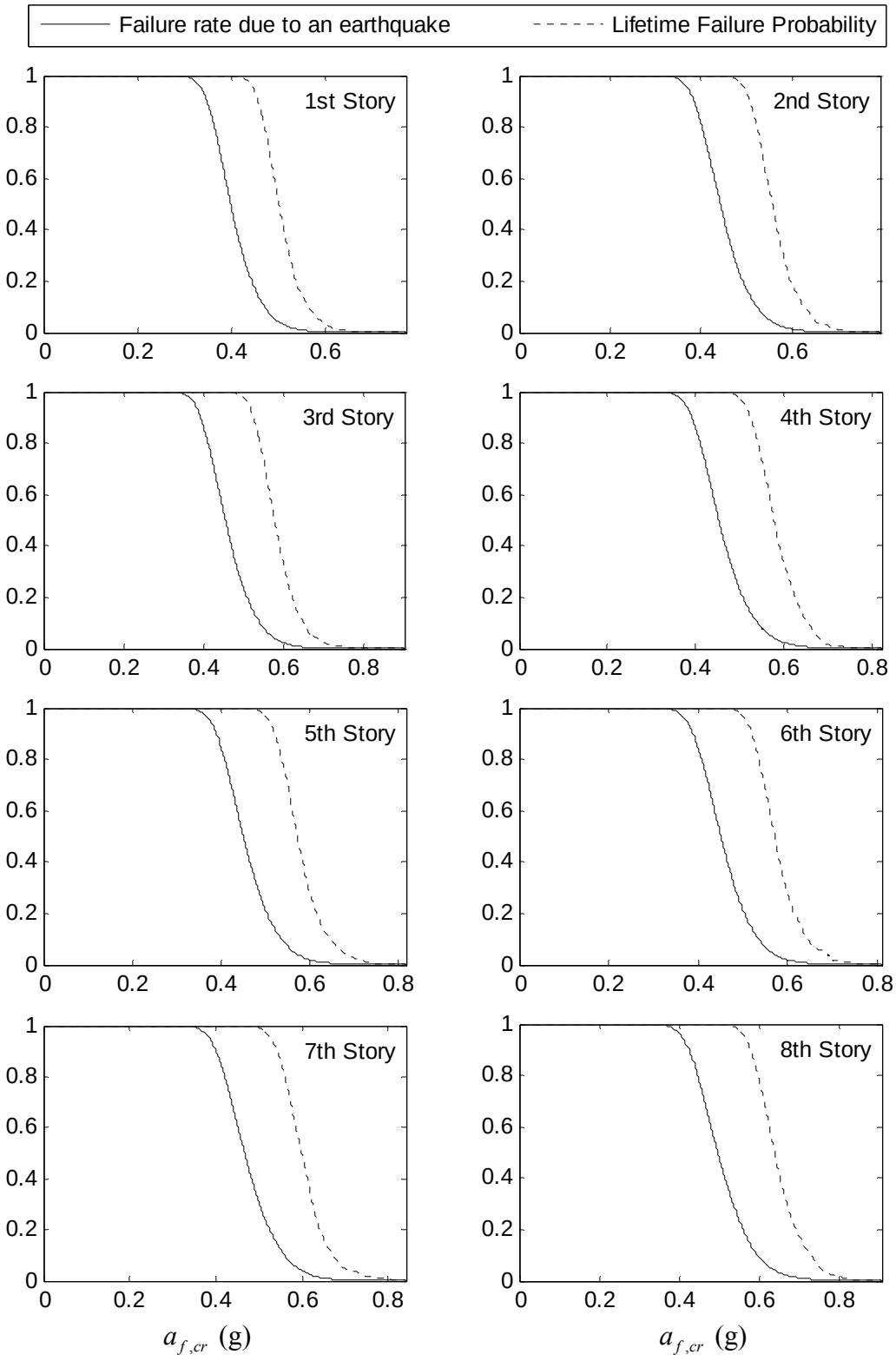

Figure 4.12: Failure rates of the eight-story building in terms of floor acceleration

4.5 Direct Economic Cost Function

In this section, basic concepts related to developing direct economic cost functions are briefly reviewed, and some characteristics of incremental dynamic analysis (IDA) curves generated by nonlinear dynamic analysis are discussed.

Similar to the previous chapter, direct economic cost functions are derived from fragility curves having four damage states, and incremental dynamic analysis method is utilized to construct fragility curves analytically.

4.5.1 Fragility Curves

The fundamentals of incremental dynamic analysis (IDA) and fragility curve were discussed in Section 3.5. Recall the definitions of IDA and fragility curve. The IDA is a parametric analysis method to estimate structural performance under several earthquake ground motions [38], and fragility curve shows the conditional probability of reaching or exceeding a particular damage state as a function of earthquake intensity measure.

Incremental Dynamic Analysis (IDA)

IDA curves are characterized by Damage Measure *DM* (maximum interstory drift ratio $\Delta_{R,\max}^{(i)}$ or floor acceleration $A_{f,\max}^{(i)}$) and Intensity Measure *IM* (first mode spectral displacement S_{d1} or acceleration S_{a1}), as introduced in Section 3.5.1. The basic procedure for developing IDA curves was outlined in Algorithm 3.1 in which a linear elastic dynamic analysis method is used to estimate *DM*. In general, nonlinear analysis method provides more reliable estimate of building performance. Thus, the nonlinear analysis method is implemented in Algorithm 3.1 by modifying Step 1-3 (b); that is, *DM* is obtained by Algorithm 4.1 and Equations (3.5) and (3.6).

IDA curves of linear elastic systems (e.g. Figure 3.16) show a linear relation between *IM* and *DM*. For nonlinear structural systems, however, the relationship between *IM* and *DM* is not linear in high intensity range in which large inelastic deformation occurs [21]. For example, consider the IDA curves in Figure 4.13 generated using four different accelerograms. Beyond the intensity measure of $S_{d1} \approx 4$ inches, the relationship between the maximum interstory drift ratio and spectral displacement is nonlinear. This shows the influence of geometric and material nonlinearities on the post-yield responses of the 1st story.

Figure 4.13 also shows that the shape or pattern of IDA curve depends on input ground acceleration. In *Incremental Dynamic Analysis*, Vamvatsikosy and Cornell [39] state that because IDA study depends on not only structural model but also ground motion, it is difficult to predict the responses of the structure. That is, when a structural model is subjected to different ground motions, distinctive responses may be observed. They present four patterns of IDA curves; "A softening case", "A bit of hardening", "Severe hardening", and "Weaving behavior" (e.g. Figure 4.13). In an extreme case of the hardening, called "structural resurrection," structures severely damaged at some intensity measure may be still sustained at a higher seismic intensity level due to excessive hardening [39]. For example, Figure 4.14 shows the 1st story of the eight-story building is forced to collapse within the intensity range of $S_{d1} \approx$ [12, 14] inches, but it experiences less damage at higher levels of the intensity measure.

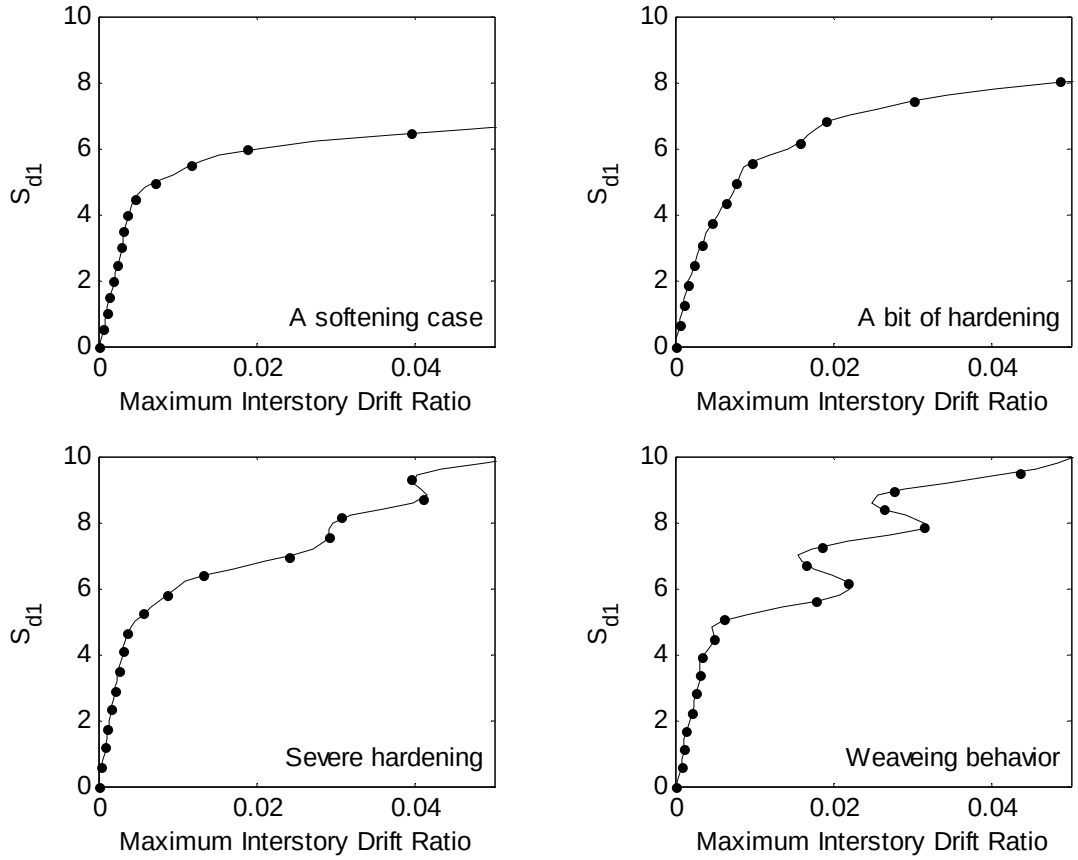

Figure 4.13: IDA curves for the 1st story of the eight-story building subjected to four different accelerograms

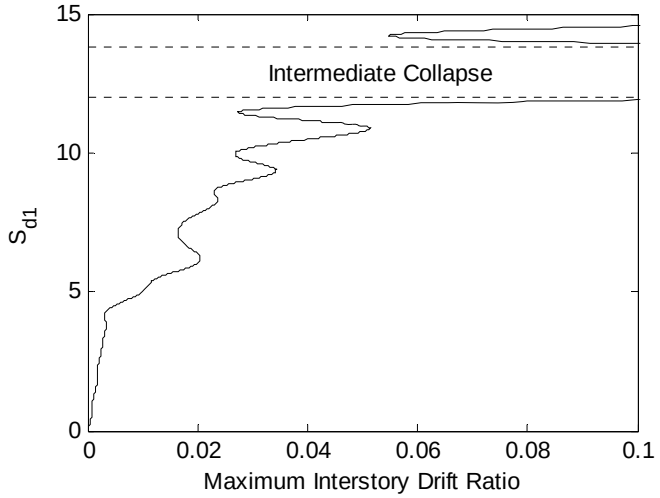

Figure 4.14: IDA curves for the 1st story showing an extreme case of hardening

In addition, IDA method results in a heavy computational burden for nonlinear structural models or may cause numerical instability in calculating *DM* at high *IM* [38],[39]. Thus, only the 100 artificial earthquake samples are used in incremental dynamic analysis of the eight-story building within the predetermined *IM* limits of $S_{d1} = 10$ inches and $S_{a1} = 1$ g. Figure 4.15 shows ten IDA curves generated for the 1st and 5th stories.

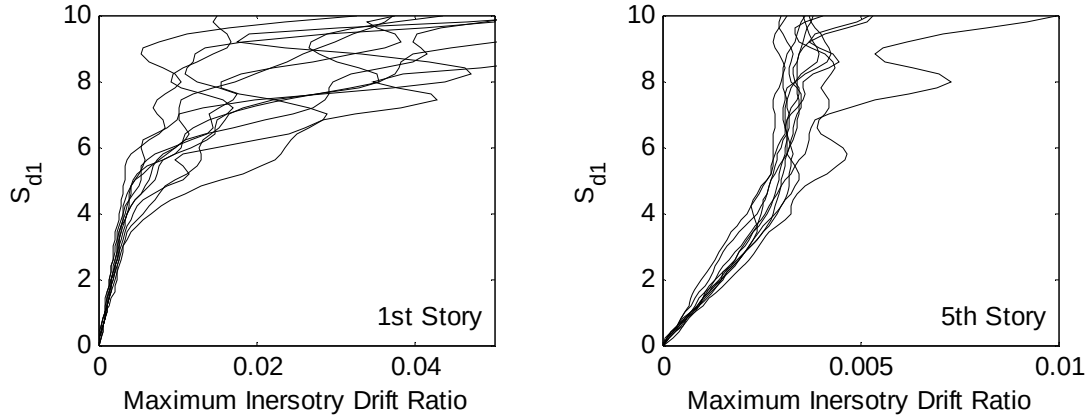

(a) Ten IDA curves as a function of spectral displacement

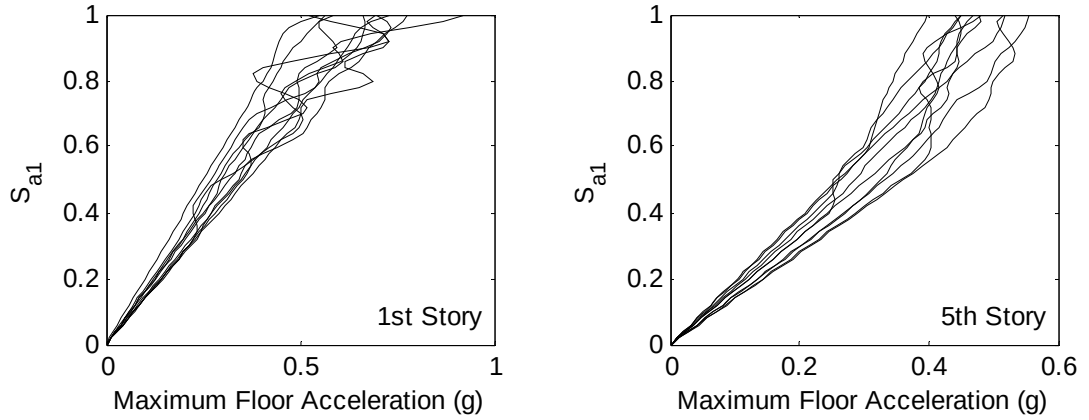

(b) Ten IDA curves as a function of spectral acceleration

Figure 4.15: Ten IDA curves for the 1st and 5th stories

Fragility Curves

Fragility curves represent the conditional probability of building damage in terms of *IM*. From the IDA results, the fragility curves are constructed analytically, and then they are expressed in the form of lognormal CDF (Refer to Steps 2 and 3 in Section 3.5.2). Same as Chapter 3, the fragility curves are constructed for structural and nonstructural (drift-sensitive and acceleration-sensitive) components based on four damage states, i.e. Slight, Moderate, Extensive, and Complete. The thresholds of each damage state given in Table 3.2 and 3.3 are used to define the damage state of each component.

The procedure to construct a fragility curve is briefly reviewed. The damage state probability at a given *IM* can be estimated using Equation (3.12). By estimating the damage-state probability for various levels of *IM*, a set of discrete points on a fragility curve is obtained. These discrete points are used to estimate median $\overline{IM}_{ds}$ and log standard deviation β_{ds} of the fragility function given in Equation (3.13). Then the conditional probabilities can be obtained at any intensity level from the fragility function.

Figure 4.16 shows the fragility curves for the 1st and 5th stories developed by nonlinear dynamic analysis. From left to right in the figure, the fragility curves represent the conditional probability of Slight, Moderate, Extensive, and Complete damages, respectively.

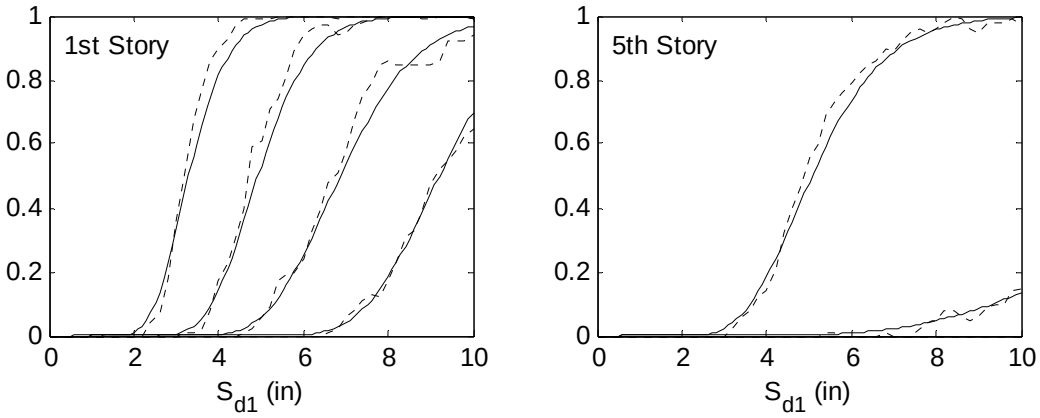

(a) Fragility curves of structural components

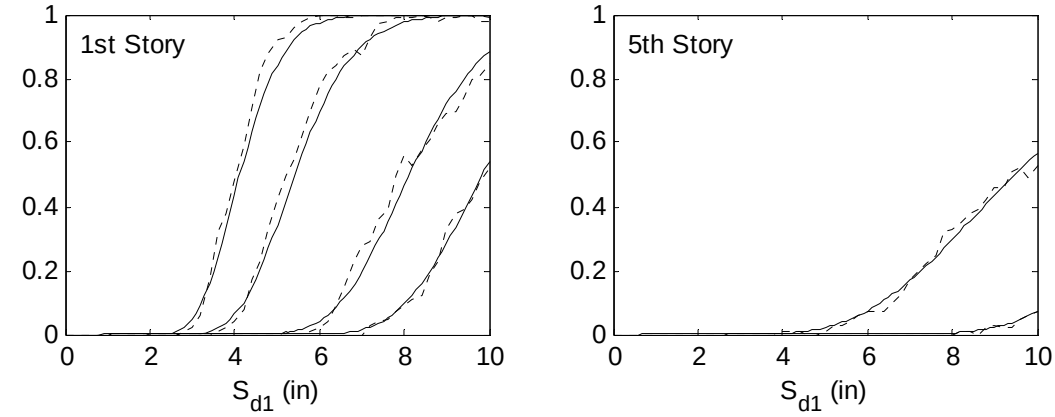

(b) Fragility curves of non-structural components (drift-sensitive)

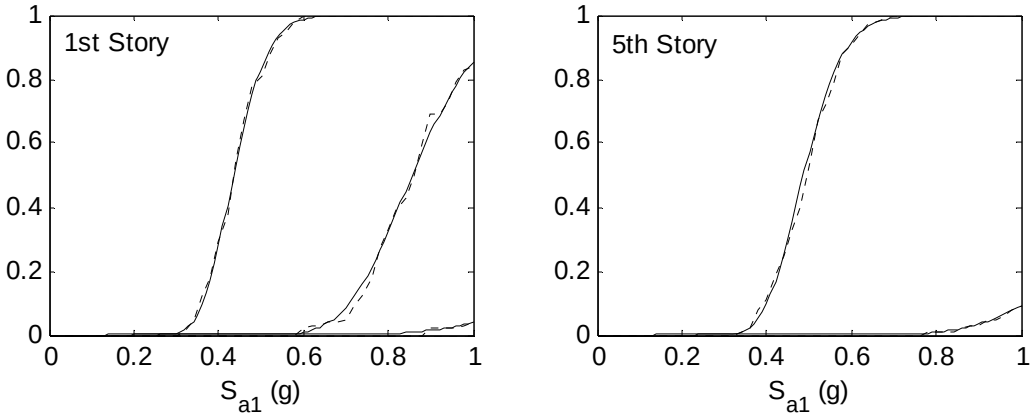

(c) Fragility curves of non-structural components (acceleration-sensitive)

Figure 4.16: Fragility curves for the 1st and 5th stories of the eight-story building (dotted lines: by IDA data, solid lines: by a lognormal fit)

4.5.2 Direct Economic Cost Functions

Direct economic cost for the eight-story building is estimated using the fragility curves developed by nonlinear analysis. For a given value of Intensity Measure *IM*, the fragility curves distribute damage of building components among the four damage states. From these curves, discrete damage state probabilities are calculated by taking the difference between the cumulative probabilities of successive damage states (Refer to Equation (3.17) in Section 3.6.1). The discrete damage state probabilities are then used as input to the estimation of the direct economic loss.

Using the repair cost functions developed in Section 3.6.2, damage state probabilities are converted to dollar loss. Repair cost for damaged component is calculated as the sum of the products of damage state cost (Table 3.8) and corresponding discrete damage state probability over all four damage states. In addition, monetary losses during recovery time are estimated as the sum of rental income loss and relocation costs. Refer to the repair cost functions in Section 3.6: Equations (3.19), (3.20) and (3.21) for damaged building components, and Equation (3.25) for monetary loss.

Direct economic costs are then estimated by the sum of costs induced by damaged structural and nonstructural (drift-sensitive and acceleration-sensitive) components and monetary loss during the recovery time. Figure 4.17 shows the direct economic cost functions for the eight story building. Based on these cost functions, the seismic performance of the existing moment frame building will be compared to an alternative structural system in terms of the exceedance probability of direct economic cost in Section 4.7.

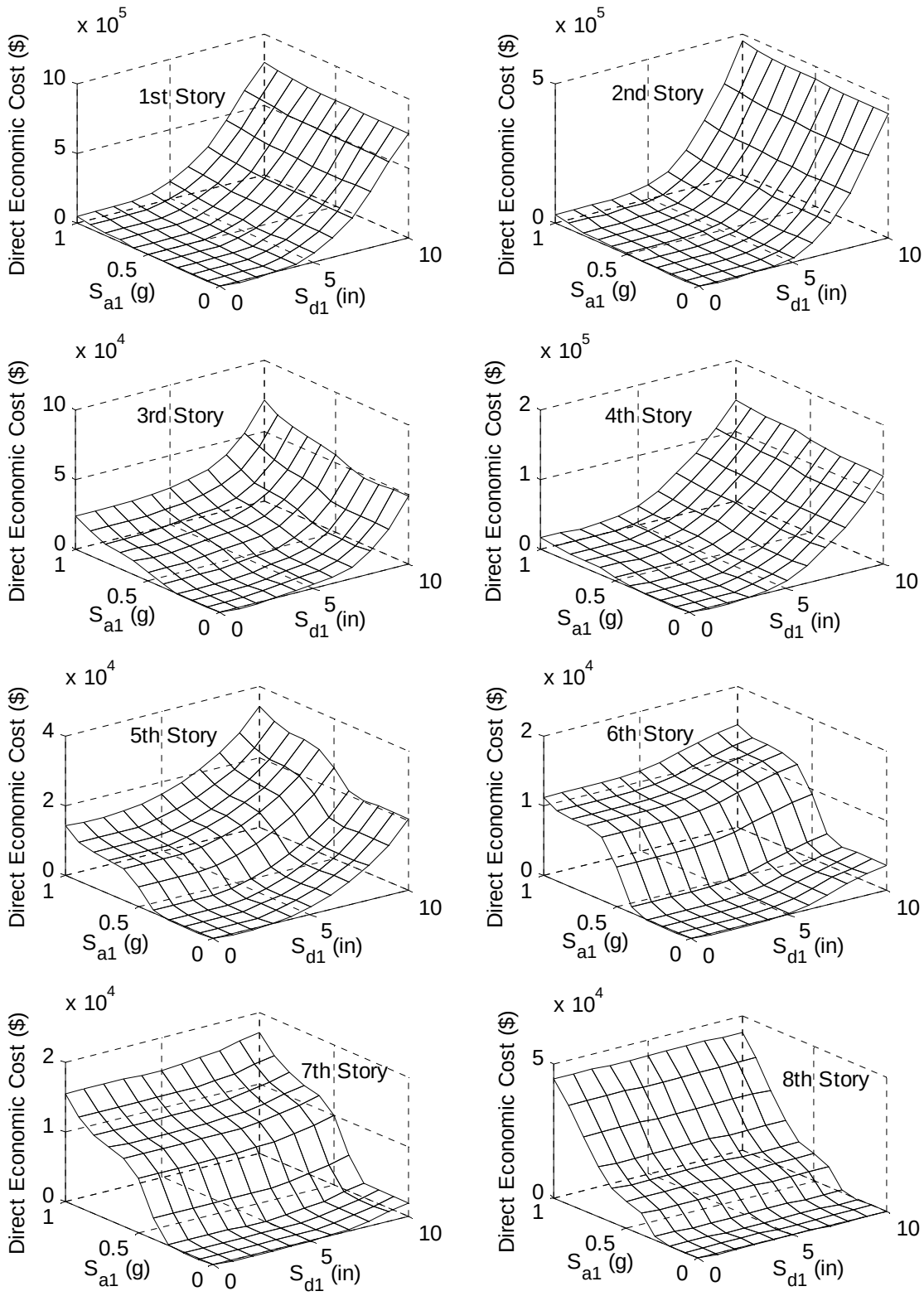

Figure 4.17: Direct economic cost functions for the eight-story building

4.6 Alternative Structural System: Braced Frame

The purpose of seismic evaluation and cost analysis for existing buildings is to estimate the probable damage due to future earthquakes and to retrofit these buildings for improved performance and stability.

In the first half of this chapter, the existing eight-story steel moment frame building has been considered for seismic evaluation using the nonlinear dynamic analysis method. Consequently, the direct economic cost functions of the building have been developed in Section 4.5. This section focuses on developing the direct economic cost functions of a seismic retrofit option. The cost functions will then be used to compare its performance to that of the existing building in terms of the exceedance probability of direct economic cost in Section 4.7.

Although several retrofit options should be considered to find an optimal alternative, this study focuses on the concentrically braced steel frame system. The braced frames are designed by providing bracing elements to the existing moment frames to increase story stiffness as shown in Figure 4.18. They are designed in accordance with the seismic design requirements of UBC 97 (Refer to Table 4.3).

Table 4.3: Bracing elements

Story	Story Shear Force (kips)	Compressive Load, P_{Brace} (kips)	Effective Length, KL (ft)	Bracing Members (A36 steel)
1	85.89	46.60	14.32	L5×5×3/4
2	88.04	58.93	14.50	L5×5×3/4
3	88.04	49.88	14.50	L5×5×3/4
4	88.04	41.21	14.50	L5×5×1/2
5	88.04	32.33	14.50	L5×5×1/2
6	88.04	23.33	14.50	L5×5×1/2
7	123.25	14.09	14.50	L5×5×3/8
8	62.81	5.89	14.50	L5×5×3/8

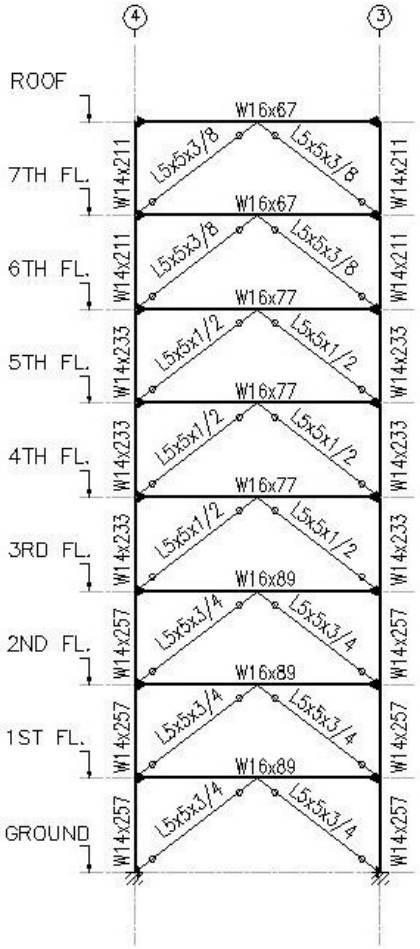

Figure 4.18: Braced frames in the N-S direction (plan view in Figure 3.3)

Nonlinear dynamic analysis of the braced frame building is performed according to the following manners: (1) the building is subjected to ground acceleration in the N-S direction, (2) the building is simplified into a lumped-mass model, (3) the additional mass of the bracing members are assumed to be negligible, (4) the story stiffnesses and yield strengths are determined from nonlinear force-displacement relation curves, and (5) the damping ratios of the first and second modes are assumed to be same as those of the existing building, i.e. $\zeta_1 = \zeta_2 = 5\%$.

4.6.1 Force–Displacement Relations

In order to perform nonlinear dynamic analysis using Algorithm 4.1, the force-displacement relations of the braced frames are characterized in a similar manner as described in Section 4.4.1. For an illustrative example, 1st-order inelastic analysis is performed on the 2nd story braced frame subjected to monotonically increasing lateral forces until the frame becomes fully plastic. Figure 4.19 shows the braced frame modeled in MASTAN2 and the locations of total eight plastic hinges. The brace elements yield at the applied load of 530.1 kips, and then the beam and columns yield at applied forces of 867.9 and 885.0 kips, respectively. Because the yield strength of the beam and columns are close, yield strength of the both elements are assumed to be 885.0 kips. Then the resulting force-displacement curve is presented in Figure 4.20 which shows a tri-linear shape.

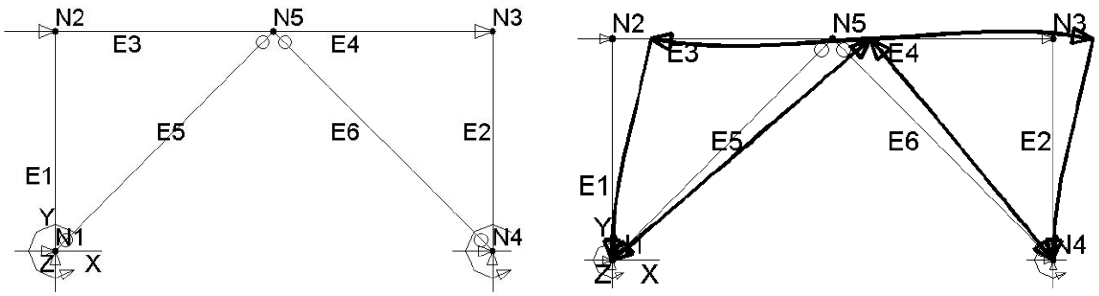

(a) A 2nd story braced frame modeled in MASTAN2

(b) Locations of total eight plastic hinges

Figure 4.19: Static pushover analysis of the 2nd story braced frame

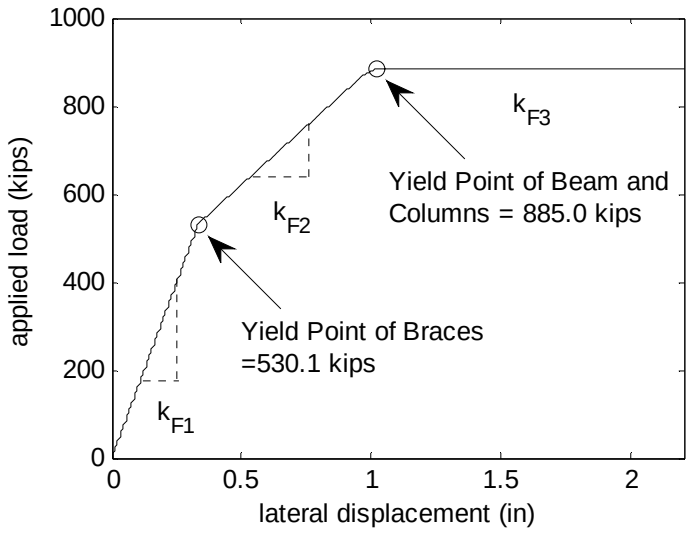

Figure 4.20: Force and displacement relationship of the 2nd story braced frame

In the force-displacement curve, the slope of each linear line represents the stiffness of the braced frame, k_{F1}, k_{F2}, or k_{F3}. Based on the assumption that story stiffness is the sum of the stiffness of the story frames, the 2nd story stiffness is equal to six times the stiffness of the story frame (six identical frames in N-S direction, see Figure 3.3). Similarly, the yield shear force for the 2nd story is six times the yield force of the story frame.

Because the tri-linear force-displacement relation is also observed in the other story frames, their stiffness and yield strength are evaluated in the same manner as in the illustrative example above. Table 4.4 summarizes yield forces, F_{y1} and F_{y2}, and story stiffness, k_{s1}, k_{s2}, and k_{s3}, of each story. Because additional bracing members are added to the existing frames, the yield forces and story stiffness are increased (see Table 4.2 and 4.4 for comparison).

Algorithm 4.4 is developed to implement the material nonlinearity of the braced frame system, having a tri-linear force-displacement relation, into Wilson's theta method, see step (c) of Algorithm 4.1.

Algorithm 4.4: Tangent stiffness matrix for braced frames (tri-linear force-displacement relationship)

Input Parameters: $\underline{k}_{s1}$, $\underline{k}_{s2}$, $\underline{k}_{s3}$, $(\underline{F_s})_{i-1}$, $\Delta\underline{x}$, and $\underline{\dot{x}}_i$

Output Parameters: $\underline{k}_t$ and $(\underline{F_s})_i$

(a) Calculate forces $(F_s^{(n)})_i$ in the n-th story frames at time t_i

for n = 1:8

if $|(F_s^{(n)})| < F_{y1}^{(n)}$,

then $(F_s^{(n)})_i = (F_s^{(n)})_{i-1} + k_{e1}\Delta x^{(n)}$

else if $F_{y1}^{(n)} \le |(F_s^{(n)})| < F_{y1}^{(n)}$ and $sign(\dot{x}_i^{(n)}) = sign(\dot{x}_{i-1}^{(n)})$

then $(F_s^{(n)})_i = (F_s^{(n)})_{i-1} + k_{s2}\Delta x^{(n)}$

else, then $(F_s^{(n)})_i = (F_s^{(n)})_{i-1} + k_{s1}\Delta x^{(n)}$

for n = 1:8

if $|(F_s^{(n)})_i| > F_{y2}^{(n)}$,

then $(F_s^{(n)})_i = sign((F_s^{(n)})_i) \cdot F_{y2}^{(n)}$

(b) Determine stiffness $k^{(n)}$ in n-th story at time t_i

for n = 1:8

if $|(F_s^{(n)})_i| < F_y^{(n)}$,

then $k^{(n)} = k_{s1}^{(n)}$

else if $F_{y1}^{(n)} \le |(F_s^{(n)})_i| < F_{y2}^{(n)}$ and $sign(\dot{x}_i^{(n)}) = sign(\dot{x}_{i-1}^{(n)})$,

then $k^{(n)} = k_{s2}^{(n)}$

else if $F_{y1}^{(n)} \le |(F_s^{(n)})_i| < F_{y2}^{(n)}$ and $sign(\dot{x}_i^{(n)}) \neq sign(\dot{x}_{i-1}^{(n)})$,

then $k^{(n)} = k_{s1}^{(n)}$

else if $|(F_s^{(n)})_i| \ge F_{y2}^{(n)}$ and $sign(\dot{x}_i^{(n)}) \neq sign(\dot{x}_{i-1}^{(n)})$,

then $k^{(n)} = k_{s2}^{(n)}$

else, then $k^{(n)} = k_{s3}^{(n)}$

(c) Construct tangent stiffness matrix $\underline{k}_t$ using $k^{(n)}$

Table 4.4: Yield forces and story stiffnesses of the braced frame structure

Story	Yield Force (kips)		Story Stiffness (kips/inches)		
	F_{y1}	F_{y2}	k_{s1}	k_{s2}	k_{s3}
1	3,255.6	5,415.0	1,0008.0	3,406.8	0.0
2	3,180.6	5,310.0	9,571.8	3,187.8	0.0
3	3,180.6	5,310.0	9,571.8	3,187.8	0.0
4	2,367.0	4,291.2	7,252.8	2,781.0	0.0
5	2,367.0	4,291.2	7,252.8	2,781.0	0.0
6	2,367.0	4,291.2	7,252.8	2,781.0	0.0
7	1,902.6	3,630.6	5,881.2	2,451.6	0.0
8	1,902.6	3,630.6	5,881.2	2,451.6	0.0

4.6.2 Direct Economic Cost Functions

To make a meaningful comparison of the existing and alternative structural systems, the same 100 samples of ground acceleration (Section 4.5.2: IDA) are used in incremental dynamic analysis of the braced frame building within the predetermined *IM* limits of $S_{d1} = 10$ inches and $S_{a1} = 1\,\text{g}$ (same as for the existing building). Based on the IDA results, fragility curves are developed in terms of spectral displacement or acceleration with lognormal distribution assumption. In the development of the fragility curves, the damage states of nonstructural components are determined based on the thresholds given in Table 3.4. However, for the structural components, the different thresholds are used to define the damage state, see Table 4.5. Then following the detailed procedure described in Section 3.6, the direct economic cost functions for the braced frame building are developed as shown in Figure 4.21.

Table 4.5: Thresholds of braced frames for structural damage [18]

Damage States	Slight	Moderate	Extensive	Complete
Structural Component (Interstory Drift Ratio)	0.0025	0.0050	0.0150	0.0400

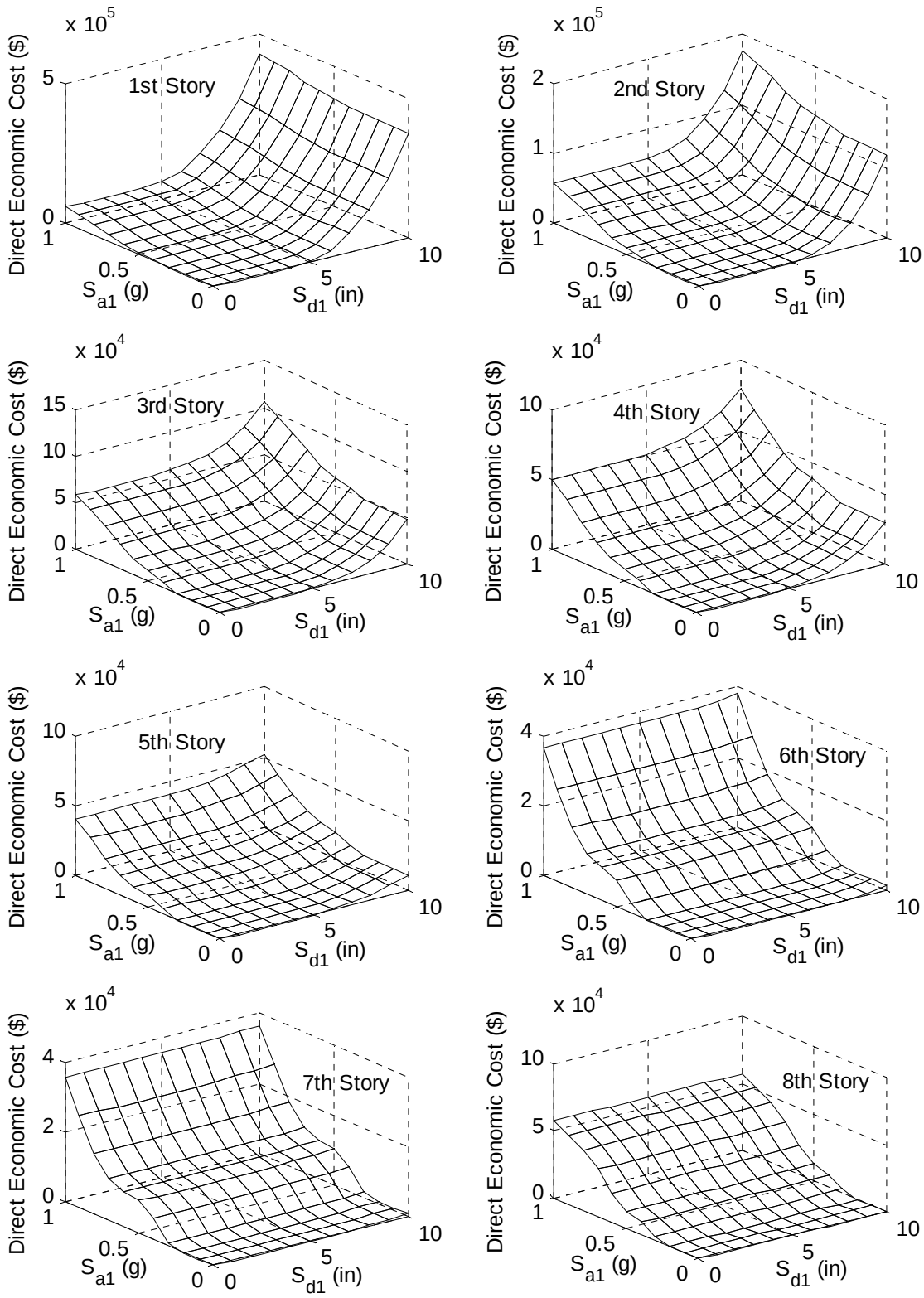

Figure 4.21: Direct economic cost functions for the braced frame building

4.7 Exceedance Probability of Direct Economic Cost

For comparison of the seismic performance of the two structural systems, exceedance probabilities of the direct economic cost are evaluated using the 10,000 samples of possible earthquake intensity measures (S_{d1}, S_{a1}) in Section 4.1 and the direct cost functions developed for each building system (see Figure 4.17 for the moment frame and Figure 4.21 for the braced frame). Given each of the intensity levels, samples of direct economic cost $C_j^{(i)}$ are obtained for each structural system (where $i = 1, 2, \ldots, 8$ and $j = 1, 2, \cdots, 10,000$).

Then the exceedance probability curves of the direct economic cost $P_{EC}(C^{(i)} > c_{cr})$ due to an earthquake are estimated using Equation (3.27), and resulting probability curves for each structural system are presented in Figure 4.22 for comparison. Also, lifetime exceedance probabilities are estimated using Equation (3.29) under the assumption of a Poisson process for the occurrence of earthquakes and compared in Figure 4.23.

Refer to Figures 4.22 and 4.23. The alternative structural system has lower exceedance probabilities for the lower stories; however, for the upper region the exceedance probabilities are higher than those for the existing building. As shown in the cost functions in Figures 4.17 and 4.21, the damage cost of the lower stories is mainly caused by drift-sensitive damage, and the cost of the upper stories is mainly influenced by acceleration-sensitive damage. Thus, the increased stiffness of the existing building by providing bracing members may help to reduce interstory displacement (i.e. help to reduce the cost influenced by drift-sensitive damage), but not floor acceleration.

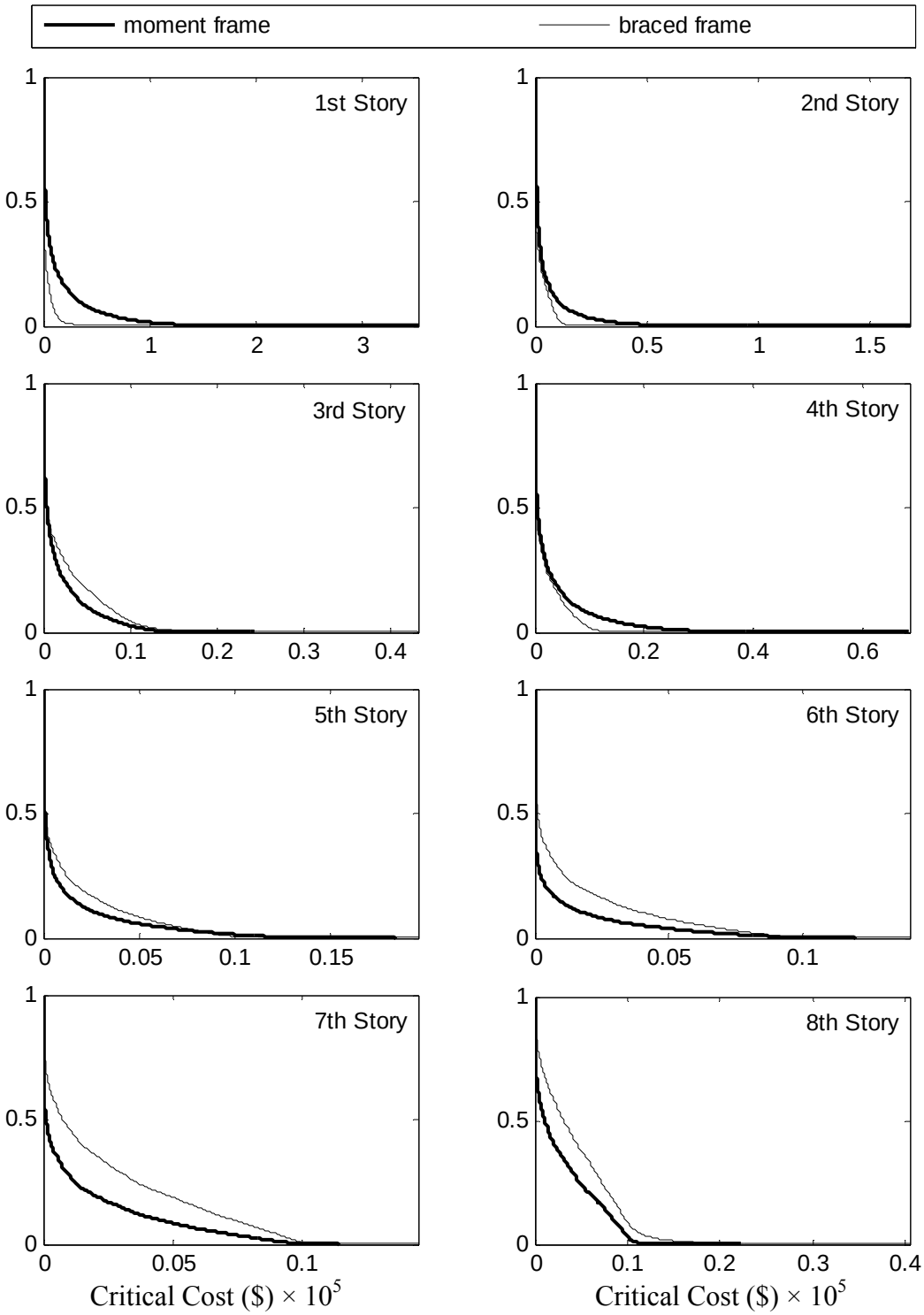

Figure 4.22: Exceedance probabilities of the direct economic cost due to an earthquake occurrence

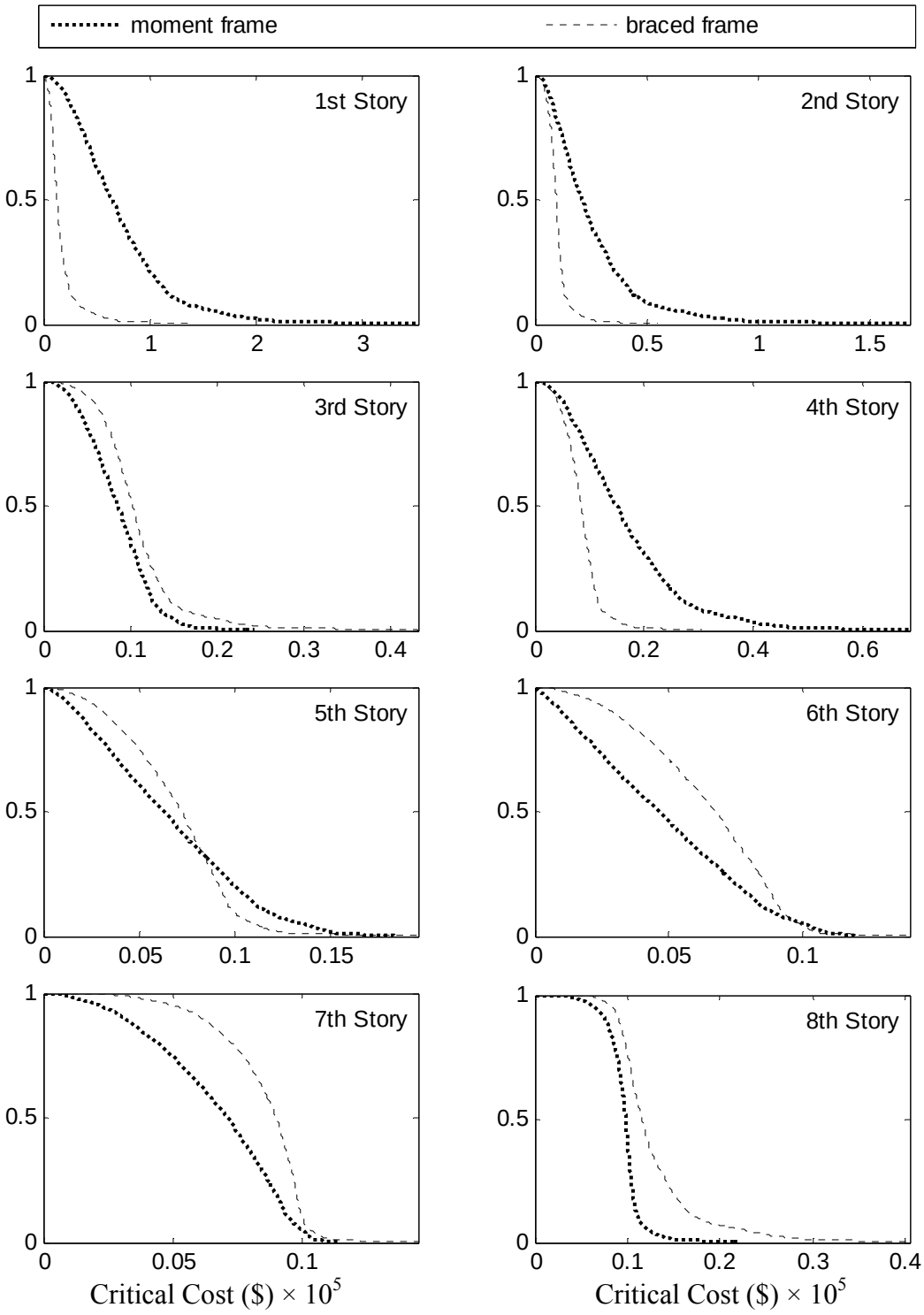

Figure 4.23: Exceedance probabilities of the direct economic cost during the lifetime

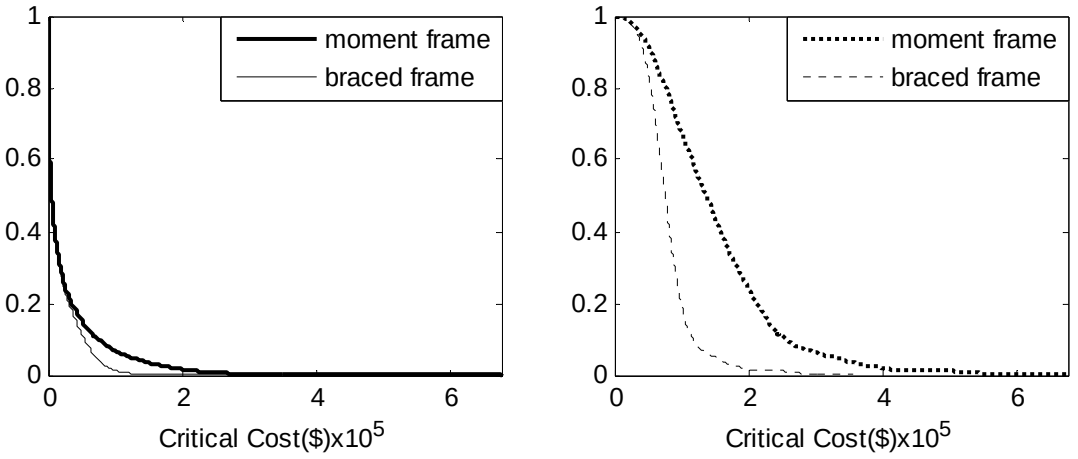

(a) Due to an earthquake (b) During the lifetime

Figure 4.24: Exceedance probabilities of direct economic cost of the entire buildings

In order to make a decision which structural system is superior, the exceedance probabilities of the overall cost of the two structural systems are compared. The total economic costs of the entire building are estimated as the sum of the repair costs of each story, see Equation (3.30). Figure 4.24 presents the comparisons of the estimated probability curves. Figure 4.24(a) does not show a large improvement by the alternative structural system; however, comparing the probability curves in Figure 4.24(b), it can be seen that the alternative structural system has better seismic performance and noticeably reduces the exceedance probability of the direct economic cost.

CHAPTER 5

SUMMARY AND CONCLUSION

This thesis presents a probabilistic procedure for estimating the damage of building-type structures subjected to earthquakes. For the evaluation of the seismic vulnerability of a building, three approaches are proposed: (1) failure rate curve, (2) fragility curve, and (3) exceedance probability of direct economic cost.

An eight-story steel moment frame building located in Los Angeles, California is used to illustrate the procedures. Stochastic processes are used to describe earthquake occurrence, ground motions, and failure. The damage to the building is measured by the maximum interstory drift and floor acceleration, and the intensity of ground motion is measured in terms of the spectral displacement and acceleration at the fundamental period of the building. These measures are obtained by numerical simulation of dynamic response.

For an initial evaluation of seismic performance of the building, a linear elastic analysis is performed to make a preliminary estimate of the damages and losses. Most buildings, however, experience inelastic deformation during strong ground motion. Hence, nonlinear analysis is carried out to provide more reliable prediction of the seismic response and a different insight into the structural behavior. While the failure rate curves derived from the linear analysis show that both structural and nonstructural components are not likely to experience moderate or severe damage, those derived from the nonlinear analysis show a considerable increase in the failure rate of the components in lower stories. Fragility curves developed by the nonlinear analysis method show the variability of the interstory drift at given intensity levels is more prominent than the variability of the curves developed by the linear analysis method.

The damages of structural and nonstructural components are closely related to monetary losses. Because the damage in terms of monetary loss provides more meaningful measure of economic impacts of earthquakes, the vulnerability of the structure is also evaluated based on the exceedance probability of the direct economic cost. The lifetime damage cost is another practical measure of the level of the safety because a desirable structural design should minimize damage cost during an intended lifetime.

In order to illustrate the use of the damage cost estimation method for finding an optimal retrofit option, an existing structural system is modified by adding braces. The braced frame is designed by placing bracing elements to the existing moment frame. The increase in stiffness due to the bracing elements helps to reduce the interstory displacement in the lower stories, and consequently, reduces the direct economic cost influenced by drift-sensitive damage. However, in the upper stories the exceedance probability of the direct economic cost is greater for the braced frame system. In order to evaluate the superiority of the two structural systems, the overall direct economic cost are compared which is the sum of the direct economic costs over all stories. In terms of the overall direct economic cost, the braced frame has a better seismic performance then the existing moment frame.

Although the methods presented in this thesis are useful to predict earthquake damage and qualify retrofit options, many assumptions have been made to simplify the dynamic response analysis and to reduce computational cost. For more realistic analysis, the assumptions herein should be verified or revised. Because earthquake direction is a source of the uncertainties, three-dimensional analysis is more desirable considering several directions of earthquake loading. The damage thresholds used to create fragility curves should be determined based on experiment or experts' opinions rather using those for generic type structures presented in HAZUS. To find an optimal

retrofit option, several alternatives should be considered with the cost required in the construction.

REFERENCES

[1] AISC Steel Construction Manual. 13th edition, 2007.

[2] H. Akiyama. Strengthening of steel frames in seismic resistance. In F. M. Mazzolani and M. Ivanyi, editors, Refurbishment of buildings and bridges, CISM Courses and Lectures No. 435 International Centre for Mechanical Sciences, 325-376, 2002.

[3] A. H-S. Ang and W. H. Tang. *Probability Concepts in Engineering Planning and Design; Volume I - Basic Principles*. Wiley, New York, 1975.

[4] A. Azarbakht and M. Dolsek. Prediction of the median IDA curve by employing a limited number of ground motion records. Earthquake Engng Struct. Dyn. 36:2401-2421, 2007

[5] R. A. Bastoni et al. *RSMeans Square Foot Costs 2007:28th Annual Edition*. Reed Construction Data, Inc. Kingston, MA, 82-83, 453, 2007.

[6] D. M. Boore. Stochastic simulation of high-frequency ground motions based on seismology models of the radiated spectra. Bulletin of the Seismological Society of America. 73(6): 1865-1894, 1983.

[7] A. K. Chopra. *Dynamics of Structures: Theory and Applications to Earthquake Engineering*. Prentice Hall,Upper Saddle River, NJ, 3rd edition, 2007.

[8] G. P. Cimellaro et al. Multi-dimensional fragility of structures: formulation and evaluation. Technical Report MCEER-06-0002, University at Buffalo, The State University of New York, Buffalo, NY, 2006.

[9] Cosmos Virtual Data Center. <http://db.cosmos-eq.org>

[10] S. H. Crandall and W. D. Mark. *Random Vibration in Mechanical Systems*. Academic Press, London, NY, 1963.

[11] FEMA-350. *Recommended Seismic Design Criteria for New Steel Moment-Frame Buildings*. Federal Emergency Management Agency, Washington, D. C., 2000.

[12] FEMA-351. *Recommended Seismic Evaluation and Upgrade Criteria for Existing Welded Steel Moment-Frame Buildings*. Federal Emergency Management Agency, Washington, D. C., 2000.

[13] R. V. Field, Jr, and M. D. Grigoriu. Reliability of dynamic systems under limited information. Sandia Report SAND2006-5580, Sandia National Laboratories, 2006.

[14] M. Grigoriu. Class Material: MATLAB Codes. CEE678: Structural Dynamics and Earthquake Engineering, Cornell University, Fall 2008.

[15] M Grigoriu. *Stochastic Calculus: Applications in Science and Engineering*, Birkhauser, Boston, 2002.

[16] M. Grigoriu. *Applied Non-Gaussian Processes: Examples, Theory, Simulation, Linear Random Vibration and MATLAB Solutions*. Prentice Hall, Englewood Cliffs, NJ, 1995.

[17] HAZUS-MH MR1. *Multi-hazard loss estimation methodology earthquake model; Advanced Engineering Building Module.* Technical and User's Manual, Federal Emergency Management Agency, Washington, D.C., 2003.

[18] HAZUS-MH MR3. *Multi-hazard loss estimation methodology earthquake model*. Technical Manual, Federal Emergency Management Agency, Washington, D.C., 2003.

[19] T.-I Hsu and M. C. Bernard. A random process for earthquake simulation. Earthquake Eng Struct Dyn, 6: 347-362, 1978.

[20] S. M. Kay, S. L. Marple, Jr. Spectrum analysis - A modern perspective. *Proc. IEEE*, 69 (11): 1380-1419, 1981.

[21] M. S. Kircil and Z. Polat, Fragility analysis of mid-rise R/C frame buildings. *Engineering Structures*, 28 (9): 1335-1345, 2006.

[22] S. C. Lee and S. W. Han. Neural-network-based models for generating artificial earthquakes and response spectra. *Computers and Structures*. 80: 1627-1638, 2002

[23] M. Lefebvre. *Applied Stochastic Processes*. Springer, New York, NY, 2007.

[24] D. G. Lignos, E. C. Stergiou, and C. J.Grantes. System reliability of steel structures based on interstory drift and direct loss demands. *5th GRACM International Congress on Computational Mechanics*, 2005.

[25] S. C. Liu and D. P. Jhaveri, Spectral and correlation analysis of ground-motion accelerograms. *Bulletin of the Seismological Society of America*. 59: 1517-1534, 1969.

[26] J. B. Mander et al. Incremental dynamic analysis applied to seismic financial risk assessment of bridge. *Engineering Structures*, 29(10): 2662–2672, 2007

[27] MASTAN2. Wiley. 2008. <http://www.mastan2.com>

[28] MATLAB. Language of Technical Computing. The MathWorks, Inc., 2007.

[29] F. Naeim, et al. Automated post-earthquake damage assessment and safety evaluation of instrumented buildings. SMIP05 Seminar on Utilization of Strong-Motion Data,71-88, 2005.

[30] G. R. Saragoni and G. C. Hart. Simulation of artificial earthquakes. Earthquake Eng Struct Dyn, 2: 249-267, 1974.

[31] N. Shome and C. A. Cornell. Probabilistic seismic demand analysis of nonlinear structures. Report No. RMS-35, Dept. of Civil Engineering, Stanford University, Stanford, CA, 1999.

[32] J. Solnes. *Stochastic Processes and Random Vibrations*. Wiley, New York, 1997

[33] T. T. Soong, *Fundamentals of Probability and Statistics for Engineers*. John Wiley, 75-112, 2004.

[34] T. T Soong and M. Grigoriu. *Random Vibration of Mechanical and Structural Systems*. Prentice-Hall, Englewood Cliffs, NJ, 1993.

[35] UBC. *1997 Uniform Building Code: Volume 2*. International Conference of Building Officials, 1997.

[36] U.S. Department of Labor. Bureau of Labor Statistics. <http://www.bls.gov/schedule/archives/cpi_nr.htm#2001>

[37] USGS. Earthquake Hazards Program: Significant Los Angeles Earthquakes. <http://earthquake.usgs.gov/regional/sca/la_eqs.php>

[38] D. Vamvatsikos and C. A. Cornell. Incremental dynamic analysis. Earthquake Eng Struct Dyn, 31(3): 491-514, 2002.

[39] D. Vamvatsikos and C. A. Cornell. The incremental dynamic analysis and its application to performance-based earthquake engineering. Proceedings of the 12th European Conference on Earthquake Engineering, 2002.

[40] E. L. Wilson. Three-Dimensional Static and Dynamic Analysis of Structures: A Physical Approach With Emphasis on Earthquake Engineering. Computers and Structures, Inc. Berkeley, CA, 2nd edition, Chapter 11, 2002 <http://www.comp-engineering.de/downloads/manuals/ETABS/English/E-MAN-008.pdf >

[41] D. Zhao and K. K. F. Wong. New approach for seismic nonlinear analysis of inelastic framed structures. *J. Engrg. Mech*. 132(9): 959-966, 2006.